dietitianCE
Continuing Education for Nutrition Professionals

Comparative Characterization of Different Stem Cell Derived Tissues

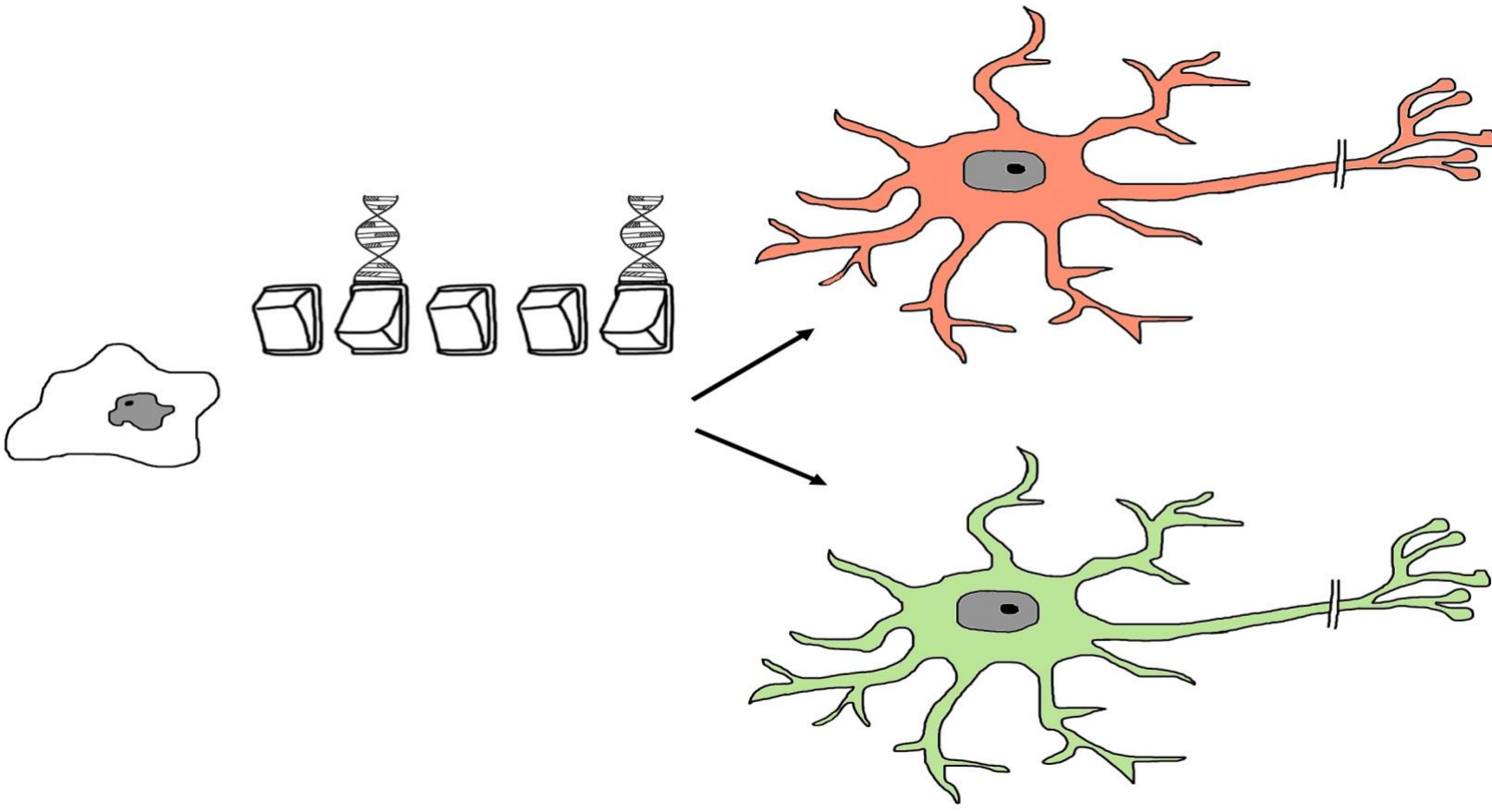

Comprehensive characterization of chorionic villi-derived mesenchymal stromal cells from human placenta

Abstract

Background: Studies in which mesenchymal stromal cells (MSC) from the placenta are compared with multiple MSC types from other sources are rare. The chorionic plate of the human placenta is mainly composed of fetal blood vessels embedded in fetal stroma tissue, lined by trophoblastic cells and organized into chorionic villi (CV) structures.

Methods: We comprehensively characterized human MSC collected from postnatal human chorionic villi of placenta (CV-MSC) by analyzing their growth and proliferation potential, differentiation, immunophenotype, extracellular matrix production, telomere length, aging phenotype, and plasticity.

Results: Immunophenotypic characterization of CV-MSC confirmed the typical MSC marker expression as defined by the International Society for Cellular Therapy. The surface marker profile was consistent with increased potential for proliferation, vascular localization, and early myogenic marker expression. CV-MSC retained multilineage differentiation potential and extracellular matrix remodeling properties. They have undergone reduced telomere loss and delayed onset of cellular senescence as they aged in vitro compared to three other MSC sources. We present evidence that increased human telomerase reverse transcriptase gene expression could not explain the exceptional telomere maintenance and senescence onset delay in cultured CV-MSC. Our in-vitro tumorigenesis detection assay suggests that CV-MSC are not prone to undergo malignant transformation during long-term in-vitro culture. Besides SOX2 expression, no other pluripotency features were observed in early and late passages of CV-MSC.

Conclusions: Our work brings forward two remarkable characteristics of CV-MSC, the first being their extended life span as a result of delayed replicative senescence and the second being a delayed aged phenotype characterized by improved telomere length maintenance. MSC from human placenta are very attractive candidates for stem cell-based therapy applications.

Background

The human placenta is a highly specialized pregnancy organ for supporting the development of a fetus. It connects the developing fetus to the wall of the mothers uterus through the umbilical cord (UC). Although the placenta originally develops from cells of fetal origin, it later consists of both maternal tissue (decidua) and fetal tissue (chorion, aminon). The chorion composition mainly consists of fetal blood vessels embedded in fetal stroma tissue and trophoblastic cells organized into ramified structures called chorionic villi (CV).

More than 10 years ago, researchers introduced the idea of using the placenta as a source for both maternal and fetal mesenchymal stromal cells (MSC) and progenitor cells [1 3]. Later, in 2007, the first international workshop on placenta-derived stem cells took place in Brescia, Italy, with the intention of setting criteria for defining MSC from human placenta [4]. However, a consensus has not yet been reached within the scientific community, as evidenced by the variety of studies published after the 2007 workshop which did not make use of the proposed criteria.

MSC from human placenta differ not only in terminology but also in harvesting and isolation methods [3, 5–20]. Studies comparing MSC from placenta with those from other sources exist, but comparative studies between CV-MSC and multiple MSC types (from other sources) are less frequent in the literature [6, 7, 21–23]. Meanwhile, early preclinical work using CV-MSC for tissue engineering applications has already started in different animal models [24–28].

It is unanimous that the use of both maternal-derived and fetal-derived MSC includes a few advantages [29–32]: noninvasive collection; no ethical concerns, often discarded as medical waste; and attractive immunological properties for allogeneic transplantations. MSC of fetal origin are particularly interesting due to their potential use for autologous applications considering the possibility for prenatal harvest and storage [33]. The possibility of MSC of fetal origin displaying a partial embryonic phenotype [34] is controversially discussed, although it could be a potential additional advantage.

In our study, we comprehensively characterize human chorionic villi-derived MSC (CV-MSC) collected from mature postnatal human placenta by analyzing their potential for growth and proliferation, differentiation, immunophenotype, extracellular matrix (ECM) production, telomere length and aging phenotype, and plasticity. A systematic comparison of CV-MSC with respective counterparts isolated from the bone marrow (BM), adipose tissue (AT), and Wharton's jelly of the UC is presented.

Methods

Isolation and culture of human chorionic villi-derived mesenchymal stem cells

Placentas from male newborns were collected after cesarean sections at the Department of Gynecology, University Hospital Aachen, in accordance with the local ethical regulations after obtaining informed consent (EK187/08). Placentas were collected from newborns delivered by elective cesarean section. Preterm birth was an exclusion criterion in our study as emergency cesareans were excluded. No further clinical data are available due to the anonymity of the donation. Before the placental tissue was dissected, the fresh placentas were washed extensively with PBS and the maternal decidua portion—identified by an experienced pathologist—was removed. CV-MSC were isolated by digestion. In brief, pieces of approximately 1 cm^3 equivalent to 4 g (wet weight) were dissected from the CV of the fetal side. Pieces were washed with PBS and transferred to centrifugation tubes for 60-minute digestion with 1 mg/ml Collagenase A (Roche Diagnostics, Germany) at 37 °C (Fig. 1a i–iii). Tissue recovery per placenta was maximized to an average of 200 g (wet weight). Digested tissue was then centrifuged and resuspended in trypsin/EDTA (PAN Biotech, Germany) for 10-minute incubation at 37 °C. Trypsinized tissue was centrifuged and transferred into a single T-25 cell culture flask containing 5 ml Bio-AMF-1 medium including supplements (Biological Industries, Israel) with additional penicillin–streptomycin at 1% and 5 mM L-Glutamine (both Thermo Fisher Scientific, Germany). Cells were kept in a humidified atmosphere at 37 °C with 5% CO_2 and passaged when 90% confluence was reached.

Isolation and culture of human bone marrow-derived mesenchymal stem cells

BM-MSC were isolated from bone marrow femoral heads following patient informed consent approved by the local Ethical Committee of the RWTH Aachen University (EK300/13). BM-MSC were isolated as described previously [35] and maintained in supplemented Mesenpan (PAN Biotech, Germany) with 2% fetal calf serum (FCS), 5 mM L-Glutamine and penicillin–streptomycin at 1% (all Thermo Fisher Scientific, Germany).

Isolation and culture of human umbilical cord-derived mesenchymal stem cells

UC-MSC were isolated from the Wharton's jelly of UCs as described previously [36]. Tissue collection was performed following local ethical guidelines and receiving informed consent (EK178/08). The cells were maintained in the same type of culture medium as described for BM-MSC.

Isolation and culture of human adipose tissue-derived mesenchymal stem cells

AT-MSC were isolated from lipoaspirates at the Department of Trauma and Hand Surgery, Medical Faculty of the Heinrich-Heine-University Düsseldorf, according to local ethics guidelines (EK-Nr. 3634). Cell isolation was carried out as described previously [37]. The lipoaspirate was first purified by centrifugation with saline solution, and subsequently by a second centrifugation for 10 minutes at $300 \times g$ in order to concentrate the cell pellet before a digestion step with 0.075% collagenase I (Biochrom, Berlin, Germany) for 45 minutes at 37 °C. The digested solution was filtered through a 250-μm filter, and the pellet was concentrated and washed with saline, before being resuspended in culture medium consisting of DMEM/F12 supplemented with 1% penicillin–streptomycin, 10% FCS (all Thermo Fisher Scientific, Germany), and 10 ng/ml bFGF (Peprotech, Germany). A panel of markers including CD16, CD31, CD49d, CD13, and CD29 was used for immunophenotypic characterization of the AT-MSC by flow cytometry (Table 1).

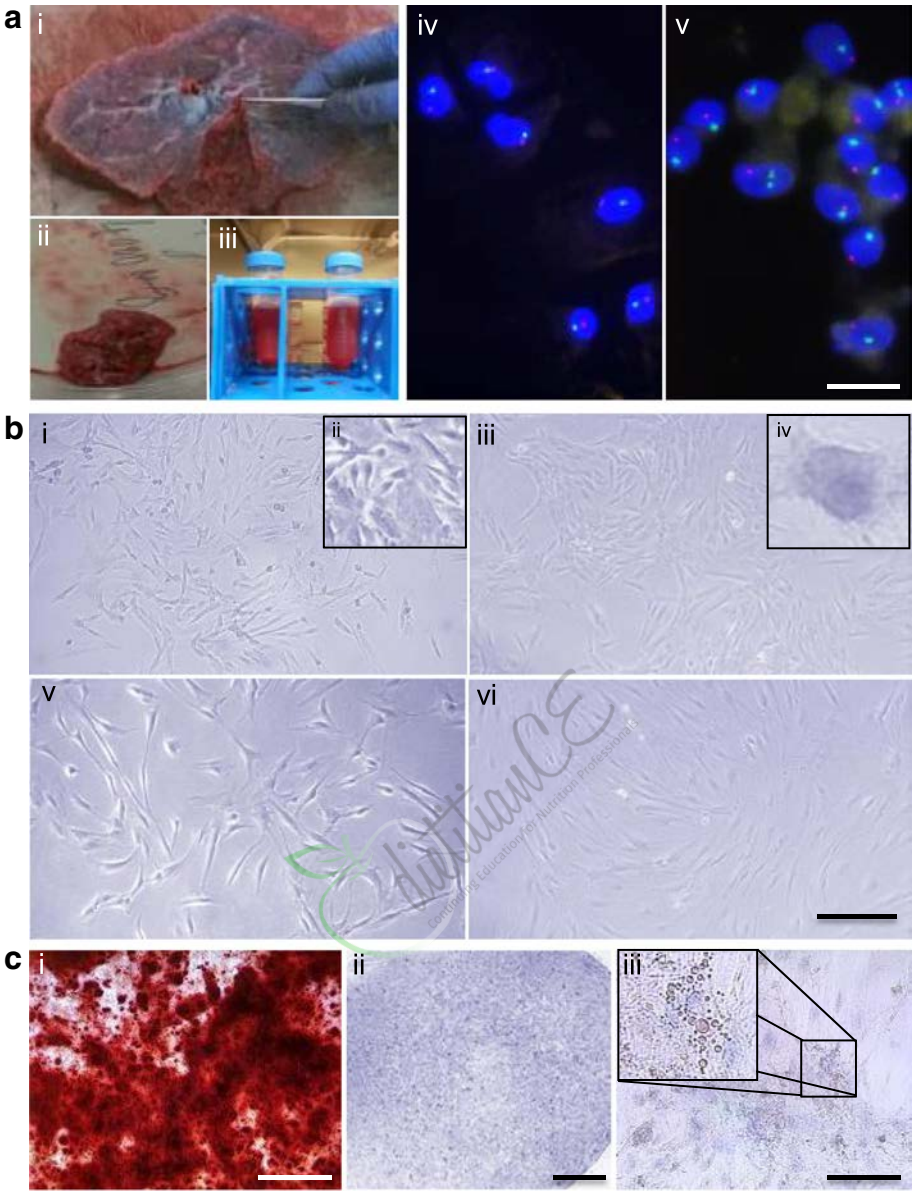

Fig. 1 **a** Isolation of human chorionic villi-derived mesenchymal stem cells (CV-CMSC) from human placenta. (i) Removal of the amnion to access the chorionic plate, (ii) pieces of CV dissected from human placenta, (iii) collagenase digestion of CV, and (iv, v) representative images of a CV-MSC donor at passage 4 (iv) and passage 9 (v) after interphase FISH analysis using a X/Y dual color probe. X chromosome fluorescence in green, Y chromosome fluorescence in orange. Scale = 25 μm. **b** Bright-field microscopy images of cultured CV-MSC (i –iv) and BM-MSC (v–vi) right after isolation and plastic adherence (ii), in passage 1 (i, v), in passage 5 (iii, iv), and in passage 10 (vi). Scale = 500 μm. **c** Representative images of Alizarin Red (calcium deposits), Toluin Blue (proteogyclans), and Oil Red O (lipid droplets) stained CV-MSC in passage 3 after respective osteogenic (i, scale = 500 μm), chondrogenic (ii, scale = 1 mm), and adipogenic (iii, scale = 100 μm) differentiation

Sex chromosome detection by fluorescence in-situ hybridization

To confirm the fetal origin of the CV-MSC isolated from placentas collected after the birth of male newborns, X/Y chromosome analysis was performed at early (p3–p4) and late (p8–p10) passages for all donors used for different subsequent experiments ($n = 5$) (Fig. 1a iv–v). The Zyto-Light CEN X/Y Dual Color Probe (Zytomed Systems, Germany) was used for detection of human α-satellites of X and Y chromosomes by fluorescence in-situ hybridization (FISH). Ten microliters of the hybridization mixture was added to the cytospun cells, and DNA denaturation was then performed at 75 °C for 2 minutes with subsequent overnight incubation using a humidified chamber. After hybridization, the cytospins were washed with cytology stringency buffer for 2 minutes at 72 °C and subsequently

Table 1 Antibodies used for flow cytometry, immunofluorescence, and western blot analysis

Flow cytometry	Source	Immunofluorescence	Source
CD44-PeCy7	560569, BD Pharmingen	SM22a	ab10135, Abcam
CD73	550256, BD Pharmingen	Calpomin	Ab700, Abcam
CD105	555690, BD Pharmingen	SM-MHC	M7786, Sigma
HLA-ABC-APC	562006, BD Pharmingen	α-SMA	A2547, Sigma
CD34-PerCP-Cy5.5	347222, BD Pharmingen	Tert (1:50)	AP33476PU-N, Acris
CD45-APC	555485, BD Pharmingen	Sox2	PA1-16968, Thermo
CD49a	559594, BD Pharmingen	Nanog	PA1-097X, Thermo
CD146-PE	561013, BD Pharmingen	Oct3/4	sc-5279, Santa Cruz Biotechnology
CD166-PE	559263, BD Pharmingen	Western blot assay	Source
CD19	555410, BD Pharmingen		
CD56-PeCy7	557747, BD Pharmingen	Tert(1:1000)	SAB4502945, Sigma
CD80-PE	560925, BD Pharmingen	Sox2 (1:2000)	PA1-16968, Thermo
CD83-PeCy7	561132, BD Pharmingen	Oct3/4(1:1000)	sc-5273, Santa Cruz Biotechnology
CD86-V450	560359, BD Pharmingen	Nanog (1:2000)	PA1-097X, Thermo
Strol	14-6688-80, eBiosciences	Erk1/2 (1:1000)	9102, Cell Signaling
CD106-PerCPCy5.5	45-0149-42, eBiosciences	pErk1/2(1:1000)	9101, Cell Signaling
CD14-PerCPCy5.5	45-0149-42, eBiosciences	β-Catenin (1:5000)	ab32572, Abcam
CD40-PeCy7	25-0409-41, eBiosciences	Smad2/3 (1:400)	AF3797, R&D Systems
CD275(B7H2)-PE	12-5889-41, eBiosciences	pSmad2/3(1:1000)	8828, Cell Signaling
CD90-APC	17-0909-42, eBiosciences	NICD(1:500)	ab8925, Abcam
HLA-DR-efluor450	48-9956-41, eBiosciences	Akt1/2(1:1000)	sc-1619, Santa Cruz Biotechnology
α-SMA	A2547, Sigma	pArk1/2(1:1000)	9271, Cell Signaling
SM22α	ab10135, Abcam	Smad1/5/9(1:2000)	ab66737, Abcam
vWF	ab8822, Abcam	PSmad1/5(1:1000)	9516, Cell Signaling

All antibodies were used in 1:100 dilutions, unless otherwise indicated

rinsed in sodium chloride/sodium citrate buffer for 1 minute at room temperature (RT). Slides were finalized using Vectashield antifade mounting medium containing 4′,6-diamidino-2-phenylindole (DAPI) (Vector Labs, Germany) and fluorescence detected on an Axiovert S135 microscope (Zeiss, Germany). The α-satellite sequences of the centromere of chromosome X were excited at 488 nm and of chromosome Y at 554 nm.

Multilineage differentiation

MSC differentiation protocols were applied as described in detail previously [35]. For adipogenic differentiation we used adipogenic induction and maintenance medium [35], alternately, twice a week for 21 days, before cells were fixed with 50% ice-cold ethanol and stained with 0.2% Oil Red O solution (Sigma, Germany) for lipid visualization. For chondrogenic differentiation, pellet cultures were performed and maintained for 21 days in serum-free chondrocyte induction medium refreshed three times a week (with freshly added TGF-β_3). Pellets were fixed in formalin and embedded in 3% agarose for paraffin block preparation. Slices were prepared and stained with 1% Toluidin Blue (Sigma, Germany) for proteogyclan visualization. For osteogenic differentiation, we applied osteogenic induction medium for 21 days, refreshed three times per week. Finally cells were fixed with 70% ice-cold ethanol and stained with 40 mM Alizarin Red (Sigma, Germany) solution for calcium deposit visualization. Staining was photographed with a Cool Snap™ HQ2 digital camera (Photometrics, USA) on an Axiophot 2 microscope (Carl Zeiss, Germany).

Long-term cultures

During long-term cultures, cell population-doubling (PD) levels were assessed by manual counting, using Neubauer chambers. In order to standardize reporting of

cellular aging, we calculated cumulative PD (cPD) after each passage by applying the following formulas:

$$2^{PD} = \text{nunmber of harvested cells/number of seeded cells},$$
$$\text{cPD} = \Sigma^{n_2}(PD\,1 + PD\,2 + \ldots + PD\,n).$$

MSC from all sources were seeded at a density of 5000 cells per cm^2 in T75 culture flasks. Cell morphology was visualized using a Cool Snap™ HQ2 digital camera (Photometrics, USA) on an Axiophot 2 microscope (Carl Zeiss, Germany).

Cell viability assays

To assess cell viability, we used the CellTiter-Blue Assay (Promega, Germany) as described previously [38]. MSC in passage 2 were seeded at 5×10^4 cells per well in 96-well plates. Viability was measured after initial cell adhesion to the culture plastic and again after 7 days in culture with one intermediate medium exchange. The assay evaluates the ability of the cells to convert resazurin into resofurin, so for the reaction we provided 100 µl fresh medium and added 20 µl viability reagent. We incubated the cells for 1 hour in a 37 °C humidified incubator before transferring 80 µl to a black 96-well plate. Fluorescence intensity was then measured using the FLUOstar OPTIMA (BMG Labtech, Germany) fluorometer. Excitation was at 560 nm and emission was at 590 nm.

Senescence-associated β-galactosidase activity

For assessment of pH-dependent senescence-associated β-galactosidase (SA-β-gal) we applied the SA-β-gal staining kit (9860; Cell Signaling Technology, USA). We followed the manufacturer's instructions to stain MSC in early and late passages. In parallel, SA-β-gal activity was assessed by flow cytometry as described by Debacq-Chainiaux et al. [39]. MSC were seeded at 1×10^3 cells per cm^2 in 24-well plates. After 7 days, the cells were incubated with 100 nM Bafilomycin A1 (Sigma, Germany) for 1 hour to alkalize the lysosomes. Next cells were incubated with 2 mM of the fluorogenic substrate C12FDG (Invitrogen, Germany) for 2 hours at RT. Fluorescence was acquired on a FACSCanto II (BD Biosciences, Germany) and data were analyzed using FlowJo (Tree Star Inc., USA).

Generation of three-dimensional collagen gels and collagen contraction quantification

Three-dimensional collagen gels were prepared as published previously [40, 41] by mixing eight volumes of acidic collagen G (3 mg/ml collagen I/III in 12 mM hydrochloric acid; Biochrom, Germany) with one volume of DMEM 4.5 g/l D-glucose 10× concentrated (Biochrom, Germany). Sodium hydroxide (2 M) was then used to neutralize the mixture and one volume of culture medium containing 1×10^6 MSC per ml was added into the mixture. Gels were polymerized at 37 °C in a humidified atmosphere for 1 hour after 500 µl of the collagen mixture was poured into each well of a 24-well plate. MSC within the gels were fed by adding 500 µl of the respective medium to top of the polymerized gels, which were kept for 28 days at 37 °C in a humidified atmosphere with two weekly medium changes. Next, gels were fixed in formaldehyde for 24 hours at 4 °C and contraction was quantified after photographing (Discovery V12, Germany) and measuring the circular area of each gel (ImageJ, open source). Collagen area is expressed as the percentage of the total collagen area of the collagen gels without cells.

Extracellular matrix remodeling

ECM remodeling was assessed by performing immunohistochemistry (IHC) of the three-dimensional collagen gels containing MSC of different sources as described previously [40]. Formaldehyde-fixed gels were cut in half and with a cross-sectional view upward for paraffin embedding. The gels were sliced in 3-µm-thick slices using a rotating microtome (Leica, Germany). For IHC we used the Dako Real detection system peroxidase/DAB+, rabbit/mouse (K5001; Dako, Germany) and stained according to the manufacturer's recommendations. Primary antibodies used were fibronectin (FN) (1:200, F3648; Sigma, Germany) and osteopontin (OPN) (1:500, sc-21742; Santa Cruz Biotechnology, Germany). Slides were dehydrated and mounted in Vitro-Clud (Langenbrinck, Germany). Images were acquired with a Cool Snap™ HQ2 digital camera (Photometrics, USA) on an Axiophot 2 microscope (Carl Zeiss, Germany).

Flow cytometry

MSC from different sources were analyzed by flow cytometry for a wide panel of markers, as presented in Table 1. The staining procedure was performed as described previously [36, 40, 41]. A minimum of 100,000 events was acquired on FACSCanto II (BD Biosciences, Germany) and the data were analyzed using FlowJo (Tree Star Inc., USA).

Immunofluorescence

For immunofluorescence, 1×10^3 MSC per cm^2 were seeded into 24-well plates and after 24 hours fixed with 4% paraformaldehyde (PFA) for 20 minutes at RT. Next cells were permeabilized with 0.2% Triton X-100 for 30 minutes and kept at 4 °C overnight in PBS. Primary antibody (Table 1) incubation was done overnight at 4 °C. Secondary antibodies donkey anti-rabbit (A21206; Thermo Fisher, Germany) or goat anti-mouse (A11001; Thermo Fisher, Germany) were used at 1:100 for 1-hour incubation at RT. Rhodamine-TRITC (50 µg/ml, P1951; Sigma, Germany) incubated for 40 minutes at RT was

used for staining the MSC F-Actin fibers. Fluorescence was acquired with a DMI 6000B microscope (Leica, Germany).

Telomere length analysis by quantitative fluorescence in-situ hybridization

Telomere length was assessed by quantitative fluorescence in-situ hybridization (Q-FISH) as described previously [42–44]. MSC from different sources in early and late passages were analyzed in parallel. Cells were fixed in methanol/acetic acid (3:1), cytospun, air dried, and dehydrated with ethanol before telomeres were stained with a Cy3-(C3TA2) peptide nucleic acid (PNA) probe (Panagene, South Korea). After 2 hours of incubation at RT in a humidified chamber, cells were washed with formalin-based buffer 2× for 15 minutes and DAPI was used for nuclei counterstain. Slides were mounted with Vectashield antifade mounting medium (Vector Labs, USA) and fluorescence was acquired with the high-resolution laser-scanning microscope LSM710 (Zeiss, Germany). Images were captured at 63× optical magnification with additional 1.2× zoom. A multi-tracking mode of 0.5-μm steps was used to acquire images of DAPI and Cy3 staining. Maximum projection of five single consecutive steps was done for TL quantification using Definiens software (Definiens, Germany). Nuclei and telomeres were detected based on the respective DAPI and Cy3 intensity. Due to the impossibility of calculating an age-adapted telomere length, the absolute telomere signal was used to calculate telomere loss (Δtelomere length) per passage in arbitrary units (a.u.) of fluorescence.

Epigenetic aging signature

The aging signature (EAS) introduced by Weidner et al. [45] uses bisulfite pyrosequencing to assess DNA methylation (DNAm) levels at three CpG sites located in the genes *ITGA2B*, *ASPA*, and *PDE4C*. For EAS analysis, genomic DNA (gDNA) was first isolated using the DNA blood kit (Qiagen, Germany) and then cleaned using the clean & concentrator kit-5 (Zymo Research, USA). Five hundred nanograms of gDNA was used for further bisulfite conversion and pyrosequencing at Varionostic GmbH (Ulm, Germany). Pyrosequencing results were used for age prediction by applying the following multivariate linear regression model:

$$\text{Age(years)} = 38.0 - 26.4\alpha - 23.7\beta + 164.7\gamma.$$

This equation was designed to predict age with a mean absolute deviation from chronological age of less than 5 years.

Real-time quantitative PCR

Quantification of mRNA expression for the assessed genes was performed by real-time quantitative PCR (qRT-PCR) using the 7300 Real-Time PCR System (Applied Biosystems, Germany). Total RNA was extracted using the universal RNA Purification Kit (Roboklon, Germany). Complementary DNA (cDNA) synthesis was performed using the cDNA Reverse Transcriptase Kit (Applied Biosystems, Germany). Amplification consisted of initial denaturation at 95 °C for 10 minutes, followed by 40 cycles of denaturation at 95 °C for 15 seconds and final extension at 60 °C for 1 minute. The housekeeping gene *GAPDH* was used for data normalization. Gene expression was set to one on human embryonic stem cells (total RNA, 5825; Sciencell, USA) using the $2^{-\Delta\Delta ct}$ method. The primers used are presented in Table 2. Seven CV-MSC donors between passages 2 and 4 were screened for pluripotency genes.

hTERT mRNA and *hTERT* splicing variant detection

To determine human telomerase reverse transcriptase (*hTERT*) mRNA levels, we performed qRT-PCR under the same conditions as before except for the use of 250 ng total RNA per reaction and the use of the following cycling conditions: 50 °C for 30 minutes, 95 °C for 15 minutes, 94 °C for 45 seconds, 60 °C for 45 seconds, 72 °C for 90 seconds for 31 cycles, and 72 °C for 10 minutes [46]. Primers are presented in Table 2. To detect *hTERT* mRNA alternative splicing, we performed qRT-PCR as before [47]. Splice variant products were amplified from 3.5 μl cDNA using primers hT2164F and hT2620R, also presented in Table 2. Cycling conditions were 94 °C for 15 minutes, 95 °C for 30 seconds (40 - cycles), 64 °C for 45 seconds, 72 °C for 45 seconds, and 72 °C for 5 minutes. Primers hT2164F and hT2620R generated a 457-bp product containing the A and the B reverse transcriptase motifs, designed to detect the presence of α and β deletions. Total human embryonic stem cell RNA (5825; Sciencell, USA) was used as a positive control.

Western blot analyses

Total protein was extracted from MSC using RIPA buffer containing protease inhibitor cocktail (Roche, Germany) and quantified using the BCA protein assay (Thermo Fisher, Germany). NuPAGE Novex 4–12% gradient Bis–Tris gels (Thermo Fisher, Germany) were used for SDS-PAGE of proteins. Proteins were transferred to nitrocellulose membranes, which were blocked using 0.5× Roti-block protein-free blocking buffer (Carl Roth, Germany) for 1 hour at room temperature. Primary antibody (Table 1) incubation was done overnight at 4 °C. Secondary HRP-linked anti-rabbit/mouse/goat IgG (1:1000; Dako, Germany) with enhanced chemiluminescence (Thermo Scientific, Germany) was used for detection. Loading

Table 2 Primers used for real-time quantitative PCR

	Forward sequence (5′–3′)	Reverse sequence (5′–3′)
GAPDH	GAAGGTGAAGGTCGGAGTCA	AATGAAGGGGTCATTGATGG
SOX2	GAGAGTGTTTGCAAAAGGGG	TGGGGCTCAAACTTCTTCTC
SOX2 (2)	CCACCTACAGCATGTCCTACTCG	GGGAGGAAGAGGTAACCACAGG
OCT4	GCAGAAGAGGATCACCCTGG	AAAGCGGCAGATGGTCGTTT
OCT4 (2)	CTGCACAGATATGCAAAGCAG	TGATCTGCTGCAGTGTGGGT
NANOG	CTTGCCTTGCTTTGAAGCAT	TTCTTGAC**C**GGGACCTTGTC
NANOG (2)	ACCTCAGCTACAAACAGGT	AAAGGCTGGGGTAGGTAGGT
hTERT	CGGAAGAGTGTCTGGAGCAA	GGATGAAGCGGAGTCTGGA
hTERT splicing variant	GCC TGA GCT GTA CTT TGT CAA	CGC AAA CAG CTT GTTCTC CAT GTC
ERK1/2 (MAPK1)	GCTAGATTCCAGCCAGGATACA	AGAACACCGATGTCTGAGCA
AKT1	ATGAGCGACGTGGCTATTGT	CCTCACGTTGGTCCACATCC
CSHL1	CTGTGGACAGCTCACCTAGC	AGCCTGGATAAGGGAACGGT
SMAD2	GTGGCAGGCGGGTCTAC	GCAAGCCACGCTAGGAAAAC
SMAD8	GTGGCCAACCTGTAGATGCC	CTCCCCAACTCGGTTGTTCA
β-Catenin	GGAGGAAGGTCTGAGGAGCAG	ATTGTCCACGCTGGATTTTCAA
SMAD1/5/9	CAGAGTGGCCAACCTGTAGA	TCCCCAACTCGGTTGTTCAG

GAPDH glyceraldehyde 3-phosphate dehydrogenase, *SOX2* sex determining region Y-box 2, *OCT4* octamer-binding transcription factor 4, *hTERT* human telomerase reverse transcriptase, *ERK* extracellular signal-regulated kinase 2, also known as mitogen-activated protein kinase 1 (*MAPK1*), *AKT* protein kinase B, *CSHL* chorionic somatomammotropin hormone like 1, *SMAD*, mothers against decapentaplegic homolog

controls were either GAPDH (1:1000, sc-32233; Santa Cruz Biotechnology, USA) or β-Actin (1:5000, ab8227; Abcam, USA). Whole human embryonic stem cell lysate (ab27198; Abcam) was used as a positive control. Hela, NIH3T3, and Jurkat lysates were used as further controls.

Statistical analysis

Results express the mean ± SD. Data were obtained from at least three independent donors unless stated otherwise. Statistics as well as graphical representations were performed using GraphPad Prism™ 5.0 (GraphPad Software Inc., USA). Statistical significance of data results from one-way ANOVA followed by Tukey's post-hoc test (analysis of three or more groups). Differences were considered significant when $p < 0.05$.

Results

CV-MSC are highly proliferative and do not enter senescence during long-term in-vitro culture

Morphology and multilineage potential

We isolated a MSC population of fetal origin from CV tissue of the placenta using collagenase digestion (Fig. 1a i–v). The isolated CV-MSC were assessed for the absence of maternal cell contaminations at passages 3–4 (early) and 8–10 (late) using FISH X/Y chromosome analysis. The male newborn karyotype was confirmed for every CV-MSC donor used in the study by the presence of an X/Y chromosome pair (Fig. 1a iv–v). The amount of cells obtained after digestion of a maximized weight of 200 g (wet weight) CV tissue per placenta resulted in approximately $5.40 \times 10^6 \pm 6.00 \times 10^5$ cells. These cells were expanded to $8.05 \times 10^7 \pm 1.2 \times 10^6$ cells for the first passage and $1.50 \times 10^8 \pm 1.02 \times 10^7$ cells by the second passage. In the second passage, CV-MSC reached a cumulative cell number corresponding to the highest PD number (3.6 ± 0.7 PD). BM-MSC reached 2.6 ± 0.6 PD, AT-MSC reached 1.4 ± 1.1 PD, and UC-MSC reached 2.5 ± 0.3 PD (Fig. 2a).

The absence of ECM, endothelial cells, hematopoietic progenitors, or blood cells in the isolated CV-MSC was verified microscopically after the first passage (Fig. 1b). CV-MSC morphology did not vary with increasing passages (Fig. 1b i, iii, iv). However, the morphology differs from the typical spindle-shaped morphology of BM-MSC (Fig. 1b v, vi), UC-MSC, and AT-MSC (Additional file 1: Figure S1B i, ii), probably relating to a more heterogeneous cell population (Fig. 1b ii).

Multilineage differentiation potential of CV-MSC was confirmed as shown in Fig. 1c i–iii and no significant differences in the potential for osteogenic, chondrogenic, and adipogenic differentiation were observed between CV-MSC, BM-MSC, UC-MSC, and AT-MSC. The latter cell source showed increased adipose differentiation potential (Additional file 1: Figure S1B i–ix).

Long-term growth, proliferation potential, and senescence

Long-term cultures shown in Fig. 2a were monitored during 15 passages. While CV-MSC reached 8 ± 4

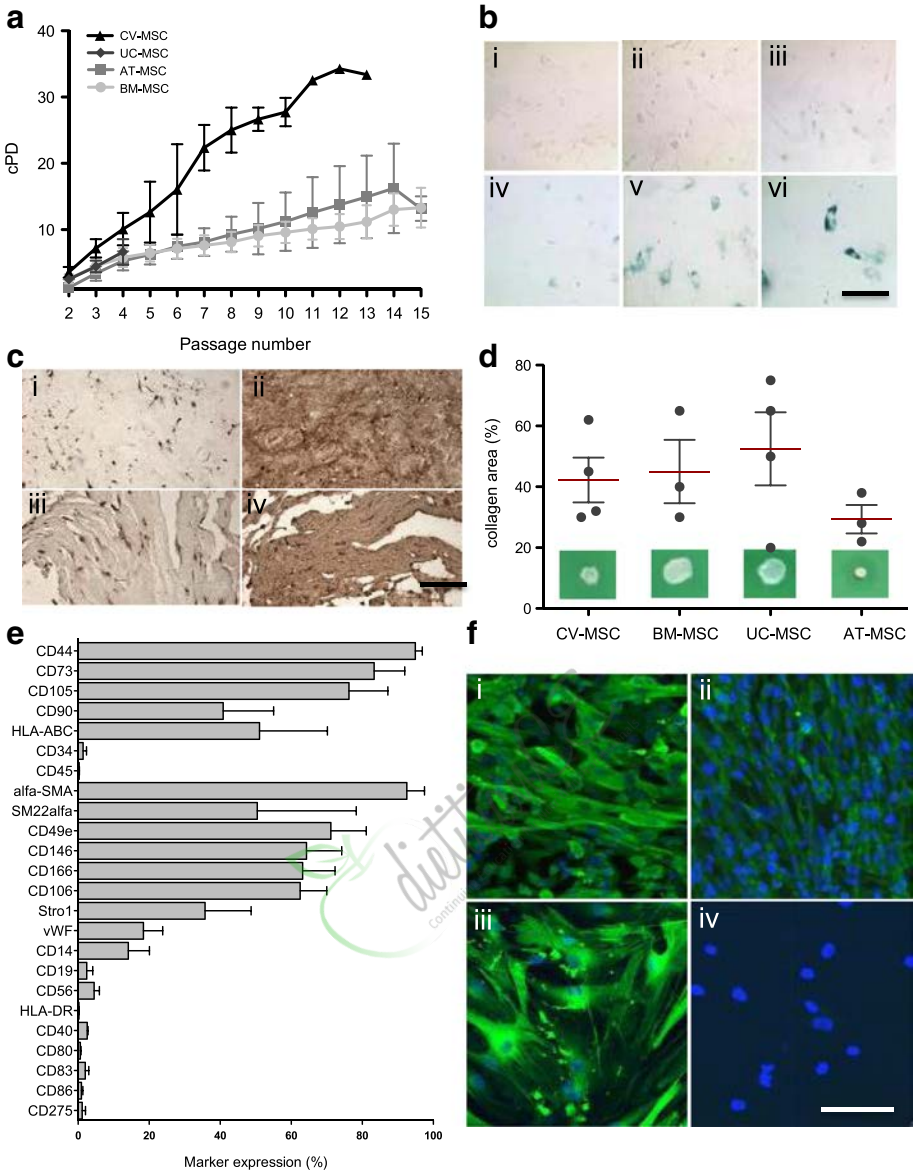

Fig. 2 **a** Cumulative population-doubling (cPD) levels versus passage number for the four different sources of MSC. Black represents CV-MSC ($n = 7$), dark gray UC-MSC ($n = 4$), medium gray AT-MSC ($n = 5$), and light gray BM-MSC ($n = 6$). **b** IHC-based senescence-associated β-galactosidase (SA-β-gal) staining of CV-MSC in early (i, passage 4) and late (ii, passage 9) passages, AT-MSC in passage 6 (iii), BM-MSC in passage 6 (iv), and UC-MSC in passage 2 (v) and passage 4 (vi). Scale = 200 μm. **c** IHC of CV-MSC (i, ii) and BM-MSC (iii, iv) stained for osteopontin (i, iii) and fibronectin (ii, iv). Scale = 1 mm. **d** Collagen area (%) after collagen contraction assay for CV-MSC ($n = 4$), BM-MSC ($n = 3$), UC-MSC ($n = 4$), and AT-MSC ($n = 3$). Cells in passage 3 were used. Results expressed as mean ± SD, percentage of the total collagen area of the collagen gels without cells. **e** Surface marker expression of CV-MSC in early passages ($n = 5$). Results expressed as mean ± SD (%). **f** Representative immunofluorescence of early passaged CV-MSC (i, iii) and BM-MSC (iii, iv) stained for SM22α (i, iii) and α-SMA (ii, iv). Scale = 50 μm. AT adipose tissue, BM bone marrow, CV chorionic villi, MSC mesenchymal stromal cells, UC umbilical cord

passages within 138 ± 64 days on average, corresponding to an average of 25 ± 3 cPD (Fig. 2a; $n = 7$; $p < 0.05$), BM-MSC reached on average 12 ± 6 passages within 329 ± 144 days, corresponding to an average of 10 ± 2 cPD ($n = 6$; $p < 0.05$). AT-MSC donors reached passage 12 approximately within 177 days, corresponding to an average number of 13 ± 5 cPD ($n = 5$), and could be expanded up to 32 passages, corresponding to an average period of 383 ± 10 days in culture and more than 30 cPD (not shown) until the cultures were intentionally stopped. UC-MSC could not be viably maintained for more than four passages (average 4 ± 2 passages; $n = 4$), corresponding to an average period of 78 ± 5 days in culture and an average of 7 ± 1 cPD. When we compare all sources after only four

passages, CV-MSC, BM-MSC, UC-MSC, and AT-MSC reached 10 ± 2 cPD, 6 ± 1 cPD, 7 ± 1 cPD, and 5 ± 1 cPD, respectively (Fig. 2a). After 12 passages the differences are dramatic, with CV-MSC having reached 34 ± 3 cPD, BM-MSC reaching 11 ± 2 cPD, and AT-MSC 13 ± 5 cPD (Fig. 2a). The higher proliferation ability of CV-MSC compared to all other cell sources was substantiated by a 7-day in-vitro cell viability assay showing that CV-MSC grow 2.85 ± 0.55 times faster than BM-MSC ($p = 0.02$) (Additional file 2: Figure S2A).

We next looked for β-gal-positive senescent cells in early and middle-to-late passages of CV-MSC and observed only marginal cell senescence from passage 3 until passage 9 (β-gal-positive cells = 7.7 ± 1.5% at passage 9; Fig. 2b, Additional file 2: Figure S2B). BM-MSC and AT-MSC showed the first signs of senescence in passage 6 (Fig. 2b), while UC-MSC reached senescence much earlier during culture, starting at passage 2 (β-gal-positive cells = 17.7 ± 2.4% at passage 4; Fig. 2b, Additional file 2: Figure S2B).

CV-MSC are heterogeneous populations demonstrating a typical MSC phenotype and remodeling potential

Matrix remodeling and immunophenotype

Next we assessed ECM remodeling ability by culturing the cells for 28 days using our collagen-based system described previously [40, 41]. CV-MSC showed equivalent ability to BM-MSC to spontaneously produce OPN and FN, two main ECM remodeling proteins, in long-term in-vitro cultures (Fig. 2c). The degree of ECM production of MSC from different sources in vitro was next quantified using the collagen contraction assay (Fig. 2d; Additional file 2: Figure S2C). Evaluation of collagen areas after contraction confirmed that CV-MSC (42.5 ± 7.4%, $n = 4$) and BM-MSC (45.0 ± 10.4%, $n = 3$) have similar remodeling potential. Weaker contraction was obtained by UC-MSC (52.50 ± 12.0%, $n = 4$) and stronger contraction by AT-MSC (29.3 ± 9.6%, $n = 3$), compared to CV-MSC.

Immunophenotypic characterizations of CV-MSC in past studies were inconsistent. We applied a wide panel of markers associated not only with MSC of BM origin but also human AT, endothelial cells, smooth muscle cells (SMC), hematopoietic cells, and pericytes to fully characterize MSC from different origins. Our flow cytometry data (Fig. 2e; Table 1) show that CV-MSC: express phenotypic markers that fit the panel defined by the International Society for Cellular Therapy (ISCT) to define human multipotent mesenchymal stromal/stem cells [48] expressing CD44, CD73, CD105, CD90, and HLA-ABC and lacking expression of CD45, CD34, CD19, and HLA-DR surface molecules; possess the non-immunogenic character of MSC by lacking expression of the immune markers CD14, CD56, CD80, CD83, CD86, CD40, and CD275 (B7-H2) [49]; show a vascular expression pattern by strongly expressing STRO-1 and CD146, which are markers for vascular niches [50]; and are prone to SMC lineage commitment by expressing high levels of α-SMA (92.5 ± 5.5%) and CD146 (64.3 ± 9.4%). SM22α was positive (approximately 50% expression) for all MSC sources (Table 3). Additionally, early myogenic markers were corroborated by immunofluorescence, which revealed positive α-SMA expression—associated with actin-positive stress fibers—and concurrent expression of SM22α in early-passage CV-MSC (Fig. 2f i, iii), consistent with increased CV-MSC potential for myogenic

Table 3 Immunophenotypic characterization of mesenchymal stromal cells

	CV-MSC (%)	BM-MSC (%)	UC-MSC (%)	AT-MSC (%)
CD44	94.9	97.4	93.3	93.9
CD73	83.4	74.2	82.2	96.4
CD105	76.3	95.7	66.3	94.0
CD90	40.8	81.0	85.8	96.9
HLA-ABC	51.1	81.0	81.9	81.0
CD34	1.4	0.5	1.5	2.5
CD45	0.3	0.2	3.4	0.1
α-SMA	92.5	18.4	9.8	27.5
SM22α	50.5	48.4	–	45.7
CD49a	71.2	91.2	52.7	–
CD146	64.3	18.8	52.1	63.1
CD166	63.2	73.1	53.6	85.2
CD106	62.5	68.0	61.2	4.3
Stro-1	44.0	9.8	2.6	2.3
vWF	18.4	12.5	6.3	6.2
CD14	14.1	2.0	1.1	0.1
CD19	2.4	0.5	0.3	–
CD56	4.5	3.5	2.8	2.0
HLA-DR	0.3	0.2	0.2	0.2
CD40	2.6	2.8	1.6	–
CD80	0.6	0.4	0.7	–
CD83	2.0	3.0	2.6	–
CD86	0.9	0.3	0.2	–
CD275	1.1	0.2	0.1	–
CD16	–	–	–	5.6
CD31	–	–	–	0.1
CD49d	–	–	–	42.2
CD13	–	–	–	75.2
CD29	–	–	–	98.2

Results expressed as mean percentage of marker expression. CV-MSC of passages 3–5 ($n = 5$), BM-MSC of passages 2–3 ($n = 4$), UC-MSC of passage 2 ($n = 4$), AT-MSC of passages 2–4 ($n = 8$)

AT adipose tissue, *BM* bone marrow, *CV* chorionic villi, *MSC* mesenchymal stromal cells, *UC* umbilical cord

lineage commitment compared to BM-MSC. The late myogenic markers SM-MHC and Calponin were absent both in CV-MSC and BM-MSC (data not shown). In contrast, BM-MSC expressed only marginal STRO-1 and CD146 expression, and showed low expression of SMC markers (α-SMA$^+$ 18.4 ± 2.8%; Fig. 2f ii, iv; Table 3).

As in other studies, the possibility of the presence of a subpopulation of pericyte-like cells or pericytes within the isolated and further cultured CV-MSC is strong in our study. This is because cultured CV-MSC have shown increased combined expression of CD146 and Stro-1 compared to the other cell sources (Table 3). However, the combined expressed markers alone do not prove the presence of pericytes.

CD49e (71.20 ± 11.7%), CD166 (62.30 ± 8.0%), and CD106 (62.5 ± 5.0%) were strongly expressed in CV-MSC, which is in line with previous studies [2, 4, 18, 49–51]. No difference was found among the expression of these three markers on cells from the different sources.

CV-MSC undergo reduced telomere loss delaying aging with increasing passages

Telomere length and methylation status

In order to understand whether the increased proliferative potential observed in CV-MSC is being recapitulated by altered telomere maintenance, we sequentially analyzed telomere length. The most dramatic telomere loss was observed in UC-MSC (–6.00 ± 0.61 a.u.; $n = 4$; two passages analyzed) (Fig. 3a, b). This was particularly dramatic, as UC-MSC could not be maintained in culture for more than four passages. As the cells aged in culture, CV-MSC suffered the least pronounced telomere loss per passage (–0.59 ± 1.055 a.u.; $n = 4$; five passages analyzed) (Fig. 3a, b). In fact, multiple intense fluorescent telomeric signals within the CV-MSC could be observed by the naked eye in early and late passages under LSCM (Fig. 3a i–iv), in contrast to all other MSC sources (Fig. 3a v–xvi). AT-MSC suffered the second least pronounced telomere loss (–1.74 ± 1.13 a.u.; n = 3; six passages analyzed), while BM-MSC suffered the third least pronounced telomere loss (–3.32 ± 0.84 a.u.; n = 2; five passages analyzed).

Next we applied the EAS as an attempt to understand whether or not the predicted aging at the telomere level will match predicted aging at the methylation level. Results showed that all cell sources were predicted to be of a far different age than their chronological age, with differences ranging from ca. 16 to 38 years either older or younger (Additional file 3: Figure S3A–C). Age predictions according to DNAm changes seem to be particularly inaccurate in the case of CV-MSC both in early and in late passages (Additional file 3: Figure S3B, C, respectively). Interestingly the predictions seem to corroborate—at least in part—the predictions based on telomere data. Predicted age in CV-MSC rapidly decreased with progressive in-vitro passaging (Additional file 3: Figure S3A), suggesting a delayed aging phenomenon already observed at the telomere level. In opposition, predicted age of all other MSC types stabilized or increased with increasing passages (Additional file 3: Figure S3A). This is in line with the establishment of an aging phenotype characterized by telomere shortening, decreased proliferation, and senescence onset.

CV-MSC express no full hTERT or shorter splicing variants

hTERT

To understand whether hTERT is the reason for the good maintenance of telomere length in late-passage CV-MSC we investigated hTERT mRNA expression. No detectable hTERT mRNA was observed in CV-MSC at passage 2 or later (Fig. 4a, b). No shorter hTERT splicing variants were detected either (Fig. 4c). At the protein level we found no indications for the production of hTERT protein in passage 4 CV-MSC using either a full-length peptide hTERT antibody (western blot analysis) or a peptide selected form the center region of hTERT (immunofluorescence) (Figure 4d i, ii, e).

CV-MSC express SOX2 but no other pluripotency markers

Pluripotency markers

Pluripotency of CV-MSC has been claimed by different groups [7–9]. In order to assess pluripotency of CV-MSC we first analyzed the expression of three genes, *NANOG*, *OCT4* variant 1 (POU5F1), and *SOX2*, associated with pluripotency and typically present in ESC. Analysis of mRNA expression of CV-MSC in passage 2 revealed a weak detectable expression of *SOX2* (0.14 ± 0.11-fold change; $n = 4$) but no expression of *OCT4* or *NANOG* (data not shown). On the protein level, we observed that CV-MSC maintained SOX2 protein expression throughout passaging (at least until passage 10; Fig. 4e), but no OCT4 isoform 1 or NANOG protein was detected (Additional file 4: Figure S4B).

Last we applied the soft agar assay in order to assess tumorigenicity in vitro, and observed no evidence for this as CV-MSC yield no tumoroids after 4 weeks in soft agar cultures (Fig. 4f).

To uncover any clue on whether there is evidence of pluripotency in CV-MSC, we looked into several signaling pathways typically involved in ESC pluripotency and self-renewal. While mRNA and protein profiles of CV-MSC were investigated extensively, no difference was observed in *Erk1/2*, *Akt1*, *Smad2*, *Smad9*, *β-Catenin*, *Smad1/5/9*, and *CSHL* gene expression between CV-MSC and BM-MSC (Additional file 4: Figure S4C). Western blot analysis confirmed gene expression results (Additional file 4: Figure S4D, E).

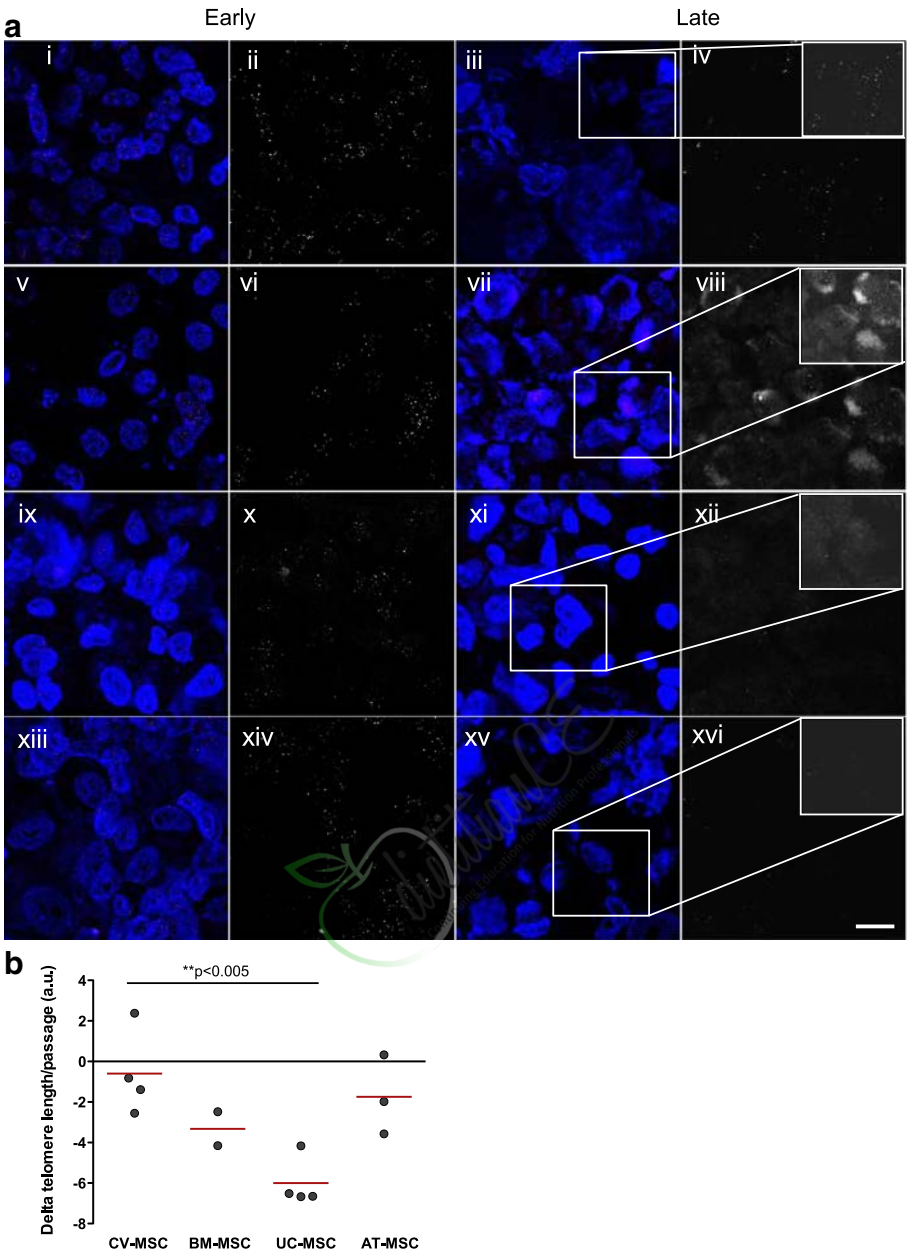

Fig. 3 a Confocal microscopy of early and late-passage CV-MSC (i–iv), BM-MSC (v–viii), AT-MSC (ix–xii), and UC-MSC (xiii–xvi) analyzed by Q-FISH. Telomeres were stained with Tel-Cy3 peptide nucleic acid probe and chromatin was stained with DAPI (overlaid image on left). Telomere signal alone (black and white image on right) shown to improve visual comparability. Shown side by side are on the left MSC in passage 3 (i, ii, v, vi, ix, x) and on the right MSC in passage 9 (iii, iv, vii, viii, xi, xii), except for UC-MSC that were on the left in passage 1 (xiii, xiv) and on the right in passage 3 (xv, xvi). Scale = 10 μm. **b** Telomere loss (Δtel) per passage (in arbitrary units (a.u.)) according to Q-FISH. CV-MSC ($n = 4$), BM-MSC ($n = 2$), UC-MSC ($n = 4$), AT-MSC ($n = 3$) (**$p < 0.005$). AT adipose tissue, BM bone marrow, CV chorionic villi, MSC mesenchymal stromal cells, UC umbilical cord

Discussion

We have successfully isolated a highly proliferative MSC population from CV of postnatal placenta while optimizing our protocols to maximize cell yield from extraction (approximately 2.7×10^7 cells/kg wet weight of CV) and after a few weeks of in-vitro culture (approximately 7.5×10^9 cells/kg wet weight of CV, after 3.6 ± 0.3 cPD). We kept CV-MSC in culture for an extended period (138 ± 64 days, corresponding to 25 ± 3 cPD) and observed delayed onset of the earlier stages of cell senescence compared to BM-MSC. In line with Barlow et al. [23], we observed that CV-MSC proliferate faster and show greater long-term growth ability than BM-MSC.

Collagenase digestion was used for cell isolation in our study so associated costs must not be overlooked as they certainly rise above those of the concurrent explant

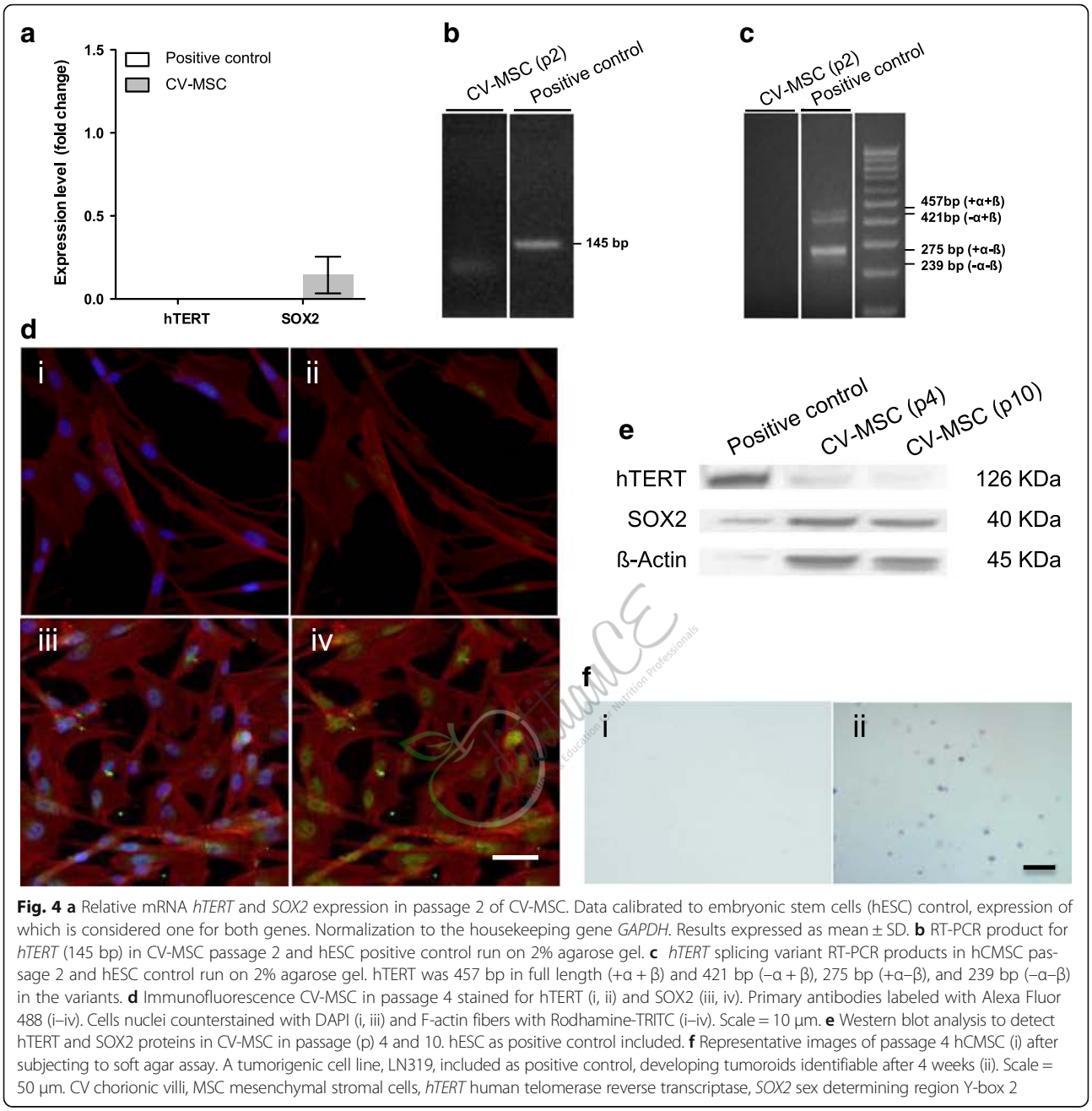

Fig. 4 a Relative mRNA *hTERT* and *SOX2* expression in passage 2 of CV-MSC. Data calibrated to embryonic stem cells (hESC) control, expression of which is considered one for both genes. Normalization to the housekeeping gene *GAPDH*. Results expressed as mean ± SD. **b** RT-PCR product for *hTERT* (145 bp) in CV-MSC passage 2 and hESC positive control run on 2% agarose gel. **c** *hTERT* splicing variant RT-PCR products in hCMSC passage 2 and hESC control run on 2% agarose gel. hTERT was 457 bp in full length (+α + β) and 421 bp (–α + β), 275 bp (+α–β), and 239 bp (–α–β) in the variants. **d** Immunofluorescence CV-MSC in passage 4 stained for hTERT (i, ii) and SOX2 (iii, iv). Primary antibodies labeled with Alexa Fluor 488 (i–iv). Cells nuclei counterstained with DAPI (i, iii) and F-actin fibers with Rodhamine-TRITC (i–iv). Scale = 10 μm. **e** Western blot analysis to detect hTERT and SOX2 proteins in CV-MSC in passage (p) 4 and 10. hESC as positive control included. **f** Representative images of passage 4 hCMSC (i) after subjecting to soft agar assay. A tumorigenic cell line, LN319, included as positive control, developing tumoroids identifiable after 4 weeks (ii). Scale = 50 μm. CV chorionic villi, MSC mesenchymal stromal cells, *hTERT* human telomerase reverse transcriptase, *SOX2* sex determining region Y-box 2

method when digesting maximized volumes of placenta tissue is a priority. However, collagenase digestion has the advantage of allowing for higher final cell yields in a short period of time. Adapted or alternative methods for isolation of placental MSC of fetal origin have been proposed [52, 53]. The preferred isolation method and in-vitro culture conditions must be assessed according to the specific requirements of each given stem cell application.

We have extensively characterized the CV-MSC cultured fraction in early and late passages. It is obvious that CV-MSC fit all MSC defining criteria [48], as reported previously [3, 50, 51, 54], including being able to differentiate into osteoblasts, adipocytes, and chondrocytes cultured in vitro in standard differentiation cocktails. We also observed that CV-MSC present a surface marker profile consistent with increased potential for proliferation (high CD44, CD73, and CD166 combined expression), vascular localization (high STRO-1, CD146, and CD106 combined expression), and predisposition for myogenic commitment (high α-SMA, SM22α, and CD146 combined expression), unlike BM-MSC. It has been introduced that combined CD146 expression and a high α-SMA expression is associated with

SMC commitment in BM-MSC [55]. Myogenic expression of CV-MSC, however, remains another topic of debate, as some studies report residual expression of α-SMA in MSC isolated from placenta tissues [56, 57] while others, such as Castrechini et al. [50], report high expression but just in CV-MSC isolated from first-trimester pregnancies.

Numerous studies report that CV-MSC isolated by collagenase digestion are prone to contamination by maternal cells, which rapidly and completely overgrow CV-MSC within one or two passages [23, 58, 59]. To address this issue we have excluded by FISH X/Y chromosome analysis the presence of maternal contamination in late-passage CV-MSC.

An often overlooked contributor to an even more complete phenotypic characterization is trophoblastic contamination in the cultures. Trophoblastic cells are the cells forming the outer layer of the blastocyst that provide nutrients to the embryo. This layer later develops into a large part of the placenta and so trophoblast-derived cells make up the majority of the chorion in the developed placenta. To determine cytotrophoblastic cells (eventually the most frequent trophoblastic cell type) in vitro, markers such as human chorionic gonadotropin, pan-cytokeratin, epidermal growth factor receptor HER2, and E-Cadherin could be investigated. Despite the controversy, most indications for trophoblastic contaminations are unlikely [20, 50].

In terms of ECM remodeling potential, CV-MSC showed the ability to produce matrix proteins (namely FN and OPN) and contract a collagen matrix in vitro similar to BM-MSC, confirming CV-MSC suitability for major stem cell-based applications.

To understand whether the observed increased potential of CV-MSC to proliferate correlated with increased telomere length, we analyzed the telomeres, repeated TTAGGG sequences at the ends of chromosomes that protect them from deterioration or fusion. Telomeres undergo progressive shortening with each cell division. Progressive telomere shortening is therefore one of the molecular mechanisms underlying aging, as critically short telomeres trigger cellular senescence and loss of cell viability [60–62]. Thus, telomere length is known to decline during in-vitro and in-vivo aging. Our results showed that CV-MSC undergo minimal telomere loss as they age in vitro compared to all other MSC sources. In contrast, UC-MSC underwent dramatic telomere loss within the very few passages we were able to keep them in vitro. At the same time we observed that UC-MSC become quickly senescent (i.e., in early passages) in β-galactosidase senescence assays. Interestingly, CV-MSC escaped in-vitro senescence—showing reduced β-galactosidase-positive cell rates—for more passages than all the other cells types due to increased potential to maintain telomere length while proliferating. The increased potential of CV-MSC to maintain telomere length over the other tissue sources reflects not only different rates of telomere loss within those tissues, but also different telomere loss rates during in-vitro passaging, potentially due to oxidative stress. Given that both CV-MSC and UC-MSC originate from postnatal tissues with virtually equivalent chronological age but dramatically different telomere length maintenance potentials, it is not clear to us why telomere erosion during in-vitro culture was so dramatic in UC-MSC. It can be related to donor variability, differential telomerase activity expression, or alternative mechanisms of telomere maintenance, as discussed later.

DNAm is known to change during aging. However, some CpG sites show almost linear changes during aging and so can be used for age prediction. Weidner et al. [45] have established an EAS to predict aging with higher precision than telomere length alone. EAS revealed predicted age in CV-MSC decreased rapidly with progressive passaging, confirming delayed aging phenomena. It is worth mentioning that our results were apparently limited by the fact that the signature was designed for age estimations from blood samples and does not seem to suit cultured cells. This leads us to a discussion based on the analysis of linear regression fits and not on absolute predictions (which fall out of the acceptable chronological age range).

hTERT is a catalytic subunit of the enzyme telomerase, which together with the telomerase RNA component (*hTERC*) comprises the most important unit of the telomerase complex. *hTERC* acts as a template for the addition of telomere units by *hTERT*. *hTERT* is expressed during early development but is absent in most somatic cells, with the exception of proliferating cells and renewal tissues [63]. In highly proliferative cells of the germline, in ESC, and in the majority of cancer cells, telomerase (by adding telomeric repeats onto the chromosome ends) prevents the replication-dependent loss of telomeres and cellular senescence [61]. The causal relationship between expression of telomerase, maintenance of telomere length, and elongated life span of the human cell has been established. We have confirmed the absence of *hTERT* mRNA in CV-MSC. *hTERT* gene expression typically corresponds to telomerase activity in many multicellular organisms. This can be untrue in some cases. Izadpanag et al., Yanada et al., Zimmermann et al., and Hiyama and Hiyama [64–67] reported that low levels of telomerase activity were found in MSC. Contradictory studies report no telomerase activity in MSC [68]. Therefore, a mechanism other than or in addition to telomerase—such as alternative lengthening of telomeres (ALT)—might play an important role in CV-MSC telomere maintenance. There are, for instance, hints

from work done on subtelomeric DNA hypomethylation facilitating telomere elongation in mammalian cells suggesting that epigenetic modifications of chromatin might occur in MSC [69]. Work done in whole chorion tissues indicates a downregulation of telomerase activity over the gestation, also supporting the idea of a decline of primitive stem cell features with aging [70]. In order to clarify the origin of our telomere observations, investigating telomerase activity levels and ALT mechanisms in CV-MSC would thus be an interesting outlook.

Previous studies using equivalent methods for isolation of CV-MSC [7–9] report the presence of panels of pluripotent markers such as *NANOG*, *OCT4*, and *SOX2* in those cells. Studies typically focus on gene expression level observations only and often PCR primer sequences or expression data are omitted. Without further concerns, some conclude that CV-MSC retain characteristics of pluripotent stem cells.

We have designed qRT-PCR primers binding to the DNA region encoding for the highly conserved AFMVW helix inside the HMG domain of the SOX2 protein. Additionally, we used *SOX2* primers to bind the DNA region encoding for the C-terminal domain of the SOX2 region, equivalent to what was done in other studies [71, 72]. Our data show that CV-MSC express SOX2 on both the gene and protein levels, an indication of improved neurogenic potential in the light of current knowledge. *SOX2*, a pluripotency marker, is also known to regulate FGF4 expression, which in turn promotes neural stem cell proliferation and differentiation in the postnatal brain [73]. The improved neurogenic potential of CV-MSC compared to BM-MSC has in fact been demonstrated [18, 20].

We did not detect the presence of *OCT4* variant 1 or *NANOG* in CV-MSC. Our data are partially supported by previous work from Jones et al. [72], who compared first-trimester to term fetal placental chorionic stem cells. They observed no detectable *OCT4A* variant 1 in the term fetal cells at the transcript level using primer pairs binding only to a larger DNA fragment within the same region as ours. Based on the absolute expression of *NANOG* reported in that work, and given the fact that one of the two primer pairs we used was equivalent to theirs, we consider the possibility of marginal but non-detectable expression of *NANOG* in our cells due to donor variability.

We nonetheless commit to exclude the possibility of pluripotency in CV-MSC given the corroborated absence of *OCT4A* variant 1. *OCT4* and *SOX2* were identified as the fundamental transcriptor factors underpinning naïve pluripotency [74], although the critical role of SOX2 might be to activate *OCT4* [75, 76]. *NANOG* becomes part of the *OCT4/SOS2/NANOG* (OSN) triumvirate as its presence is crucial for the acquisition but not the maintenance of naive pluripotency [77, 78].

One other indisputable feature of pluripotent stem cells is the formation of teratomas in vivo. We applied the equivalent in-vitro assay, designed to assess the tumorigenic potential of cells in culture—the soft agar assay—and found no evidence for malignant transformation of CV-MSC, as suggested previously [16, 79].

In human ESC the predominant signaling pathways involved in pluripotency and self-renewal [80] are TGF-β (signaling through SMAD2/3/4, activating the MAPK and AKT pathways) and the noncanonical WNT pathway (β-CATENIN signaling). Pluripotency signaling through these pathways relies predominantly upon the key transcription factors *OCT4*, *SOX2*, and *NANOG*. When NANOG is inhibited, differentiation takes place via the BMP pathway (Smad1/5/9 signaling) and NOTCH intracellular domain (NICD, CSHL1). After investigating multiple pathways we found no evidence of any pathways being differentially activated/deactivated leading to pluripotency of CV-MSC.

Placental-derived MSC have been reported to be capable of neural, retinal cell, pancreatic progenitor cell, and hepatic cell differentiation [8, 81], an indication for greater plasticity. We have no evidence, however, to support the notion that a putative pluripotent stem cell population is present within CV-MSC or that CV-MSC are less differentiated than BM-MSC.

Conclusions

In our comprehensive characterization study of CV-MSC, we show that CV-MSC hold great promise for tissue engineering applications. CV-MSC are nonimmunogenic, have multilineage differentiation potential, hold increased proliferation ability, and display a retarding aging phenotype. Our data suggest that the exceptional proliferation of CV-MSC ability might be linked with telomere length control mechanisms.

Additional files

Additional file 1: Figure S1. A Bright-field microscopy images of cultured UC-MSC in passage 3 (i) and AT-MSC in passage 24 (ii). Scale = 500 μm. **B** Visualization of calcium deposits after Alizarin Red stain (i–iii, scale = 500 μm), proteogyclans after Toluin Blue stain (iv–vi, scale = 1 mm), and lipid droplets after Oil Red O stain (vii–ix, scale = 100 μm) of differentiated AT-MSC (i, iv, vii), BM-MSC (ii, v, viii), and UC-MSC (iii, vi, ix) all in passage 3. (JPG 86 kb)

Additional file 2: Figure S2. A Viability of hMSC of all sources during a 7-day follow-up period during early passages (passages 3–5) in culture (results expressed as arbitrary units of normalized fluorescence). Black depicts CV-MSC ($n = 3$), dark gray UC-MSC ($n = 3$), medium gray AT-MSC ($n = 3$), and light gray BM-MSC ($n = 3$). **B** Histograms for CV-MSC in passage 9 ($n = 3$) and UC-MSC in passage 4 ($n = 3$) stained for β-galactosidase assessed by flow cytometry. **C** Visualization of collagen contraction potential by CV-MSC (i), BM-MSC (ii), UC-MSC (iii), and AT-MSC (iv). All donors shown. Scale = 1 cm. **D** Immunofluorescence of early passaged BM-MSC (i, iv), UC-MSC (ii–v), and AT-MSC (iii, vi) stained for SM22α (i–iii) and α-SMA (iv–vi). Scale = 50 μm. All conditions $n \geq 3$. (JPG 63 kb)

Additional file 3: Figure S3. A Difference between predicted and chronological MSC donor age (years) after EAS: CV-MSC 37.75 ± 5.43 years ($n = 4$), BM-MSC −16.00 ± 10.06 years ($n = 4$), UC-MSC 25.50 ± 1.84 years ($n = 4$), AT-MSC 17.00 ± 5.00 ($n = 2$), from passage 2 to passage 5 (**$p < 0.005$). **B** Difference between predicted and chronological MSC donor age (years) after EAS: CV-MSC 29.25 ± 4.46 years ($n = 4$), BM-MSC −26.40 ± 10.52 years ($n = 5$), AT-MSC 32.80 ± 9.65 ($n = 5$), from passage 6 to passage 15 (**$p < 0.005$). It was not possible to keep UC-MSC until late passages. **C** Predicted age (years) versus passage number EAS: one representative donor shown for CV-MSC (black), UC-MSC (dark gray), AT-MSC (medium gray), and BM-MSC (light gray). (JPG 33 kb)

Additional file 4: Figure S4. A Immunofluorescence CV-MSC in passage 5 stained for Oct3/4 (i) and Nanog (ii). Alexa Fluor-488 (Green) was used to label the primary antibodies (i–iv). Rhodamine-TRITC was used for F-Actin fiber labeling (i–iv) and DAPI for nuclei counterstain (i, iii). Scale = 10 μm. **B** Western blot analysis for detection of Oct3/4 and Nanog proteins in passage 4 and passage 10 CV-MSC. hESC are positive control. **C** Relative *ERK1/2*, *AKT1*, *CSHL1*, *SMAD2*, *SMAD9*, *β-CATENIN*, and *SMAD1/5/9* gene expression in CV-MSC in passage 4 and BM-MSC in passage 3. Data calibrated to positive control, expression of which is considered one for both genes. Housekeeping gene *GAPDH* used for normalization. **D, E** Western blot analysis to detect Erk1/2, pErk1/2, β-Catenin, Smad2/3, pSmad2/3, NICD, Akt1/2, pAkt, Smad1/5/9, and pSmad1/5 proteins in CV-MSC and BM-MSC. hESC, Hela, NIH3T3, and Jurkat controls included. (JPG 71 kb)

Abbreviations

AKT: Protein kinase B; ALT: Alternative lengthening of telomeres; AT: Adipose tissue; BCA: Bicinchoninic acid; bFGF: Basic fibroblast growth factor; BM: Bone marrow; cDNA: Complementary deoxyribonucleic acid; CSHL: Chorionic somatomammotropin hormone Like 1; CV: Chorionic villi; DAPI: 4′,6-Diamidino-2-phenylindole; DMEM: Dulbecco's modified Eagle's medium; DNAm: deoxyribonucleic acid methylation; EAS: Epigenetic signature; EDTA: Ethylenediaminetetraacetic acid; ERK: Extracellular signal-regulated kinase 2 (also known as MAPK1); ESC: Embryonic stem cells; F12: Nutrient mixture F-12; FISH: Fluorescent in-situ hybridization; FN: Fibronectin; GAPDH: Glyceraldehyde 3-phosphate dehydrogenase; gDNA: Genomic deoxyribonucleic acid; HER2: Epidermal growth factor receptor; HLA-ABC: Human leukocyte antigen, major histocompatibility complex, class I, A, B, C; HRP: Horseradish peroxidase; hTERC: Human telomerase RNA component; hTERT: Human telomerase reverse transcriptase; IHC: Immunohistochemistry; ISCT: International Society for Cellular Therapy; MAPK1: Mitogen-activated protein kinase 1 (also known as ERK); mRNA: Messenger ribonucleic acid; MSC: Mesenchymal stromal cells; NICD: Notch intracellular domain; OCT4: Octamer-binding transcription factor 4; OPN: Osteopontin; PBS: Phosphate-buffered saline; PD: Population doubling; PFA: Paraformaldehyde; PNA: Peptide nucleic acid; Q-FISH: Quantitative fluorescent in-situ hybridization; qRT-PCR: Quantitative real-time polymerase chain reaction; RIPA: Radioimmunoprecipitation assay; RNA: Ribonucleic acid; RT: Room temperature; SA-β-gal: Senescence-associated β-galactosidade; SM22α: Smooth muscle protein 22 alfa (transgelin); SMAD: Mothers against decapentaplegic homolog; SMC: Smooth muscle cells; SM-MHC: Smooth muscle myosin heavy chain; SOX2: sex determining region Y-box 2 (also known as SRY); TGF: Transforming growth factor; UC: Umbilical cord; α-SMA: Alpha smooth muscle actin

Competing interests

The authors declare that they have no competing interests.

References

1. Fukuchi Y, Nakajima H, Sugiyama D, Hirose I, Kitamura T, Tsuji K. Human placenta-derived cells have mesenchymal stem/progenitor cell potential. Stem Cells. 2004;22(5):649–58.
2. In 't Anker PS, Scherjon SA, Kleijburg-van der Keur C, de Groot-Swings GM, Claas FH, Fibbe WE, Kanhai HH. Isolation of mesenchymal stem cells of fetal or maternal origin from human placenta. Stem Cells. 2004;22(7):1338–45.
3. Igura K, Zhang X, Takahashi K, Mitsuru A, Yamaguchi S, Takashi TA. Isolation and characterization of mesenchymal progenitor cells from chorionic villi of human placenta. Cytotherapy. 2004;6(6):543–53.
4. Parolini O, Alviano F, Bagnara GP, Bilic G, Buhring HJ, Evangelista M, Hennerbichler S, Liu B, Magatti M, Mao N, Miki T, Marongiu F, Nakajima H, Nikaido T, et al. Concise review: isolation and characterization of cells from human term placenta: outcome of the first international workshop on placenta derived stem cells. Stem Cells. 2008;26(2):300–11.
5. Oliveira MS, Barreto-Filho JB. Placental-derived stem cells: culture, differentiation and challenges. World J Stem Cells. 2015;7(4):769–75.
6. Li X, Bai J, Ji X, Li R, Xuan Y, Wang Y. Comprehensive characterization of four different populations of human mesenchymal stem cells as regards their immune properties, proliferation and differentiation. Int J Mol Med. 2014;34(3):695–704.
7. Shaer A, Azarpira N, Aghdaie MH, Esfandiari E. Isolation and characterization of human mesenchymal stromal cells derived from placental decidua basalis; umbilical cord Wharton's jelly and amniotic membrane. Pakistan J Med Sci. 2014;30(5):1022–6.
8. Sabapathy V, Ravi S, Srivastava V, Srivastava A, Kumar S. Long-term cultured human term placenta-derived mesenchymal stem cells of maternal origin displays plasticity. Stem Cells Int. 2012;2012:174328.

9. Koo BK, Park IY, Kim J, Kim JH, Kwon A, Kim M, Kim Y, Shin JC, Kim JH. Isolation and characterization of chorionic mesenchymal stromal cells from human full term placenta. J Korean Med Sci. 2012;27(8):857–63.
10. Vellasamy S, Sandrasaigaran P, Vidyadaran S, George E, Ramasamy R. Isolation and characterisation of mesenchymal stem cells derived from human placenta tissue. World J Stem Cells. 2012;4(6):53–61.
11. Rus Ciuca D, Soritau O, Susman S, Pop VI, Mihu CM. Isolation and characterization of chorionic mesenchyal stem cells from the placenta. Rom J Morphol Embryol. 2011;52(3):803–8.
12. Kanematsu D, Shofuda T, Yamamoto A, Ban C, Ueda T, Yamasaki M, Kanemura Y. Isolation and cellular properties of mesenchymal cells derived from the decidua of human term placenta. Differentiation. 2011;82(2):77–88.
13. Li X, Ling W, Pennisi A, Wang Y, Khan S, Heidaran M, Pal A, Zhang X, He S, Zeitlin A, Abbot S, Faleck H, Hariri R, Shaughnessy Jr JD, et al. Human placenta-derived adherent cells prevent bone loss, stimulate bone formation, and suppress growth of multiple myeloma in bone. Stem Cells. 2011;29(2):263–73.
14. Mihu CM, Rus Ciuca D, Soritau O, Susman S, Mihu D. Isolation and characterization of mesenchymal stem cells from the amniotic membrane. Rom J Morphol Embryol. 2009;50(1):73–7.
15. Huang YC, Yang ZM, Chen XH, Tan MY, Wang J, Li XQ, Xie HQ, Deng L. Isolation of mesenchymal stem cells from human placental decidua basalis and resistance to hypoxia and serum deprivation. Stem Cell Rev. 2009;5(3): 247–55.
16. Shin KS, Na KH, Lee HJ, Kim DG, Shin SJ, Kim JK, Kim GJ. Characterization of fetal tissue-derived mesenchymal stem cells. Int J Stem Cells. 2009;2(1):51–8.
17. Soncini M, Vertua E, Gibelli L, Zorzi F, Denegri M, Albertini A, Wengler GS, Parolini O. Isolation and characterization of mesenchymal cells from human fetal membranes. J Tissue Eng Regen Med. 2007;1(4):296–305.
18. Portmann-Lanz CB, Schoeberlein A, Huber A, Sager R, Malek A, Holzgreve W, Surbek DV. Placental mesenchymal stem cells as potential autologous graft for pre- and perinatal neuroregeneration. Am J Obstet Gynecol. 2006;194(3):664–73.
19. Battula VL, Bareiss PM, Treml S, Conrad S, Albert I, Hojak S, Abele H, Schewe B, Just L, Skutella T, Buhring HJ. Human placenta and bone marrow derived MSC cultured in serum-free, b-FGF-containing medium express cell surface frizzled-9 and SSEA-4 and give rise to multilineage differentiation. Differentiation. 2007;75(4):279–91.
20. Yen BL, Huang HI, Chien CC, Jui HY, Ko BS, Yao M, Shun CT, Yen ML, Lee MC, Chen YC. Isolation of multipotent cells from human term placenta. Stem Cells. 2005;23(1):3–9.
21. Du WJ, Chi Y, Yang ZX, Li ZJ, Cui JJ, Song BQ, Li X, Yang SG, Han ZB, Han ZC. Heterogeneity of proangiogenic features in mesenchymal stem cells derived from bone marrow, adipose tissue, umbilical cord, and placenta. Stem Cell Res Ther. 2016;7(1):163.
22. Han ZC, Du WJ, Han ZB, Liang L. New insights into the heterogeneity and functional diversity of human mesenchymal stem cells. Biomed Mater Eng. 2017;28(s1):S29–45.
23. Barlow S, Brooke G, Chatterjee K, Price G, Pelekanos R, Rossetti T, Doody M, Venter D, Pain S, Gilshenan K, Atkinson K. Comparison of human placenta- and bone marrow-derived multipotent mesenchymal stem cells. Stem Cells Dev. 2008;17(6):1095–107.
24. Wang A, Brown EG, Lankford L, Keller BA, Pivetti CD, Sitkin NA, Beattie MS, Bresnahan JC, Farmer DL. Placental mesenchymal stromal cells rescue ambulation in ovine myelomeningocele. Stem Cells Transl Med. 2015;4(6):659–69.
25. Chen YJ, Chung K, Pivetti C, Lankford L, Kabagambe SK, Vanover M, Becker J, Lee C, Tsang J, Wang A, Farmer DL. Fetal surgical repair with placenta-derived mesenchymal stromal cell engineered patch in a rodent model of myelomeningocele. J Pediatr Surg; 2017. https://doi.org/10.1016/j.jpedsurg.2017.10.040, https://www.ncbi.nlm.nih.gov/pubmed/29096888.
26. Long C, Lankford L, Kumar P, Grahn R, Borjesson DL, Farmer D, Wang A. Isolation and characterization of canine placenta-derived mesenchymal stromal cells for the treatment of neurological disorders in dogs. Cytometry A; 2017. https://doi.org/10.1002/cyto.a.23171, https://www.ncbi.nlm.nih.gov/pubmed/28715613.
27. Lu Y, Gao H, Zhang M, Chen B, Yang H. Glial cell line-derived neurotrophic factor-transfected placenta-derived versus bone marrow-derived mesenchymal cells for treating spinal cord injury. Med Sci Monit. 2017;23: 1800–11.
28. Fan ZX, Lu Y, Deng L, Li XQ, Zhi W, Li-Ling J, Yang ZM, Xie HQ. Placenta-versus bone-marrow-derived mesenchymal cells for the repair of segmental bone defects in a rabbit model. FEBS J. 2012;279(13):2455–65.
29. Patel J, Shafiee A, Wang W, Fisk NM, Khosrotehrani K. Novel isolation strategy to deliver pure fetal-origin and maternal-origin mesenchymal stem cell (MSC) populations from human term placenta. Placenta. 2014;35(11):969–71.
30. Ilancheran S, Moodley Y, Manuelpillai U. Human fetal membranes: a source of stem cells for tissue regeneration and repair? Placenta. 2009;30(1):2–10.
31. Parolini O, Caruso M. Review: preclinical studies on placenta-derived cells and amniotic membrane: an update. Placenta. 2011;32 Suppl 2:S186–95.
32. Lankford L, Selby T, Becker J, Ryzhuk V, Long C, Farmer D, Wang A. Early gestation chorionic villi-derived stromal cells for fetal tissue engineering. World J Stem Cells. 2015;7(1):195–207.
33. Schmidt D, Mol A, Breymann C, Achermann J, Odermatt B, Gossi M, Neuenschwander S, Pretre R, Genoni M, Zund G, Hoerstrup SP. Living autologous heart valves engineered from human prenatally harvested progenitors. Circulation. 2006;114(1 Suppl):I125–31.
34. Pipino C, Shangaris P, Resca E, Zia S, Deprest J, Sebire NJ, David AL, Guillot PV, De Coppi P. Placenta as a reservoir of stem cells: an underutilized resource? Br Med Bull. 2013;105:43–68.
35. Neuss S, Becher E, Woltje M, Tietze L, Jahnen-Dechent W. Functional expression of HGF and HGF receptor/c-met in adult human mesenchymal stem cells suggests a role in cell mobilization, tissue repair, and wound healing. Stem Cells. 2004;22(3):405–14.
36. Ferreira MS, Jahnen-Dechent W, Labude N, Bovi M, Hieronymus T, Zenke M, Schneider RK, Neuss S. Cord blood-hematopoietic stem cell expansion in 3D fibrin scaffolds with stromal support. Biomaterials. 2012;33(29):6987–97.
37. Alharbi Z, Oplander C, Almakadi S, Fritz A, Vogt M, Pallua N. Conventional vs. micro-fat harvesting: how fat harvesting technique affects tissue-engineering approaches using adipose tissue-derived stem/stromal cells. J Plast Reconstr Aesthet Surg. 2013;66(9):1271–8.
38. Ferreira MV, Labude N, Piroth D, Jahnen-Dechent W, Knuchel R, Hieronymus T, Zenke M, Neuss S. Compatibility of different polymers for cord blood-derived hematopoietic progenitor cells. J Mater Sci Mater Med. 2012;23(1):109–16.
39. Debacq-Chainiaux F, Erusalimsky JD, Campisi J, Toussaint O. Protocols to detect senescence-associated beta-galactosidase (SA-betagal) activity, a biomarker of senescent cells in culture and in vivo. Nat Protoc. 2009;4(12):1798–806.
40. Leisten I, Kramann R, Ventura Ferreira MS, Bovi M, Neuss S, Ziegler P, Wagner W, Knuchel R, Schneider RK. 3D co-culture of hematopoietic stem and progenitor cells and mesenchymal stem cells in collagen scaffolds as a model of the hematopoietic niche. Biomaterials. 2012;33(6):1736–47.
41. Ventura Ferreira MS, Bergmann C, Bodensiek I, Peukert K, Abert J, Kramann R, Kachel P, Rath B, Rutten S, Knuchel R, Ebert BL, Fischer H, Brummendorf TH, Schneider RK. An engineered multicomponent bone marrow niche for the recapitulation of hematopoiesis at ectopic transplantation sites. J Hematol Oncol. 2016;9:4.
42. Hummel S, Ventura Ferreira MS, Heudobler D, Huber E, Fahrenkamp D, Gremse F, Schmid K, Muller-Newen G, Ziegler P, Jost E, Blasco MA, Brummendorf TH, Holler E, Beier F. Telomere shortening in enterocytes of patients with uncontrolled acute intestinal graft-versus-host disease. Blood. 2015;126(22):2518–21.
43. Ziegler S, Schettgen T, Beier F, Wilop S, Quinete N, Esser A, Masouleh BK, Ferreira MS, Vankann L, Uciechowski P, Rink L, Kraus T, Brummendorf TH, Ziegler P. Accelerated telomere shortening in peripheral blood lymphocytes after occupational polychlorinated biphenyls exposure. Arch Toxicol. 2017; 91(1):289–300.
44. Schneider RK, Schenone M, Ferreira MV, Kramann R, Joyce CE, Hartigan C, Beier F, Brummendorf TH, Germing U, Platzbecker U, Busche G, Knuchel R, Chen MC, Waters CS, et al. Rps14 haploinsufficiency causes a block in erythroid differentiation mediated by S100A8 and S100A9. Nat Med. 2016; 22(3):288–97.
45. Weidner CI, Lin Q, Koch CM, Eisele L, Beier F, Ziegler P, Bauerschlag DO, Jockel KH, Erbel R, Muhleisen TW, Zenke M, Brummendorf TH, Wagner W. Aging of blood can be tracked by DNA methylation changes at just three CpG sites. Genome Biol. 2014;15(2):R24.
46. Calado RT, Yewdell WT, Wilkerson KL, Regal JA, Kajigaya S, Stratakis CA, Young NS. Sex hormones, acting on the TERT gene, increase telomerase activity in human primary hematopoietic cells. Blood. 2009;114(11):2236–43.
47. Hartmann U, Brummendorf TH, Balabanov S, Thiede C, Illme T, Schaich M. Telomere length and hTERT expression in patients with acute myeloid leukemia correlates with chromosomal abnormalities. Haematologica. 2005;90(3):307–16.
48. Dominici M, Le Blanc K, Mueller I, Slaper-Cortenbach I, Marini F, Krause D, Deans R, Keating A, Prockop D, Horwitz E. Minimal criteria for defining

multipotent mesenchymal stromal cells. The international society for cellular therapy position statement. Cytotherapy. 2006;8(4):315–7.
49. Abumaree MH, Al Jumah MA, Kalionis B, Jawdat D, Al Khaldi A, AlTalabani AA, Knawy BA. Phenotypic and functional characterization of mesenchymal stem cells from chorionic villi of human term placenta. Stem Cell Rev. 2013;9(1):16–31.
50. Castrechini NM, Murthi P, Gude NM, Erwich JJ, Gronthos S, Zannettino A, Brennecke SP, Kalionis B. Mesenchymal stem cells in human placental chorionic villi reside in a vascular Niche. Placenta. 2010;31(3):203–12.
51. Qin SQ, Kusuma GD, Al-Sowayan B, Pace RA, Isenmann S, Pertile MD, Gronthos S, Abumaree MH, Brennecke SP, Kalionis B. Establishment and characterization of fetal and maternal mesenchymal stem/stromal cell lines from the human term placenta. Placenta. 2016;39:134–46.
52. Shafiee A, Fisk NM, Hutmacher DW, Khosrotehrani K, Patel J. Fetal endothelial and mesenchymal progenitors from the human term placenta: potency and clinical potential. Stem Cells Transl Med. 2015;4(5):419–23.
53. Mathews S, Lakshmi Rao K, Suma Prasad K, Kanakavalli MK, Govardhana Reddy A, Avinash Raj T, Thangaraj K, Pande G. Propagation of pure fetal and maternal mesenchymal stromal cells from terminal chorionic villi of human term placenta. Sci Rep. 2015;5:10054.
54. Ryan JM, Barry FP, Murphy JM, Mahon BP. Mesenchymal stem cells avoid allogeneic rejection. J Inflamm. 2005;2:8.
55. Espagnolle N, Guilloton F, Deschaseaux F, Gadelorge M, Sensebe L, Bourin P. CD146 expression on mesenchymal stem cells is associated with their vascular smooth muscle commitment. J Cell Mol Med. 2014;18(1):104–14.
56. Li CD, Zhang WY, Li HL, Jiang XX, Zhang Y, Tang PH, Mao N. Mesenchymal stem cells derived from human placenta suppress allogeneic umbilical cord blood lymphocyte proliferation. Cell Res. 2005;15(7):539–47.
57. Talele NP, Fradette J, Davies JE, Kapus A, Hinz B. Expression of alpha-smooth muscle actin determines the fate of mesenchymal stromal cells. Stem Cell Rep. 2015;4(6):1016–30.
58. Pelekanos RA, Sardesai VS, Futrega K, Lott WB, Kuhn M, Doran MR. Isolation and expansion of mesenchymal stem/stromal cells derived from human placenta tissue. J Vis Exp. 2016;(112). https://doi.org/10.3791/54204, https://www.ncbi.nlm.nih.gov/pubmed/27340821.
59. Heazlewood CF, Sherrell H, Ryan J, Atkinson K, Wells CA, Fisk NM. High incidence of contaminating maternal cell overgrowth in human placental mesenchymal stem/stromal cell cultures: a systematic review. Stem Cells Transl Med. 2014;3(11):1305–11.
60. Collins K, Mitchell JR. Telomerase in the human organism. Oncogene. 2002;21(4):564–79.
61. Blasco MA. Telomeres and human disease: ageing, cancer and beyond. Nat Rev Genet. 2005;6(8):611–22.
62. Wright WE, Shay JW. Telomere biology in aging and cancer. J Am Geriatr Soc. 2005;53(9 Suppl):S292–4.
63. Shay JW, Wright WE. Senescence and immortalization: role of telomeres and telomerase. Carcinogenesis. 2005;26(5):867–74.
64. Izadpanah R, Trygg C, Patel B, Kriedt C, Dufour J, Gimble JM, Bunnell BA. Biologic properties of mesenchymal stem cells derived from bone marrow and adipose tissue. J Cell Biochem. 2006;99(5):1285–97.
65. Yanada S, Ochi M, Kojima K, Sharman P, Yasunaga Y, Hiyama E. Possibility of selection of chondrogenic progenitor cells by telomere length in FGF-2-expanded mesenchymal stromal cells. Cell Prolif. 2006;39(6):575–84.
66. Zimmermann S, Voss M, Kaiser S, Kapp U, Waller CF, Martens UM. Lack of telomerase activity in human mesenchymal stem cells. Leukemia. 2003;17(6):1146–9.
67. Hiyama E, Hiyama K. Telomere and telomerase in stem cells. Br J Cancer. 2007;96(7):1020–4.
68. Fehrer C, Lepperdinger G. Mesenchymal stem cell aging. Exp Gerontol. 2005;40(12):926–30.
69. Gonzalo S, Jaco I, Fraga MF, Chen T, Li E, Esteller M, Blasco MA. DNA methyltransferases control telomere length and telomere recombination in mammalian cells. Nat Cell Biol. 2006;8(4):416–24.
70. Kyo S, Takakura M, Tanaka M, Kanaya T, Sagawa T, Kohama T, Ishikawa H, Nakano T, Shimoya K, Inoue M. Expression of telomerase activity in human chorion. Biochem Biophys Res Commun. 1997;241(2):498–503.
71. Okolicsanyi RK, Camileri ET, Oikari LE, Yu C, Cool SM, van Winjen AJ, Griffiths LR, Haupt LM. Human mesenchymal stem cells retain multilineage differentiation capacity including neural marker expression after extended in vitro expansion. PLoS One. 2015;10(9):e0137255.
72. Jones GN, Moschidou D, Puga-Iglesias TI, Kuleszewicz K, Vanleene M, Shefelbine SJ, Bou-Gharios G, Fisk NM, David AL, De Coppi P, Guillot PV. Ontological differences in first compared to third trimester human fetal placental chorionic stem cells. PLoS One. 2012;7(9):e43395.
73. Kosaka N, Kodama M, Sasaki H, Yamamoto Y, Takeshita F, Takahama Y, Sakamoto H, Kato T, Terada M, Ochiya T. FGF-4 regulates neural progenitor cell proliferation and neuronal differentiation. FASEB J. 2006;20(9):1484–5.
74. Young RA. Control of the embryonic stem cell state. Cell. 2011;144(6):940–54.
75. Avilion AA, Nicolis SK, Pevny LH, Perez L, Vivian N, Lovell-Badge R. Multipotent cell lineages in early mouse development depend on SOX2 function. Genes Dev. 2003;17(1):126–40.
76. Masui S, Nakatake Y, Toyooka Y, Shimosato D, Yagi R, Takahashi K, Okochi H, Okuda A, Matoba R, Sharov AA, Ko MS, Niwa H. Pluripotency governed by Sox2 via regulation of Oct3/4 expression in mouse embryonic stem cells. Nat Cell Biol. 2007;9(6):625–35.
77. Chambers I, Silva J, Colby D, Nichols J, Nijmeijer B, Robertson M, Vrana J, Jones K, Grotewold L, Smith A. Nanog safeguards pluripotency and mediates germline development. Nature. 2007;450(7173):1230–4.
78. Silva J, Nichols J, Theunissen TW, Guo G, van Oosten AL, Barrandon O, Wray J, Yamanaka S, Chambers I, Smith A. Nanog is the gateway to the pluripotent ground state. Cell. 2009;138(4):722–37.
79. Abdulrazzak H, Moschidou D, Jones G, Guillot PV. Biological characteristics of stem cells from foetal, cord blood and extraembryonic tissues. J R Soc Interface. 2010;7 Suppl 6:S689–706.
80. Hackett JA, Surani MA. Regulatory principles of pluripotency: from the ground state up. Cell Stem Cell. 2014;15(4):416–30.
81. Yu J, Su X, Zhu C, Pan Q, Yang J, Ma J, Shen L, Cao H, Li L. GFP labeling and hepatic differentiation potential of human placenta-derived mesenchymal stem cells. Cell Physiol Biochem. 2015;35(6):2299–308.

The multi-functional roles of menstrual blood-derived stem cells in regenerative medicine

Abstract

Menstrual blood-derived stem cells (MenSCs) are a novel source of mesenchymal stem cells (MSCs). MenSCs are attracting more and more attention since their discovery in 2007. MenSCs also have no moral dilemma and show some unique features of known adult-derived stem cells, which provide an alternative source for the research and application in regenerative medicine. Currently, people are increasingly interested in their clinical potential due to their high proliferation, remarkable versatility, and periodic acquisition in a non-invasive manner with no other sources of MSCs that are comparable in adult tissue. In this review, the plasticity of pluripotent biological characteristics, immunophenotype and function, differentiative potential, and immunomodulatory properties are assessed. Furthermore, we also summarize their therapeutic effects and functional characteristics in various diseases, including liver disease, diabetes, stroke, Duchenne muscular dystrophy, ovarian-related disease, myocardial infarction, Asherman syndrome, Alzheimer's disease, acute lung injury, cutaneous wound, endometriosis, and neurodegenerative diseases. Subsequently, the clinical potential of MenSCs is investigated. There is a need for a deeper understanding of its immunomodulatory and diagnostic properties with safety concern on a variety of environmental conditions (such as epidemiological backgrounds, age, hormonal status, and pre-contraceptive). In summary, MenSC has a great potential for reducing mortality and improving the quality of life of severe patients. As a kind of adult stem cells, MenSCs have multiple properties in treating a variety of diseases in regenerative medicine for future clinical applications.

Keywords: Menstrual blood-derived stem cells, Cellular therapy, Adult stem cells, Menstrual blood, Regenerative medicine

Background

Mesenchymal stem cells (MSCs), a heterogeneous subgroup of progenitor cells, have self-renewing capacity and differentiating potential into various specialized cell types, including osteoblasts, chondrocytes, and adipocytes [1]. MSC can be harvested from several adult tissues, such as bone marrow (BM), peripheral blood (PB), adipose tissue (AD), umbilical cord (UC), and placenta [2–6]. BM-MSCs have received the preferential attentions for exploring a variety of diseases in animal models and clinical trials [7–9]. Although BM-MSCs have obtained great priorities and predominant studies, the difficulty of separating BM-MSCs is a limiting factor owing to the requirements of invasive operation and ethical issue of donors [10, 11]. Therefore, exploring novel source of MSCs can be effectively used without these limitations.

Approximately a decade ago, Meng et al. and Cui et al. discovered a novel source of MSCs from human menstrual fluid, named menstrual blood-derived stem cells (MenSCs) [12, 13]. Throughout these years, more and more studies are focusing on MenSCs, a representative comparison was presented in six sources of MSCs, suggesting that MenSCs possessed higher proliferation rates and painless procedures, and almost no ethical issues

[14]. In addition, some papers focus on the therapeutic potential and underlying mechanism of MenSCs. The purpose of this review is to provide an update based on current knowledge about MenSCs in their native environment, the basic characteristic, and a detailed description for therapeutic ways in a variety of diseases.

Basic characteristic of MenSCs

Definition and immunophenotype

At first, MenSCs are termed as endometrial regenerative cells [12, 15]. Subsequently, with advantages of non-invasive collection processes, high proliferation rate, pluripotency, and low immunogenicity, MenSCs were extensively studied [16–20]. Of course, there are some other names which were described by many researchers [21–37]. At present, the existing nomenclatures and detailed information of MenSCs are listed in Table 1. In this review, MenSCs are described with the uniform and convenient name throughout the paper.

In Table 2, we have completed a detailed comparison of the phenotypes published in the existing papers [12, 13, 16, 17, 19–21, 23, 26–28, 30–32, 34, 36–43]. According to Table 2, MenSCs were positive for several surface molecules, such as CD9, CD29, CD44, CD73, CD90, CD105, octamer binding transcription factor 4 (OCT-4), CD166, major histocompatibility complex I (MHC I), and C-X-C chemokine receptor type 4 (CXCR4). Among these molecules above, CD29, CD73, CD90, and CD105 were commonly identified for MSC markers. MenSCs also remained to have negative expressions for hematopoietic stem cell markers, such as CD34, CD45, and CD133. And CD14, CD38, and human leukocyte antigen-DR isotype (HLA-DR) were also negative. Interestingly, some papers were reported for the positive expression of embryonic markers and intracellular multipotent markers, such as OCT-4, c-kit proto-oncogene (c-kit)/CD117, and stage-specific embryonic antigen-4 (SSEA-4), which have not existed in MSCs from other sources. However, these findings were controversial, and some researchers showed that the expressions of c-kit and SSEA-4 were negative [12, 23, 26, 27, 42]. In our lab, we also performed these cells with surface molecule examination, and they were stable and consistent [19, 20, 34, 35, 38].

Table 1 The existing nomenclatures for MenSCs in different literatures

Names	References
Endometrial regenerative cells	[12, 15]
Menstrual blood-derived stem cells	[16–20]
Menstrual-derived stem cells	[21]
Menstrual blood stem cells	[22]
Menstrual blood stromal stem cells	[23–25]
Menstrual stem cells	[26]
Menstrual blood-derived stromal stem cells	[27, 28]
Endometrial stem cells	[29]
Menstrual blood-derived endometrial stem cells	[30, 31]
Menstrual blood-derived mesenchymal stem cells	[32–34]
Menstrual blood progenitor cells	[35]
Endometrial mesenchymal stem cells	[36, 37]

Proliferation and differentiation

Studies by Meng et al. and our group have reported that MenSCs from young and healthy women could increase to one doubling every 20 h supplied with sufficient culture conditions, which was twice as fast as BM-MSCs (estimated 40–45 h) [12, 35]. MenSCs have similar phenotypes and properties compared with BM-MSCs, including spindles, classical three-line differentiation, and surface marker expression. A high rate of proliferation was contributed to the high expression of embryonic trophic factors and extracellular matrix (ECM) in MenSCs [44]. A high proliferative capacity is critical for future clinical research because cell-based treatment is usually dose-dependent along with cells from the lower passages; therefore, increasing the yield of the preliminary cells is necessary and considerable in clinical research. In addition, MenSCs have been extensively expanded in vitro and hardly showed obvious chromosomal abnormalities by our group and others [12, 23, 35]. Such a highly proliferating rate and stably genetic characteristic, as well as the apparent pluripotency, suggest that the novel stem cells may exhibit unexpected therapeutic properties.

MenSCs are also remarkable for their broad differentiation capacity. Currently, MenSCs can be induced as endothelial, cardiomyocytic, neurocytic, cartilaginous, myocytic, respiratory epithelial, pancreatic, hepatic, adipocytic, and osteogenic parts using appropriate differentiation techniques [12, 14, 26]. Hida et al. found that MenSCs exhibited cardiogenic differentiation in a scaffold culture system [45]. Lai's team has confirmed that the differentiation of MenSCs into germ cells was induced in the appropriate medium [46]. Similarly, Liu et.al also proved that MenSCs had the capacity to differentiate into ovarian tissue-like cells [22]. Furthermore, our group and Khanjani et al. have shown that MenSCs could differentiate into functional hepatocyte-like cells by checking mature hepatocyte functions [17, 33, 39]. In addition, MenSCs had a potential for differentiation into glial lineages (neurosphere-like cells) by examining the expression of glial fibrillary acidic protein, oligosaccharide-2, and myelin basic protein [47].

Immunomodulation properties

The extensive progress has been made in immunomodulatory properties for a multitude of inflammatory responses

Table 2 Comparison of the different immunophenotypic profile of MenSCs

Markers	12	40	23	42	13	39	19, 20, 34, 38	16	27	26	17	36	43	28	32	37	21	41	30, 31
CD14	–				–					–			–		–			–	
CD34	–		–	–	–		–		–	–		–	–	–	–	–	–	–	–
CD38	–		–						–					–					
CD45	–		–	–	–	–	–		–	–	–	–	–	–		–	–	–	–
CD133	–		–		–	–			–						–		–	–	
STRO-1	–								–										
SSEA-4	–		+	+					–	–				–					+
Nanog	–	+																	+
CD9	+		+						+										
CD29	+		+	+	+		+		+	+			+	+		+	+			+
CD73	+				+		+		+		+	+			+	+		+	+	+
CD41a	+																		
CD44	+		+	+	+				+	+	+			+	+	+		+	+	+
CD90	+		+	+	+		+		+		+		+	+	+	+	+	+	+	+
CD105	+		+	+	+	+	+		+	+	+	+			+	+	+		+	+
OCT-4	+	+		+		+			+	+		+	+							
CXCR4		+	+																	
CD166			+	+		+											+			
CD49f			+																	
MHC I			+		+					+									+	+
MHC II (HLA-DR)			–		–		–			–		–			–				–	–
LIN			–																	
CD117 (c-kit)			+	+	–		–			–	–	–					–			
CD13					+															
CD54					+															
CD55					+															
CD31					–					–										
CD50					–															
CD106						–														
Vimentin						+														
CD10									+	+										
CD271										–										
EpCAM										–										
CD49a										–							+			
SSEA-3										–										
TRA-1-60										–										
CD146											+						+			
CD40															–					
CD83															–					
CD86															–					
CD19																		–		
Sox2																		–	+	
c-myc																		–	+	

STRO-1 stromal cell antigen 1, *LIN* lineage, *EpCAM* epithelial cell adhesion molecule, *TRA-1-60* tumor-rejection antigen-1-60, *Sox2* SRY (sex determining region Y)-box 2, *c-myc* c-myelocytomatosis

in inhibiting dendritic cells, B lymphocyte cells, T lymphocyte cells, mixed lymphocyte reaction (MLR), and promoting regulatory T cells (Tregs) [48]. However, the research on the immunomodulation of MenSCs is still in its infancy. It is worth noting that the endometrium is a part of the mucosal immune system, and MenSCs are extracted from menstrual blood, and their original sources are deciduous endometrial stem cells [44]. In fact, we only knew sporadic information of MenSC in animal disease models with autoimmune diseases [24, 25]. This emphasized the necessity for further research to assess immunosuppressive effects on immune-related molecules (such as MHC I, MHC II, CD40, and CD80/86) and other inflammatory-related cytokines (such as interferon-γ (IFN-γ), tumor necrosis factor α (TNF-α), interleukin-1 alpha (IL-1α), and interleukin-1 beta (IL-1β)) in MenSCs [49]. Therefore, immunoregulatory properties of MenSCs are currently unrecognized despite the unified management mechanism of MenSC-based therapy is explored in animal models and clinical researches.

Practical application of MenSCs in tissue regeneration and disease therapy

At present, more and more registrations for a variety of diseases support the therapeutic benefits of MSC transplantation in clinical trials (www.clinicaltrials.gov). In contrast, the registrations of MenSCs are still few, and no more than 10 clinical trials are presented by searching "menstrual blood stem cells". Actually, the therapeutic potential of MenSCs has already been recognized in several kinds of diseases in pre-clinical research, which is fundamental for future clinical applications in tissue repair and regenerative medicine. Similar to BM-MSCs, MenSCs also have several merits, including the ability to migrate into injury sites, differentiation into different cell lineages, secretion of soluble factors, and regulation of immune responses. Therefore, more researches need to be explored before MenSC becomes a common use in clinical application and treatment.

Liver disease

Liver fibrosis is the universal phase of various chronic liver diseases and causes a huge public health issue due to high rates for the morbidity and mortality worldwide [50]. Fibrosis was a reversible process along with wound healing and characterized by accumulation of ECM protein at the site of an injured liver [51]. At present, orthotopic liver transplantation (OLT) is the most effective strategy for patients at the end stage of liver disease. However, due to lack of organ donors, surgical complications, lifelong immunosuppression, and high cost, its application has been limited to a large number of patients in the current condition. Recently, we have studied the therapeutic effect of MenSC transplantation in a mouse model of liver fibrosis induced by CCl_4 (carbon tetrachloride) [20]. The results showed that MenSC had the effect on treating liver fibrosis. Liver function was improved via targeting activated hepatic stellate cells (HSCs), and collagen deposition was reduced after cell transplantation in liver fibrotic mice. Co-culture experiments showed that MenSCs restrained the proliferation of LX-2 cells (HSC line) through secretion of paracrine cytokines, including interleukin-6 (IL-6), IL-8, hepatocyte growth factor (HGF), monocyte chemoattractant protein 1 (MCP-1), growth-related oncogene (GRO), and osteoprotegerin (OPG). The results suggest that MenSC may be an attractive treatment for chronic liver disease by targeting HSCs via paracrine mediators.

Fulminant hepatic failure (FHF) is a life-threatening and sharply pathological reaction, which results in relatively high mortality by rapid necrosis of liver cells with the stimulation of a variety of acute injuries, such as hepatotoxic drugs, immune-mediated attacks, or viral infections [52]. The exosomes contain microRNA/lncRNA and adhesion molecules as well as small vesicles of secreted proteins, which mediate cellular signaling pathways both in vivo and in vitro [53]. Our group proved that MenSC-derived exosomes (MenSC-Ex) possessed therapeutic potential by inhibiting hepatocyte apoptosis in D-galactosamine (D-Gal) and lipopolysaccharide (LPS) induced FHF in mice, and we further showed that the levels of TNF-α, IL-6, and IL-1β were reduced by co-culture with AML12 hepatocytes (a normal mouse hepatocyte cell line) in vitro [19]. The study suggests that MenSC-Ex can improve liver function to increase the rate of survival in FHF model mice.

Diabetes

Type 1 diabetes mellitus (T1DM), known as a kind of autoimmune diabetes, is a multifactorial disease by the deficiency of secreting insulin in islet β cells to influence the normal organism metabolism, ultimately leading to elevated blood glucose levels and a severe decline in insulin secretion [54]. Transplantation of human islets is currently the most effective treatment; due to the lack of pancreatic donors, it has been greatly restricted in the widespread application. Our team has studied the therapeutic effect of MenSCs and the underlying mechanism of β cell regeneration after MenSC transplantation in the T1DM mouse model [35]. From our study, MenSCs could facilitate β-cell regeneration and enhance the number of β cells by increasing the expressions of neurogenin 3 (ngn 3), forkhead box A2 (foxa 2), pancreatic and duodenal homeobox 1 (pdx 1), NK homeobox factor 6.1 (nkx 6.1), and paired box gene (pax) to activate endogenous progenitor cell differentiation post MenSC

transplantation in T1DM mice. Clarifying the precise mechanism involved in MenSC-induced β-cell regeneration will facilitate the future use of MenSCs to treat diabetes.

Ischemic stroke

Ischemic stroke, one of the leading causes of long-term disability, is a chain reaction of functional impairment that initially occurs during the identification phase of rapid physical and mental fluctuations [55]. Currently, ischemic stroke causes many patients producing permanent nerve damage, and stem cell therapy will help to improve and possibly restore the nerve function. Borlongan et al. demonstrated that MenSCs improved ischemic stroke in an oxygen glucose deprivation (OGD) rat model in vitro [40]. The behavioral and histological disorders were also significantly improved in the rat model of ischemic stroke by intracerebral/intravenous transplantation. Co-culture experiments showed that MenSCs significantly reduced cell death of OGD-exposed rat primary neurons through increasing vascular endothelial growth factor (VEGF), brain-derived neurotrophic factor (BDNF), and neurotrophin 3 (NT-3). The neurostructural and behavioral benefits afforded by transplanted MenSCs support their use as a kind of stem cell source for cell therapy in treating ischemic stroke.

Duchenne muscular dystrophy

Duchenne muscular dystrophy (DMD) is a deadly x-linked muscle degeneration disease that consists of a potential genetic defect characterized by an enhanced inflammatory response [56]. DMD is an important part of the muscular dystrophy glycoprotein complex (DGC), which is involved in the relative stabilization of the sarcolemma and regulation of the interaction between the cytoskeleton and skeletal muscle and myocardial ECM. Umezawa's team showed that MenSCs could restore muscle degeneration and repair skeletal muscle abnormalities by increasing muscle-like protein expression in immunodeficient DMD model mice [13]. In addition, MenSCs effectively differentiated into myoblasts/muscle cells after co-culture with mouse myoblast C2C12 in vitro, and these differentiated cells could express anti-atrophy muscle protein. It is suggested that MenSCs transform muscular dystrophic cells into anti-atrophic cells through trans-differentiation both in vitro and in vivo.

Critical limb ischemia

Critical limb ischemia (CLI) refers to the final clinical stage along with the limb damage due to severe blood loss causing a series of pathological and physiological abnormalities that lead to limb pain or insufficient nutrition to support the legs [57]. Currently, although clinical trials have reported that autologous stem cells improve their symptoms by stimulating angiogenesis, the appropriate cell population of MSCs is still needed to explore. Murphy et al. demonstrated that administration of MenSCs improved CLI in a mouse model [58]. Although they did not explore the precise mechanism, they pointed out three possible reasons: (1) producing high levels of growth factors, IL-4, hypoxia inducible factor-1 alpha (HIF-1α), and matrix metalloproteinases (such as MMP3 and MMP10) with a paracrine role; (2) inhibiting the inflammatory response and blocking the pro-inflammatory signaling pathway; (3) producing a large amount of endothelial progenitor cells to mediate cell differentiation. Collectively, they suggest that MenSC represents a novel approach for treating the CLI by supplying an "off the shelf" therapeutic way, and it will provide a guideline for the feasibility of the proposed clinical trial in future.

Ovarian-related disease

Ovarian cancer is one of the most deadly gynecological diseases for ambiguous symptoms and lack of reliable screening methods in many developed countries [59]. At present, platinum-based combination chemotherapy is the standard treatment for the past decade, but there is almost no improvement and progress. Cancer patients, especially women under the age of 40, are often suffering from reproductive damage related with premature ovarian failure (POF) and infertility in women. Lai et al. have demonstrated that MenSCs improved the estrous cycle and restored mouse fertility in the POF mouse model [36]. Wang et al. further explored that MenSCs could significantly improve the ovarian microenvironment by reducing granulosa cell apoptosis and ovarian interstitial fibrosis [21]. Transplanted MenSCs played an important role in ovarian function by secreting cytokines such as fibroblast growth factor 2 (FGF 2). MenSCs repair ovarian injury, improve ovarian function, and stimulate ovarian regeneration, which suggest that MenSCs may be a novel and effective strategy for the treatment of POF in regenerative medicine.

In addition, epithelial ovarian cancer (EOC) has been found to be advanced in most cases, with a combination of extensive abdominal metastasis, high recurrence, and chemoresistance [60]. Recently, Lai group found that MenSCs could improve the symptoms of EOC through tumor transplant animal model in vivo. Moreover, they further discovered that MenSCs induced angiogenic ability by inhibiting AKT/PKB (protein kinase B)-mediated degradation of the forkhead O-3a (FoxO3a) to induce cell cycle arrest, promote apoptosis, interfere with mitochondrial membrane function, and reduce EOC cells in co-culture models in vitro. These results suggest that MenSCs inhibit AKT-induced degradation of FoxO3a,

which facilitates the anti-tumor properties of MenSCs on EOC in future regenerative medicine.

Myocardial infarction

Myocardial infarction (MI), a type of coronary artery disease (CAD), is pathologically defined as the death of cardiomyocytes because of excessive ischemic condition [61]. Since MI has a long-term undiscovered phase, it can also be a major catastrophic event that causes sudden death or severe hemodynamic deterioration in patients. Hida et al. confirmed that the transplanted MenSCs significantly restored the damaged cardiac function in nude rat model [45]. In addition, Jiang et al. further demonstrated that MenSCs significantly reduced apoptosis, promoted cell proliferation, and recruited c-kit$^+$ cells in an immunological MI model rats [29]. MenSCs could express some specific cytokines to activate AKT/extracellular signal-regulated kinases 1 and 2 (ERK 1/2)/signal transducers and activator of transcription 3 (STAT 3) and suppress p38 signaling pathway. Then Wang's team found that MenSCs inhibited endothelial cell to mesenchymal transition (EMT), which helped to reduce the total number of cardiac fibroblasts and tissue fibrosis progression [62]. In addition, they verified that secreted exosomes of miR-21 mediated and enhanced the paracrine and cytoprotective effects through a transwell co-culture system in vitro. Exosomal microRNA (miR) array revealed that miR-21 targeted phosphatase and tensin homolog (PTEN) and the downstream of AKT [37]. These results suggest that MenSCs improve the damaged cardiac function in MI mainly through paracrine role and miRs deriving from exosome.

Asherman syndrome

Asherman syndrome is caused by the formation of adhesions in the uterine cavity. Women with this disease often have many comprehensive and complicated symptoms, such as infertility, irregular menstruation (including amenorrhea, less menstruation, or dysmenorrhea), and repeated pregnancy loss [63]. Autologous MenSC transplantation significantly increased endometrial thickness (ET) in Asherman syndrome women in a total of 7 patients with Asherman syndrome in a non-controlled prospective and 3-year clinical study [28]. They showed that the ET of 5 women was significantly increased to 7 mm (a thickness to ensure embryo implantation). Four of these patients were subjected to frozen embryo transfer (FET). Surprisingly, one patient developed a spontaneous pregnancy only after the second MenSC transplant. This study suggests that autologous MenSC transplantation is a possible option for the treatment of Asherman syndrome in women.

Alzheimer's disease

Alzheimer's disease, caused by amyloid-beta (Aβ) production, is progressive memory loss and cognitive dysfunction, and its neuropathological features are induced by the hyperphosphorylated tau proteins, which are composed of extracellular Aβ plaque deposits and intracellular neurofibrillary tangles (NTFs) [64]. Our group found that transplantation of MenSC in the brain of APP/PS1 mice could significantly improve the spatial learning characteristics and memory ability of AD in mouse model [34]. In addition, MenSCs significantly improved amyloid plaques in vivo and reduced tau hyperphosphorylation. It is worth noting that we also proved that intracranial transplantation of MenSCs significantly increased the expression of Aβ-degrading enzymes and decreased the level of pro-inflammatory cytokines to alter the microglia-associated phenotype. This result indicates that MenSCs can degrade Aβ and play an anti-inflammatory effect for improving AD in vivo.

Acute lung injury

Acute lung injury (ALI) is a severe health burden worldwide due to its rapid attack and high mortality. Many factors can cause ALI, such as tidal volume, mechanical ventilation, or hypoxia; these injuries are often accompanied by inflammatory reactions, and once inflammatory reactions are sustained, the patients will face suffocation or even death [65]. Our group showed that MenSCs promoted the repair of injured lung by inhibiting the inflammatory response in LPS-induced ALI in mice [38]. Furthermore, MenSCs not only improved pulmonary microvascular permeability, reduced histopathological injury, and downregulated the expressions of IL-1β and caspase-3, but also upregulated the levels of IL-10, proliferating cell nuclear antigen (PCNA), and keratinocyte growth factor (KGF) in bronchoalveolar lavage fluid (BALF). MenSCs could also increase the survival rate of BEAS-2B cells (human normal lung epithelial cells) and inhibit LPS-induced cell apoptosis in a co-culture experiment. These results suggest that MenSC-based treatment may become an attractive strategy for improving ALI in regenerative medicine.

Cutaneous wound

Cutaneous wound is repaired by coordinated biological progress to restore the original stage of damaged tissue, including cell proliferation and differentiation, and a variety of cell apoptosis, thereby producing multiple layers of connective tissue. The repaired skin is usually cured in the form of a scar, and the main purposes of the cutaneous regeneration are to understand how to induce skin to reconstruct damaged parts without forming scars [66]. Cuenca et al. revealed that MenSCs significantly improved wound healing and enhanced new

blood vessel formation in a mouse excisional wound model [41]. They further discovered that MenSCs secreted some cytokines, including angiopoietin (Angpt), platelet-derived growth factor (PDGF), elastin (Eln), MMP3, and MMP10, allowing them to participate in wound repair. These results suggest that MenSCs promote wound healing and contribute to cutaneous regeneration.

Endometriosis

Endometriosis is a common gynecological disorder defined as endometrial glands and interstitial growth outside the uterus, which is currently present in approximately 10% of women at reproductive age and 30% of infertile women [67]. Clinical interest and research are mainly focused on lesions and the directly affected diseases for the lack of understanding and exploration of the pathogenesis of women in different periods. Nikoo et al. found that MenSCs played a very important role by comparing the ability in morphology, CD marker expression, cell proliferation, invasion, adhesion, and some immunomodulatory molecules between women with endometriosis (E-MenSCs) and non-endometriosis (NE-MenSCs) [27]. In addition, the expressions of indoleamine 2,3-dioxygenase-1 (IDO1), cyclooxygenase-2 (COX-2), IFN-γ, IL-10, and MCP-1 were increased, and the level of forkhead transcription factor-3 (FOXP3) was reduced in co-culture of E-MenSCs and peripheral blood mononuclear cells (PBMCs) in vitro. These finding suggests that MenSC has a critical role in improving endometriosis.

Clinical applications and safety concerns of MenSCs

Cellular therapies using MSCs are undergoing extensive preclinical and clinical trials. Especially, the progress of clinical trials of BM-MSCs is encouraging, a variety of diseases are researched in the I or II stage [68]. Compared to the most common BM-MSCs, the clinical trials of MSCs from other tissue sources (such as AD, PB, UC, and placenta, amniotic membrane, and menstrual blood) are a drop in the bucket. Bianco proposed that different human diseases could be reasonably used with different sources of MSCs, which was better to establish the physiological and pathological system to treat a variety of diseases for clinical applications [1]. Because MenSCs possess good immunosuppressive properties, they are able to intravenously inject large amounts of cells to injured body. From short-term studies, they are safe and reliable after cell transplantation, and they migrate into the inflammatory or injured sites, which has a regenerative inhibitory effect on inflammation [49]. Currently, no evidence of tumor or toxicity following administration of MenSC has been found in nude mice. Moreover, we assessed that MenSCs had significant inhibitory effects on tumor growth in a mouse glioma model [69]. No obvious physiological or serological abnormalities were observed in four patients with multiple sclerosis for the use of MenSCs [15]. Although researches indicate that MenSCs are rapidly evolving, it is not yet determined how long MenSCs can survive in foreign bodies and there are no data guaranteeing their long-term safety owing to lack of specific markers to monitor these cells in vivo [10, 68].

From a safety point of view, people are concerned with the collection procedure with standard process and isolated MenSCs are carried out under aseptic conditions in compliance with good manufacturing practice (GMP) release standards. At present, the high-quality and high-consistency of MenSCs are still scarce because there are no golden standardization and ideal molecular markers to verify them. The heterogeneity of MenSCs is derived from the variability of donors, different procedures of cell cultures, and a variety of environmental conditions (such as epidemiological backgrounds, age, hormonal status, and pre-contraceptive). These interventions may make MenSC transplantation of a routine clinical treatment and avoid unproven treatments that possess a health risk to the patients and may compromise the reputation of stem cell research and therapy.

Future perspectives and conclusions

MenSCs have been broadly used in preclinical studies, and many of which have shown effectively therapeutic functions in prevention and control of various diseases, including liver disease, diabetes, stroke, Duchenne muscular dystrophy, ovarian-related disease, myocardial infarction, Asherman syndrome, Alzheimer's disease, acute lung injury, cutaneous wound, endometriosis, and neurodegenerative diseases (Fig. 1). The potential of multidirectional differentiation of MenSCs suggests its potential for repair of various tissue damages. However, the therapeutic effect of MenSCs should not be simply considered as a single reason, we should use a more comprehensive horizon coordinated with the local microenvironment. Especially, some novel hotspots are explored, such as vesicles and exosomes, single-cell RNA-sequencing, and cell-targeted therapy for precision medicine.

In order to achieve the end goal of the use of MenSCs in clinical implementation, the standard criterion of sample collections is needed to produce high quality and high consistency of MenSCs; more importantly, fundamental pre-clinical research is demanded for establishing more treatment strategies and exploring precise signaling pathways. Finally, the long-term safety of MenSCs should be assessed before they are used in clinical medicine. In summary, although more work needs to be

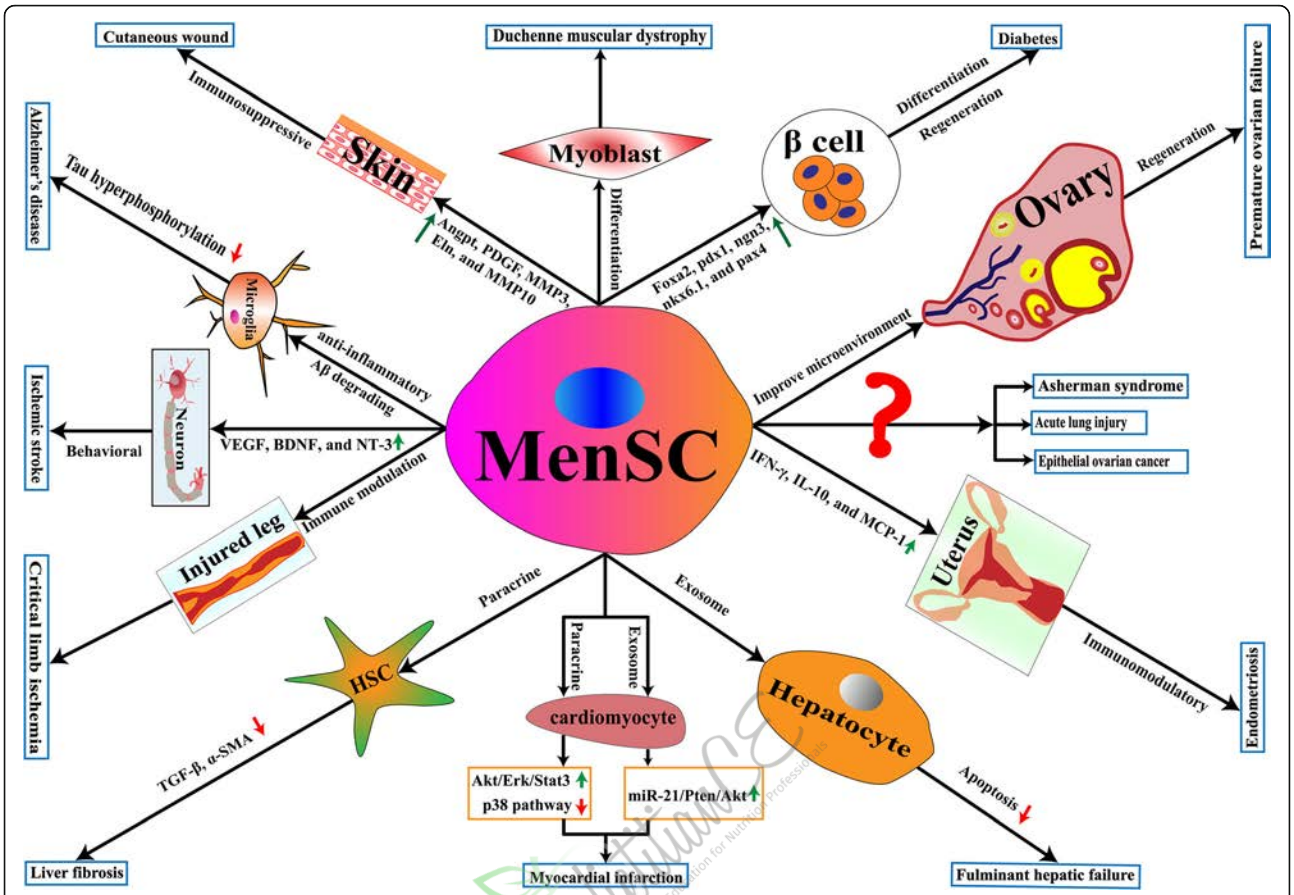

Fig. 1 Schematic diagram of MenSCs in treating a diversity of diseases, including liver fibrosis, fulminant hepatic failure, diabetes, stroke, Duchenne muscular dystrophy, epithelial ovarian cancer, premature ovarian failure, myocardial infarction, Asherman syndrome, Alzheimer's disease, acute lung injury, cutaneous wound, endometriosis, and neurodegenerative diseases. The blue boxes with characters show various diseases, the green arrow represents enhancement, and the red arrow represents decrement. Abbreviations: Erk, extracellular signal-regulated kinases; Stat 3, signal transducers and activator of transcription 3; Akt, PKB (protein kinase B); miR-21, microRNAs 21; Pten, phosphatase and tensin homolog; Aβ, amyloid-beta; IL-10, interleukin 10; α-SMA, α-smooth muscle actin; TGF-β, transforming growth factor-β; IFN-γ, interferon-γ; VEGF, vascular endothelial growth factor; BDNF, brain derived neurotrophic factor; NT-3, neurotrophin 3; Angpt, angiopoietin; PDGF, platelet-derived growth factor; Eln, elastin; MMP, matrix metalloproteinases; pax, paired box gene; ngn 3, neurogenin 3; nkx 6.1, NK homeobox factor 6.1; foxa 2, forkhead box A2; pdx 1, pancreatic and duodenal homeobox 1; and MCP-1, monocyte chemoattractant protein 1

done, MenSCs have been proved to play multi-functional roles in treating a variety of diseases through diversely therapeutic strategies in preclinical research, which will be contributed to the development of MenSC-based treatment in regenerative medicine and clinical applications.

Abbreviations

AD: Adipose tissue; AKT/PKB: Protein kinase B; ALI: Acute lung injury; Angpt: Angiopoietin; Aβ: Amyloid-beta; BALF: Bronchoalveolar lavage fluid; BDNF: Brain-derived neurotrophic factor; BM: Bone marrow; CAD: Coronary artery disease; CCl_4: Carbon tetrachloride; c-kit: c-kit proto-oncogene; CLI: Critical limb ischemia; c-myc: c-myelocytomatosis; COX-2: Cyclooxygenase-2; CXCR4: C-X-C chemokine receptor type 4; D-Gal: D-galactosamine; DGC: Dystrophy glycoprotein complex; DMD: Duchenne muscular dystrophy; ECM: Extracellular matrix; Eln: Elastin; EMT: Endothelial cell to mesenchymal transition; EOC: Epithelial ovarian cancer; EpCAM: Epithelial cell adhesion molecule; ERK: Extracellular signal-regulated kinases; ET: Endometrial thickness; FET: Frozen embryo transfer; FGF 2: Fibroblast growth factor 2; FHF: Fulminant hepatic failure; foxa 2: Forkhead box A2; FoxO3a: Forkhead O-3a; FOXP3: Forkhead transcription factor-3; GMP: Good manufacturing practice; GRO: Growth-related oncogene; HGF: Hepatocyte growth factor; HIF-1α: Hypoxia inducible factor-1 alpha; HLA-DR: Human leukocyte antigen-DR isotype; HSCs: Hepatic stellate cells; IDO1: Indoleamine 2,3-dioxygenase-1; IFN-γ: Interferon-γ; IL: Interleukin; KGF: Keratinocyte growth factor; LIN: Lineage; LPS: Lipopolysaccharide; MCP-1: Monocyte chemoattractant protein 1; MenSC-Ex: MenSC-derived exosomes; MenSCs: Menstrual blood-derived stem cells; MHC: Major histocompatibility complex; MI: Myocardial infarction; miRs: MicroRNAs; MLR: Mixed lymphocyte reaction; MMP: Matrix metalloproteinases; MSCs: Mesenchymal stem cells; NE: Non-endometriosis; ngn 3: Neurogenin 3; nkx 6.1: NK homeobox factor 6.1; NT-3: Neurotrophin 3; NTFs: Neurofibrillary tangles; OCT-4: Octamer binding transcription factor 4; OGD: Oxygen glucose deprivation; OLT: Orthotopic liver transplantation; OPG: Osteoprotegerin; pax: Paired box gene; PB: Peripheral blood; PBMCs: Peripheral blood mononuclear cells; PCNA: Proliferating cell nuclear antigen; PDGF: Platelet-derived growth factor; pdx 1: Pancreatic and duodenal homeobox 1; POF: Premature ovarian failure; PTEN: Phosphatase and tensin homolog; Sox2: SRY (sex determining region Y)-box 2; SSEA-4: Stage-specific embryonic antigen-4; STAT 3: Signal transducers and activator of transcription 3; STRO-1: Stromal cell antigen 1; T1DM: Type 1 diabetes mellitus; TNF-α: Tumor necrosis factor α; TRA-1-60: Tumor-rejection antigen-1-60; Tregs: Regulatory T cells; UC: Umbilical cords; VEGF: Vascular endothelial growth factor

Competing interests
The authors declare that they have no competing interests.

References

1. Bianco P. "Mesenchymal" stem cells. Annu Rev Cell Dev Biol. 2014;30: 677–704.
2. Barry FP, Murphy JM. Mesenchymal stem cells: clinical applications and biological characterization. Int J Biochem Cell Biol. 2004;36:568–84.
3. Lee OK, Kuo TK, Chen WM, et al. Isolation of multipotent mesenchymal stem cells from umbilical cord blood. Blood. 2004;103:1669–75.
4. Zuk PA, Zhu M, Ashjian P, et al. Human adipose tissue is a source of multipotent stem cells. Mol Biol Cell. 2002;13:4279–95.
5. In 't Anker PS, Scherjon SA, Kleijburg-van der Keur C, et al. Isolation of mesenchymal stem cells of fetal or maternal origin from human placenta. Stem Cells. 2004;22:1338–45.
6. Korbling M, Anderlini P. Peripheral blood stem cell versus bone marrow allotransplantation: does the source of hematopoietic stem cells matter? Blood. 2001;98:2900–8.
7. Uccelli A, Moretta L, Pistoia V. Mesenchymal stem cells in health and disease. Nat Rev Immunol. 2008;8:726–36.
8. Samsonraj RM, Raghunath M, Nurcombe V, et al. Concise review: multifaceted characterization of human mesenchymal stem cells for use in regenerative medicine. Stem Cells Transl Med. 2017;6:2173–85.
9. Galipeau J, Sensebe L. Mesenchymal stromal cells: clinical challenges and therapeutic opportunities. Cell Stem Cell. 2018;22:824–33.
10. Ren G, Chen X, Dong F, et al. Concise review: mesenchymal stem cells and translational medicine: emerging issues. Stem Cells Transl Med. 2012;1:51–8.
11. Si Y-L, Zhao Y-L, Hao H-J, et al. MSCs: biological characteristics, clinical applications and their outstanding concerns. Ageing Res Rev. 2011;10:93–103.
12. Meng X, Ichim TE, Zhong J, et al. Endometrial regenerative cells: A novel stem cell population. J Transl Med. 2007;5:57.
13. Cui CH, Uyama T, Miyado K, et al. Menstrual blood-derived cells confer human dystrophin expression in the murine model of Duchenne muscular dystrophy via cell fusion and myogenic transdifferentiation. Mol Biol Cell. 2007;18:1586–94.
14. Khoury M, Alcayaga-Miranda F, Illanes SE, et al. The promising potential of menstrual stem cells for antenatal diagnosis and cell therapy. Front Immunol. 2014;5:205.
15. Zhong Z, Patel AN, Ichim TE, et al. Feasibility investigation of allogeneic endometrial regenerative cells. J Transl Med. 2009;7:15.
16. Khanmohammadi M, Khanjani S, Edalatkhah H, et al. Modified protocol for improvement of differentiation potential of menstrual blood-derived stem cells into adipogenic lineage. Cell Prolif. 2014;47:615–23.
17. Khanjani S, Khanmohammadi M, Zarnani AH, et al. Efficient generation of functional hepatocyte-like cells from menstrual blood-derived stem cells. J Tissue Eng Regen Med. 2015;9:E124–34.
18. Zheng SX, Wang J, Wang XL, et al. Feasibility analysis of treating severe intrauterine adhesions by transplanting menstrual blood-derived stem cells. Int J Mol Med. 2018;41:2201–12.
19. Chen L, Xiang B, Wang X, et al. Exosomes derived from human menstrual blood-derived stem cells alleviate fulminant hepatic failure. Stem Cell Res Ther. 2017;8:9.
20. Chen L, Zhang C, Chen L, et al. Human menstrual blood-derived stem cells ameliorate liver fibrosis in mice by targeting hepatic stellate cells via paracrine mediators. Stem Cells Transl Med. 2017;6:272–84.
21. Wang Z, Wang Y, Yang T, et al. Study of the reparative effects of menstrual-derived stem cells on premature ovarian failure in mice. Stem Cell Res Ther. 2017;8:11.
22. Liu T, Huang Y, Zhang J, et al. Transplantation of human menstrual blood stem cells to treat premature ovarian failure in mouse model. Stem Cells Dev. 2014;23:1548–57.
23. Patel AN, Park E, Kuzman M, et al. Multipotent menstrual blood stromal stem cells: isolation, characterization, and differentiation. Cell Transplant. 2008;17:303–11.
24. Nikoo S, Ebtekar M, Jeddi-Tehrani M, et al. Effect of menstrual blood-derived stromal stem cells on proliferative capacity of peripheral blood mononuclear cells in allogeneic mixed lymphocyte reaction. J Obstet Gynaecol Res. 2012;38:804–9.
25. Bozorgmehr M, Moazzeni SM, Salehnia M, et al. Menstrual blood-derived stromal stem cells inhibit optimal generation and maturation of human monocyte-derived dendritic cells. Immunol Lett. 2014;162:239–46.
26. Alcayaga-Miranda F, Cuenca J, Luz-Crawford P, et al. Characterization of menstrual stem cells: angiogenic effect, migration and hematopoietic stem cell support in comparison with bone marrow mesenchymal stem cells. Stem Cell Res Ther. 2015;6:32.
27. Nikoo S, Ebtekar M, Jeddi-Tehrani M, et al. Menstrual blood-derived stromal stem cells from women with and without endometriosis reveal different phenotypic and functional characteristics. Mol Hum Reprod. 2014;20:905–18.

28. Tan J, Li P, Wang Q, et al. Autologous menstrual blood-derived stromal cells transplantation for severe Asherman's syndrome. Hum Reprod. 2016;31: 2723–9.
29. Jiang Z, Hu X, Yu H, et al. Human endometrial stem cells confer enhanced myocardial salvage and regeneration by paracrine mechanisms. J Cell Mol Med. 2013;17:1247–60.
30. Liu Y, Niu R, Yang F, et al. Biological characteristics of human menstrual blood-derived endometrial stem cells. J Cell Mol Med. 2018;22:1627–39.
31. Liu Y, Yang F, Liang S, et al. N-cadherin upregulation promotes the neurogenic differentiation of menstrual blood-derived endometrial stem cells. Stem Cells Int. 2018;2018:3250379.
32. Moreno R, Rojas LA, Villellas FV, et al. Human menstrual blood-derived mesenchymal stem cells as potential cell carriers for oncolytic adenovirus. Stem Cells Int. 2017;2017:3615729.
33. Mou XZ, Lin J, Chen JY, et al. Menstrual blood-derived mesenchymal stem cells differentiate into functional hepatocyte-like cells. J Zhejiang Univ Sci B. 2013;14:961–72.
34. Zhao Y, Chen X, Wu Y, et al. Transplantation of human menstrual blood-derived mesenchymal stem cells alleviates Alzheimer's disease-like pathology in APP/PS1 transgenic mice. Front Mol Neurosci. 2018;11:140.
35. Wu X, Luo Y, Chen J, et al. Transplantation of human menstrual blood progenitor cells improves hyperglycemia by promoting endogenous progenitor differentiation in type 1 diabetic mice. Stem Cells Dev. 2014; 23:1245–57.
36. Lai D, Wang F, Yao X, et al. Human endometrial mesenchymal stem cells restore ovarian function through improving the renewal of germline stem cells in a mouse model of premature ovarian failure. J Transl Med. 2015;13:155.
37. Wang K, Jiang Z, Webster KA, et al. Enhanced cardioprotection by human endometrium mesenchymal stem cells driven by exosomal MicroRNA-21. Stem Cells Transl Med. 2017;6:209–22.
38. Xiang B, Chen L, Wang X, et al. Transplantation of menstrual blood-derived mesenchymal stem cells promotes the repair of LPS-induced acute lung injury. Int J Mol Sci. 2017;18:689.
39. Khanjani S, Khanmohammadi M, Zarnani AH, et al. Comparative evaluation of differentiation potential of menstrual blood- versus bone marrow-derived stem cells into hepatocyte-like cells. PLoS One. 2014;9:e86075.
40. Borlongan CV, Kaneko Y, Maki M, et al. Menstrual blood cells display stem cell-like phenotypic markers and exert neuroprotection following transplantation in experimental stroke. Stem Cells Dev. 2010;19:439–52.
41. Cuenca J, Le-Gatt A, Castillo V, et al. The reparative abilities of menstrual stem cells modulate the wound matrix signals and improve cutaneous regeneration. Front Physiol. 2018;9:464.
42. Allickson JG, Sanchez A, Yefimenko N, et al. Recent studies assessing the proliferative capability of a novel adult stem cell identified in menstrual blood. Open Stem Cell J. 2011;3:4–10.
43. Ren H, Sang Y, Zhang F, et al. Comparative analysis of human mesenchymal stem cells from umbilical cord, dental pulp, and menstrual blood as sources for cell therapy. Stem Cells Int. 2016;2016:1–13.
44. Gargett CE, Masuda H. Adult stem cells in the endometrium. Mol Hum Reprod. 2010;16:818–34.
45. Hida N, Nishiyama N, Miyoshi S, et al. Novel cardiac precursor-like cells from human menstrual blood-derived mesenchymal cells. Stem Cells. 2008;26: 1695–704.
46. Lai D, Guo Y, Zhang Q, et al. Differentiation of human menstrual blood-derived endometrial mesenchymal stem cells into oocyte-like cells. Acta Biochim Biophys Sin. 2016;48:998–1005.
47. Azedi F, Kazemnejad S, Zarnani AH, et al. Differentiation potential of menstrual blood-versus bone marrow-stem cells into glial-like cells. Cell Biol Int. 2014;38:615–24.
48. Shi Y, Su J, Roberts AI, et al. How mesenchymal stem cells interact with tissue immune responses. Trends Immunol. 2012;33:136–43.
49. Wang Y, Chen X, Cao W, et al. Plasticity of mesenchymal stem cells in immunomodulation: pathological and therapeutic implications. Nat Immunol. 2014;15:1009–16.
50. Friedman SL. Hepatic fibrosis -- overview. Toxicology. 2008;254:120–9.
51. Schuppan D, Kim YO. Evolving therapies for liver fibrosis. J Clin Invest. 2013; 123:1887–901.
52. Wang YH, Wu DB, Chen B, et al. Progress in mesenchymal stem cell-based therapy for acute liver failure. Stem Cell Res Ther. 2018;9:227.
53. Phinney DG, Pittenger MF. Concise review: MSC-derived exosomes for cell-free therapy. Stem Cells. 2017;35:851–8.
54. Katsarou A, Gudbjornsdottir S, Rawshani A, et al. Type 1 diabetes mellitus. Nat Rev Dis Primers. 2017;3:17016.
55. Hess DC, Borlongan CV. Cell-based therapy in ischemic stroke. Expert Rev Neurother. 2014;8:1193–201.
56. Ichim TE, Alexandrescu DT, Solano F, et al. Mesenchymal stem cells as anti-inflammatories: implications for treatment of Duchenne muscular dystrophy. Cell Immunol. 2010;260:75–82.
57. Varu VN, Hogg ME, Kibbe MR. Critical limb ischemia. J Vasc Surg. 2010;51: 230–41.
58. Murphy MP, Wang H, Patel AN, et al. Allogeneic endometrial regenerative cells: an "off the shelf solution" for critical limb ischemia? J Transl Med. 2008;6:45.
59. Falconer H, Yin L, Gronberg H, et al. Ovarian Cancer Risk After Salpingectomy: A Nationwide Population-Based Study. J Natl Cancer Inst. 2015;107:dju410.
60. Kurman RJ, Shih IM. The origin and pathogenesis of epithelial ovarian cancer: a proposed unifying theory. Am J Surg Pathol. 2010;34:433–43.
61. Thygesen K, Alpert JS, Jaffe AS, et al. Third universal definition of myocardial infarction. J Am Coll Cardiol. 2012;60:1581–98.
62. Zhang Z, Wang JA, Xu Y, et al. Menstrual blood derived mesenchymal cells ameliorate cardiac fibrosis via inhibition of endothelial to mesenchymal transition in myocardial infarction. Int J Cardiol. 2013;168:1711–4.
63. Myers EM, Hurst BS. Comprehensive management of severe Asherman syndrome and amenorrhea. Fertil Steril. 2012;97:160–4.
64. De Strooper B, Karran E. The cellular phase of Alzheimer's disease. Cell. 2016; 164:603–15.
65. Rubenfeld GD, Herridge MS. Epidemiology and outcomes of acute lung injury. Chest. 2007;131:554–62.
66. Bielefeld KA, Amini-Nik S, Alman BA. Cutaneous wound healing: recruiting developmental pathways for regeneration. Cell Mol Life Sci. 2012;70:2059–81.
67. Taylor HS, Osteen KG, Bruner-Tran KL, et al. Novel therapies targeting endometriosis. Reprod Sci. 2011;18:814–23.
68. Trounson A, McDonald C. Stem cell therapies in clinical trials: progress and challenges. Cell Stem Cell. 2015;17:11–22.
69. Wang X-J, Xiang B-Y, Ding Y-H, et al. Human menstrual blood-derived mesenchymal stem cells as a cellular vehicle for malignant glioma gene therapy. Oncotarget. 2017;8:58309–21.

Comparative analysis of mesenchymal stem cells derived from amniotic membrane, umbilical cord, and chorionic plate under serum-free condition

Abstract

Background: Mesenchymal stem cells (MSCs) have emerged as a promising regenerative tool, owing mainly to their multi-differentiation potential and immunosuppressive capacity. When compared with MSCs classically derived from the adult bone marrow (BM), MSCs of neonatal origins exhibit superior proliferation ability, lower immunogenicity, and possible lower incorporated mutation; hence, they are considered as an alternative source for clinical use. Several researches have focused on the biological differences among some neonatal MSCs cultured in serum-containing medium (SCM). However, since it has been reported that MSCs possess different biological characteristics when cultured in serum-free medium (SFM), these comparative studies in SCM cannot exactly represent the results under the serum-free Good Manufacturing Practice (GMP) standard.

Methods: Here, MSCs were isolated from three neonatal tissues, namely amniotic membrane (AM), umbilical cord (UC), and chorionic plate (CP), from the same donor, and their morphologies, immunophenotypes, trilineage differentiation potentials, global gene expression patterns, and proliferation abilities were systematically compared under chemical-defined SFM.

Results: Our study demonstrated that these three neonatal MSCs exhibited a similar morphology and immunophenotypic pattern but various mesodermal differentiation potentials under SFM: amniotic membrane-derived MSCs showed a higher rate for osteogenic differentiation; chorionic plate-derived MSCs presented better adipogenic induction efficiency; and all these three neonatal MSCs exhibited similar chondrogenic potential. Moreover, by the analysis of global gene expression patterns, we speculated a possible higher proliferation ability of CP-MSCs in SFM, and we subsequently validated this conjecture.

Conclusions: Collectively, these results suggest that MSCs of different neonatal origins possess different biological features in SFM and thus may represent an optimal choice for different clinical applications.

Keywords: Mesenchymal stem cells, Serum-free medium, Amniotic membrane, Umbilical cord, Chorionic plate, Trilineage differentiation efficiency, Gene expression pattern

Background

Mesenchymal stem cells (MSCs) are somatic stem cells which originate from mesoderm, and can differentiate into multi-lineages including adipocytes, osteocytes, chondrocytes, epithelial cells, neuron-like cells, and hepatocyte-like cells [1–3]. In addition, because of their low immunogenicity and capability to potently suppress or ameliorate immune responses [4], MSCs are considered as ideal candidates for therapeutic applications. After the first successful isolation from bone marrow (BM) in 1976 [5], MSCs have been subsequently isolated from a wide range of other tissues, such as adipose tissues, umbilical cord blood, placenta, skin, and hair follicles [6–9]. Over the past few years, MSCs derived from placentome tissues have attracted intensive attentions of more and more researchers [10], owing mainly to their non-invasive isolation methods, large-scale supply, and minimized ethical issues [11]. Moreover, it has been reported that mutations accumulate steadily over time and intrinsic mutational processes in adult stem cells can initiate tumorigenesis [12]. Hence, in comparison with those derived from adult BM or adipose tissues, MSCs derived from term placentome tissues can be immature cells with superior proliferation ability, lower immunogenicity [13], and possible lower incorporated mutation [14], which make them better options for clinical use. Different MSCs have been successively isolated from different layers of placentome tissues, including umbilical cord (UC), amniotic membrane (AM), chorionic plate (CP), chorionic villi (CV), and maternal decidua [15–18]. Considering the partly maternal origin of CV tissues [19], we thus focused on MSCs derived from the rest three neonatal tissues, namely amniotic membrane-derived MSCs (AM-MSCs), umbilical cord-derived MSCs (UC-MSCs), and chorionic plate-derived MSCs (CP-MSCs).

Meanwhile, as a heterogenous population of multi-potent stem cells with typical fibroblast-like morphology, MSCs of different tissue origins or culture conditions may exhibit diverse biological potentials [20]. Although AM-MSCs, UC-MSCs, and CP-MSCs share many more similarities and present even closer relations when compared with MSCs derived from adult tissues, it has been demonstrated that they also present different faces with each other. Wegmeyer et al. [15] reported that AM-MSCs and UC-MSCs showed different growth characteristics and distinct gene expression patterns. Kim et al. [18] reported that CP-MSCs possessed higher expression of adipogenesis-related genes but lower ability of mineralized matrix accumulation ability when compared with UC-MSCs. Araújo et al. [17] reported that MSCs of four neonatal sources (AM, UC, chorionic membrane, and placental decidua) presented relatively lower ability of adipogenesis but superior efficiency in osteogenesis. However, studies mentioned above paid their attention on neonatal MSCs cultured in serum-containing medium (SCM), which might bring uncertainties to the results owing to the appreciable batch-to-batch variation of serum. Even worse, the safety issues associated with animal or human serum can be never ignored, thus the utilization of SCM might thoroughly hinder the further clinical applications of these MSCs, due to a risk of the infectious pathogen contamination. Furthermore, it has been reported that human UC-MSCs cultured in serum-free medium (SFM) exhibited differently in growth rate, telomerase, and gene expression profile [21], which suggested that the comparative work performed in SCM cannot exactly represent the results in SFM.

Within this context, we designed the present study to systematically compare AM-MSCs, UC-MSCs, and CP-MSCs in chemical-defined SFM. These three MSCs were isolated from the placenta of the same donor, cultured in SFM; their morphologies, immunophenotypes, trilineage differentiation potentials, and proliferation abilities were compared and their different gene expression patterns were analyzed to evaluate their potential clinical applications in cell therapies in further studies.

Methods

Isolation and culture of AM-MSCs, UC-MSCs, and CP-MSCs

Healthy full-term human placental samples were collected according to the policy of the Ethics Committee of the 306th Hospital of the Chinese People's Liberation Army, Beijing, China. Written informed consents were obtained from all donors before this study. Collected placentas were sterilely kept on ice and processed by explant methods within 4 h post-delivery. All the samples were used in accordance with standard experimental protocols approved by the Ethical Committee of Institute of Zoology, Chinese Academy of Sciences.

Briefly, UC tissues were cut into small sections, and the veins and arteries were clearly removed. Then, the AM and CP tissues were successively peeled from the human placenta. All the tissues were thoroughly washed with cold Dulbecco's phosphate-buffered saline (DPBS; Gibco, Grand Island, NY, USA) and then separately cut into 0.5–1 mm^3 small pieces. Minced small explants were transferred into 100-mm plates (Corning, NY, USA). A chemical-defined SFM (MSCGM-CD; Lonza, Walkersville, MD, USA) was carefully added. The plates were kept in 37 °C, 5% CO_2 humidified atmosphere (Thermo Fisher Scientific, San Diego, CA, USA), and fresh medium was changed every other day. Colonies with fibroblast morphology usually appeared 10–14 days afterwards. At around 80% confluence, cells were detached using TrypLE™ Express (Invitrogen, Carlsbad, CA, USA) and then spilt at the ratio of 1: 3. Cells at passage 5 were utilized for all the further experiments.

Flow cytometric analysis

The immunophenotype of MSCs was analyzed with the following antibodies: FITC-conjugated CD14, CD19, and

CD45, and PE-conjugated CD34, CD73, CD90, CD105, and HLA-DR. Corresponding isotype-matched antibodies were used as controls. All the antibodies were purchased from BD Pharmingen (Franklin Lakes, NJ, USA). Cells were analyzed by flow cytometry using CytoFLEX (Beckman Coulter, Indianapolis, IN, USA). Data analysis was performed with CytExpert software (Beckman Coulter).

Trilineage differentiation

Adipogenic, osteogenic, and chondrogenic differentiation experiments were performed following the instructions of human mesenchymal stem cell functional identification kit (R&D systems, Inc., Wiesbaden, Germany).

For adipogenic differentiation, MSCs were seeded into a 24-well plate at the density of 3.7×10^4 cells/well, and maintained in culture medium until 100% confluency. Cells were then exposed to adipogenic differentiation medium for 3 weeks. Lipid droplets of the resultant differentiated cells were detected using Oil red staining (Sigma-Aldrich, St. Louis, MO, USA).

For osteogenic differentiation, 4.2×10^3 cells were seeded per well. When cells reached 50–70% confluency, the medium was replaced with osteogenic differentiation medium and kept for 3 weeks. To assess osteogenic differentiation, Alizarin Red S staining (Sigma-Aldrich) was performed for the calcium-rich extracellular matrix.

For chondrogenic differentiation, 2.5×10^5 cells resuspended in chondrogenic differentiation medium were centrifuged for 5 min at 200×*g* in a 15-mL conical tube (Corning). After 3 weeks, a chondrogenic pellet was harvest and fixed in 4% paraformaldehyde (PFA). Cryosection was performed and sections were stained with Alcian Blue (Sigma-Aldrich).

RNA extraction and real-time PCR

Total RNA was isolated from MSCs using Trizol Reagent (Invitrogen) according to manufacturer's instructions. Quality of RNA was controlled with NanoDrop 2000 spectrophotometer (Thermo Fisher Scientific). The cDNA was prepared by SuperScript™ II (Thermo Fisher Scientific) using 2 μg RNA.

To comparatively analyze the expression level of trilineage differentiation-related genes, the SYBR Green (TaKaRa, Dalian, China) detection method was employed and real-time quantitative PCR was performed on LightCycler 480 (Roche Applied Science, Indianapolis, IN, USA) with an annealing temperature of 60 °C using customized Real-Time ready 384 Panel (Roche Applied Science). The relative expression level of the differentiation-related genes in one particular induced MSC sample was normalized to 1, and the relative expression fold in other induced MSC samples was shown as $2^{-\Delta\Delta Ct}$. Real-time PCR was performed with samples from three independent donors, and each sample was tested in triplicate. Primers involved were listed in Additional file 1: Table S1.

Transcriptome analysis

Four pairs of AM-MSC, UC-MSC, and CP-MSC RNA samples (12 samples in total) were sent to Annoroad Company for mRNA sequencing (RNA-Seq). The sequencing library for Illumina HiSeq 4000 sequencer was constructed with 0.2 μg of total RNA of each sample by PE150 strategy. Raw data and processed data were uploaded to the NCBI Gene Expression Omnibus database (accession number GSE118808). Data analysis was executed as previously reported [22]. Low expressed genes were removed. All 0 FPKM values were replaced by 0.01. We eventually identified 763 differentially expressed genes among these three MSCs based on twofold differences from 6637 genes. Unsupervised hierarchical clustering analysis was performed using Cluster 3.0 [23]. After the log-transformation of the input data, we then selected center genes with median. The adjusted data on genes and arrays were clustered using the average linkage method. Clustering results were presented and exported by TreeView 1.1.6r4 [23]. The principal component analysis (PCA) was made by R (3.5.0)/Bioconductor (3.7) with the "edgeR" and "limma" packages [24]. Kyoto Encyclopedia of Genes and Fenomes (KEGG) [25] and gene ontology–biological process (GO-BP) [26] enrichment analyses were performed using R/Bioconductor with the "clusterProfiler" package [27]. The Venn diagram was constructed at http://genevenn.sourceforge.net /.

Colony-forming unit (CFU) assay

To assess the self-renewal capacity of MSCs, CFU-F efficiency assay was performed. 1×10^3 viable cells at passage 5 were seeded in 100-mm plates (Corning). Following the cultivation for around 14 days (before colonies began to merge), the MSCs were washed with DPBS (Invitrogen), fixed with 4% PFA for 10 min and then stained with 1% toluidine blue (Sigma-Aldrich) solution for 30 min at room temperature. Stained colonies with at least 50 cells were counted for further analysis.

Cell Counting Kit-8 (CCK8) assay

The experiments were performed following the instructions of Cell Counting Kit-8 (Sigma-Aldrich). MSCs of all three neonatal origins at passage 5 were utilized for the assay. Briefly, a total of 2×10^3 viable cells were plated in each well of the 96-well plates (Corning). After the incubation for the first 24 h, the viable cell number was then tested every 24 h for seven consecutive days. To determine the number of viable MSCs, the optical density value at 450 nm was detected with Enspire™ Multimode Plate Reader (PerkinElmer, Baesweiler, Germany).

Statistical analysis

Statistical analysis was performed using GraphPad Prism 5.0 software (Graph Pad Software, Inc., San Diego, CA, USA). All data were presented as the mean ± SEM. One-way ANOVA followed by Bonferroni multiple comparisons was utilized to determine the statistical significance. The result was considered of statistical significance when $p < 0.05$.

Results

AM-MSCs, UC-MSCs, and CP-MSCs exhibited similar morphology and immunophenotypic profiles

For the establishment of these three neonatal MSCs, healthy full-term placental samples were collected and processed within 4 h post-delivery. After the isolation of primary AM-MSCs, UC-MSCs, and CP-MSCs using explant methods, these MSCs were respectively expanded in the chemical-defined SFM. The morphologies of MSCs at passage 5 were assessed using inverted phase contrast microscopy. MSCs derived from all these three neonatal sources retained a fibroblast-like morphology and exhibited the spiral-shaped characteristics when reached confluence (Fig. 1a).

Flow cytometric analysis was then performed according to the MSC criteria proposed by the International Society for Cellular Therapies (ISCT) [1], which stipulated that the MSC population must express (≥ 95%) CD105, CD73, and CD90 but lack expression (≤ 2% positive) of CD45, CD34, CD14 or CD11b, CD79a or CD19, and HLA class II. MSC samples from three individual donors were analyzed, and our data demonstrated that all the three MSCs were negative for the MHC class II molecule HLA-DR, showed low expression of endothelial and hematopoietic markers (CD45, CD34, CD19, and CD14), and highly expressed typical MSC markers (CD73, CD90, and CD105) (Fig. 1b). It was revealed that there was no difference among these three MSCs in terms of immunophenotypic patterns (see Additional file 2: Figure S1).

CP-MSCs exhibited superior adipogenic potential

To test the adipogenic potentials of AM-MSCs, UC-MSCs, and CP-MSCs expanded in SFM, these three MSCs at passage 5 were cultured in the commercial adipogenic induction medium. At around 7 days post induction, MSCs turned to be flat and lipid vacuoles started to appear in the induced cells. After 21 days of induction, cells were fixed, and then the adipogenesis was verified by Oil Red O staining. The accumulation of cytoplasmic oil droplets could be distinctly observed in CP-MSCs while relatively weakly stained in UC-MSCs or AM-MSCs (Fig. 2a–c), indicating the superior adipogenic potential of CP-MSCs.

Real-time PCR was then performed to further confirm the adipogenic efficiency of these three MSCs. The quantification of *LEP*, *PPARG*, and *ADIPSIN* mRNA expression levels revealed that CP-MSCs exhibited the highest adipogenic efficiency (Fig. 2d–f), which was consistent with the results of Oil Red O staining. It was also shown that UC-MSCs expressed significantly higher *LEP* (Fig. 2d; $p < 0.001$) and *PPARG* (Fig. 2e; $p < 0.01$) than AM-MSCs, which indicated a superior adipogenic potential of UC-MSCs over AM-MSCs. Thus, it was concluded that among these three neonatal MSCs, the adipogenic potential was high in CP-MSCs, moderate in UC-MSCs, but relatively low in CP-MSCs.

AM-MSCs showed superior osteogenic potential

To test the osteogenic potentials of AM-MSCs, UC-MSCs, and CP-MSCs, these three MSCs at passage 5 were cultured in the commercial osteogenic induction medium. After the incubation in osteogenic induction medium for around 21 days, Alizarin Red staining was performed when cells started to detach. The staining results confirmed that all the three MSCs underwent osteogenic differentiation, but with variable efficiencies. The red staining results indicating calcium deposit were very clear in AM-MSCs and moderate in UC-MSCs, while weak in CP-MSCs, which indicated a gradient descent of osteogenic potentials from AM-MSCs, UC-MSCs, to CP-MSCs (Fig. 3a–c).

The osteogenic capacity was then further evaluated by measuring the relative mRNA expression of related markers. According to the expression of *ON*, *OCN*, and *RUNX2*, expression level was three times higher in AM-MSCs than in CP-MSCs (Fig. 3d–e; $p < 0.001$). The expression level of *ON* showed a significant decrease from AM-MSCs to UC-MSCs and from UC-MSCs to CP-MSCs (Fig. 3d; $p < 0.05$). The quantification of *OCN* and *RUNX2* expression also showed to be three times higher in AM-MSCs than in UC-MSCs (3E-F; $p < 0.001$). Taken together with the Alizarin Red staining results, it was concluded that among these three neonatal MSCs, osteogenic efficiency was high in AM-MSCs, moderate in UC-MSCs, and low in CP-MSCs.

AM-MSCs, UC-MSCs, and CP-MSCs displayed a similar chondrogenic potential

To test the chondrogenic potentials of AM-MSCs, UC-MSCs, and CP-MSCs expanded in SFM, these three MSCs at passage 5 were centrifuged in a 15-mL conical tube. After culture with the commercial chondrogenic induction medium for around 21 days, the chondrocyte pellets formed and were fixed and frozen sectioning was performed. The sections were then stained with Alcian Blue indicating cartilage proteoglycans. All tested MSCs exhibited positive staining results, and there was no obvious difference among AM-MSCs, UC-MSCs, and CP-MSCs (Fig. 4a–c).

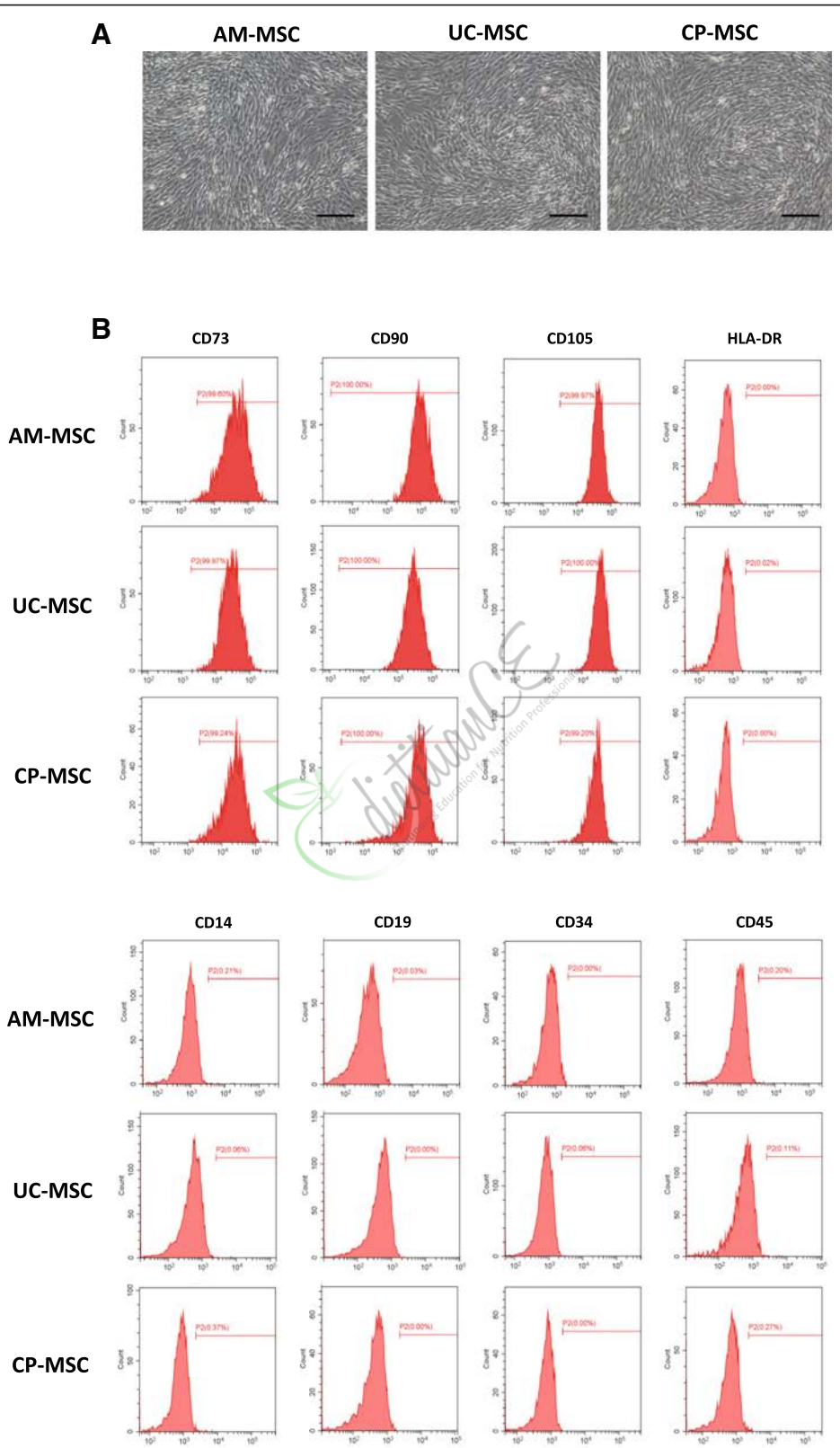

Fig. 1 Morphology and immunophenotype of MSCs derived from AM, UC, and CP. **a** Phase-contrast microscope images of MSCs at passage 5. *Scale bar* = 200 μm. **b** Representative pictures of flow cytometric analysis of the surface marker expression on AM-MSCs, UC-MSCs and CP-MSCs

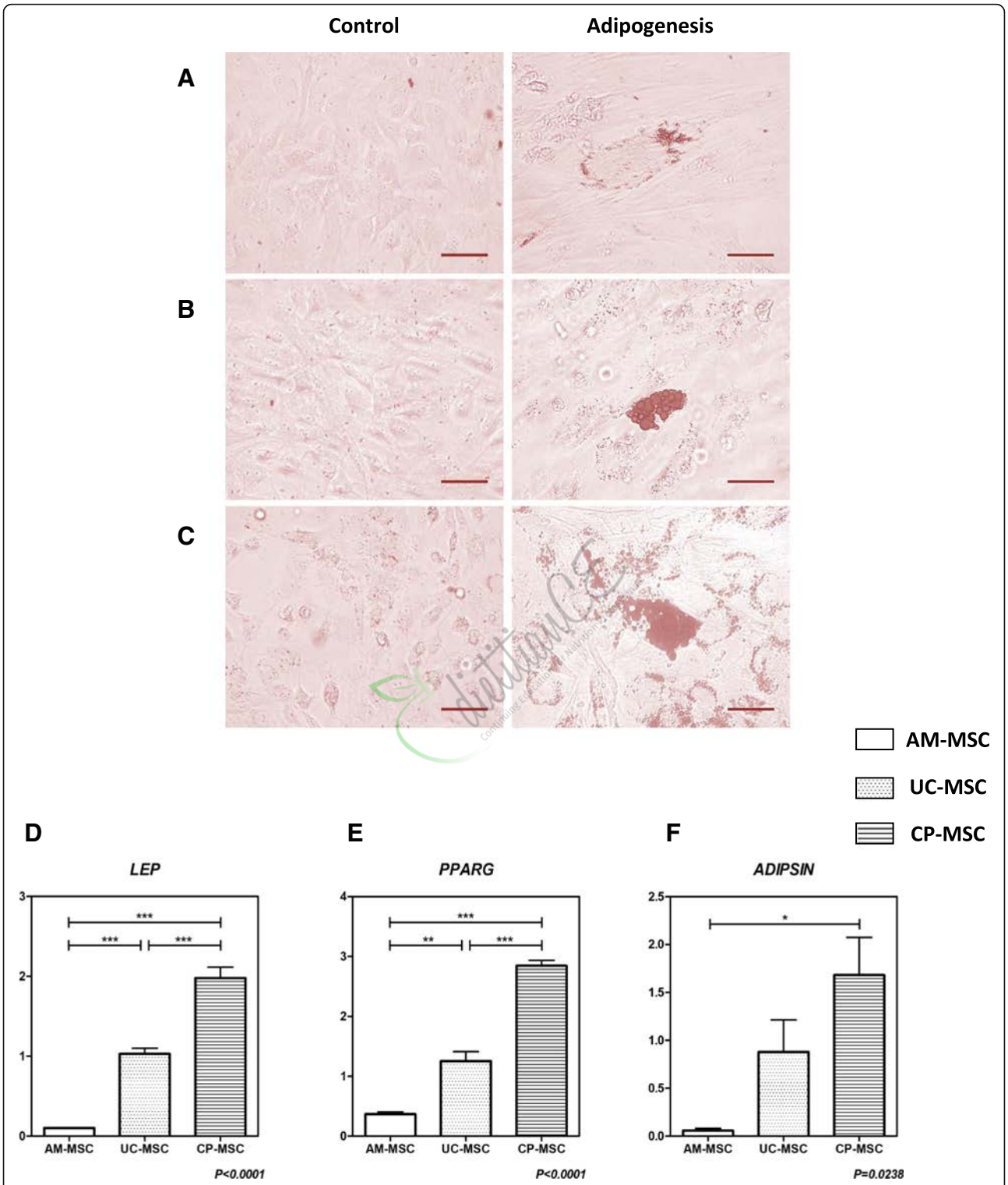

Fig. 2 Adipogenesis of AM-MSCs, UC-MSCs, and CP-MSCs. **a–c** Representative pictures of three MSCs before and after the adipogenic differentiation were shown. The differentiation results of AM-MSCs (**a**), UC-MSCs (**b**), and CP-MSCs (**c**) were confirmed by Oil Red O staining. *Scale bar* = 50 μm. **d–f** Real-time PCR was performed to measure the relative expression levels of adipogenic differentiation related genes: *LEP* (**d**), *PPARG* (**e**), and *ADIPSIN* (**f**). All data were presented as the mean ± SEM ($n = 3$). Each sample was replicated in triplicates. *$p < 0.05$; **$p < 0.01$; ***$p < 0.001$

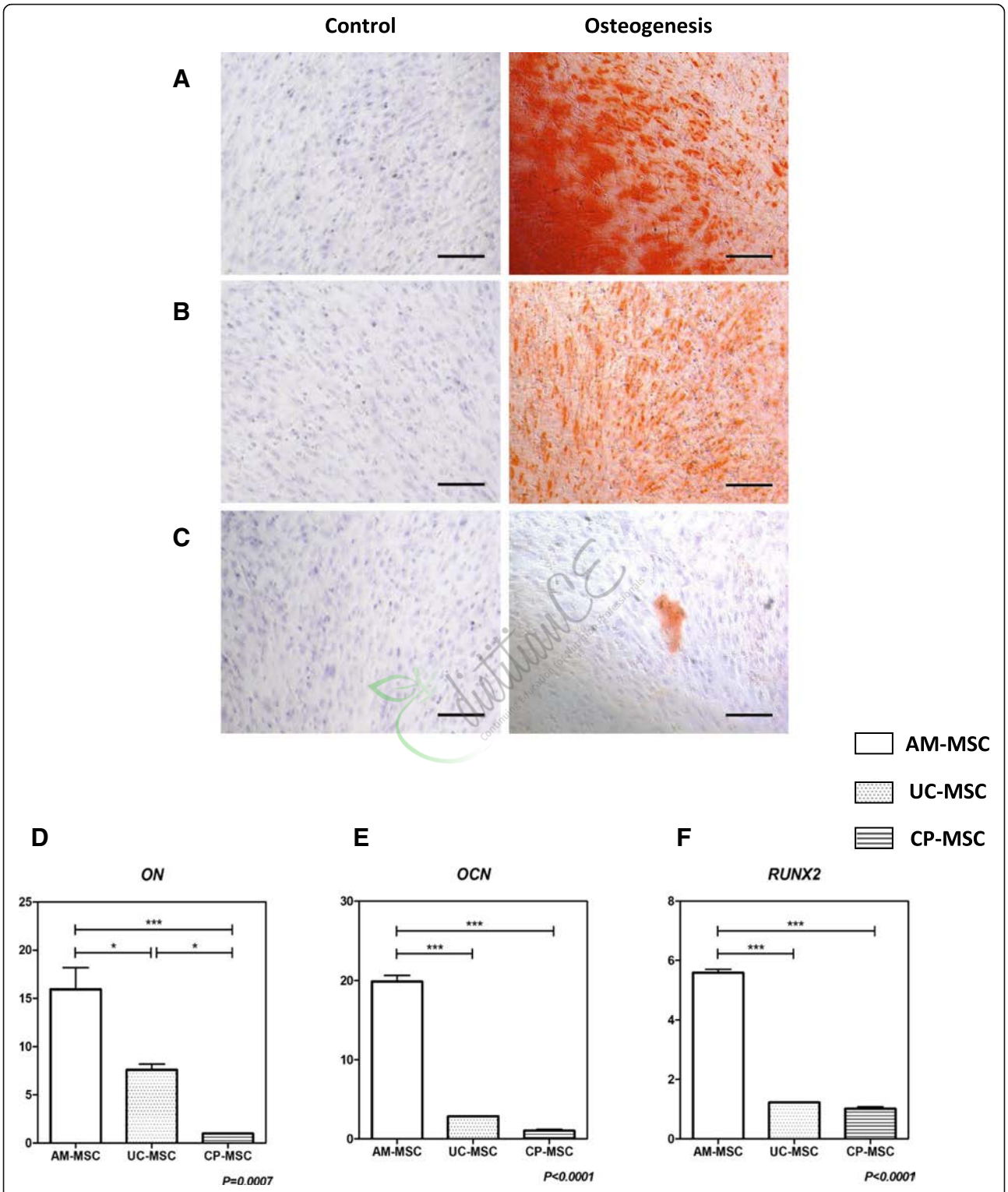

Fig. 3 Osteogenesis of AM-MSCs, UC-MSCs, and CP-MSCs. **a–c** Representative pictures of three MSCs before and after the osteogenic differentiation were shown. The differentiation results of AM-MSCs (**a**), UC-MSCs (**b**), and CP-MSCs (**c**) were confirmed by Alizarin Red staining. *Scale bar* = 200 μm. **d–f** Real-time PCR was performed to measure the relative expression levels of osteogenic differentiation related genes: *ON* (**d**), *OCN* (**e**), and *RUNX2* (**f**). All data were presented as the mean ± SEM ($n = 3$). Each sample was replicated in triplicates. *$p < 0.05$; ***$p < 0.001$

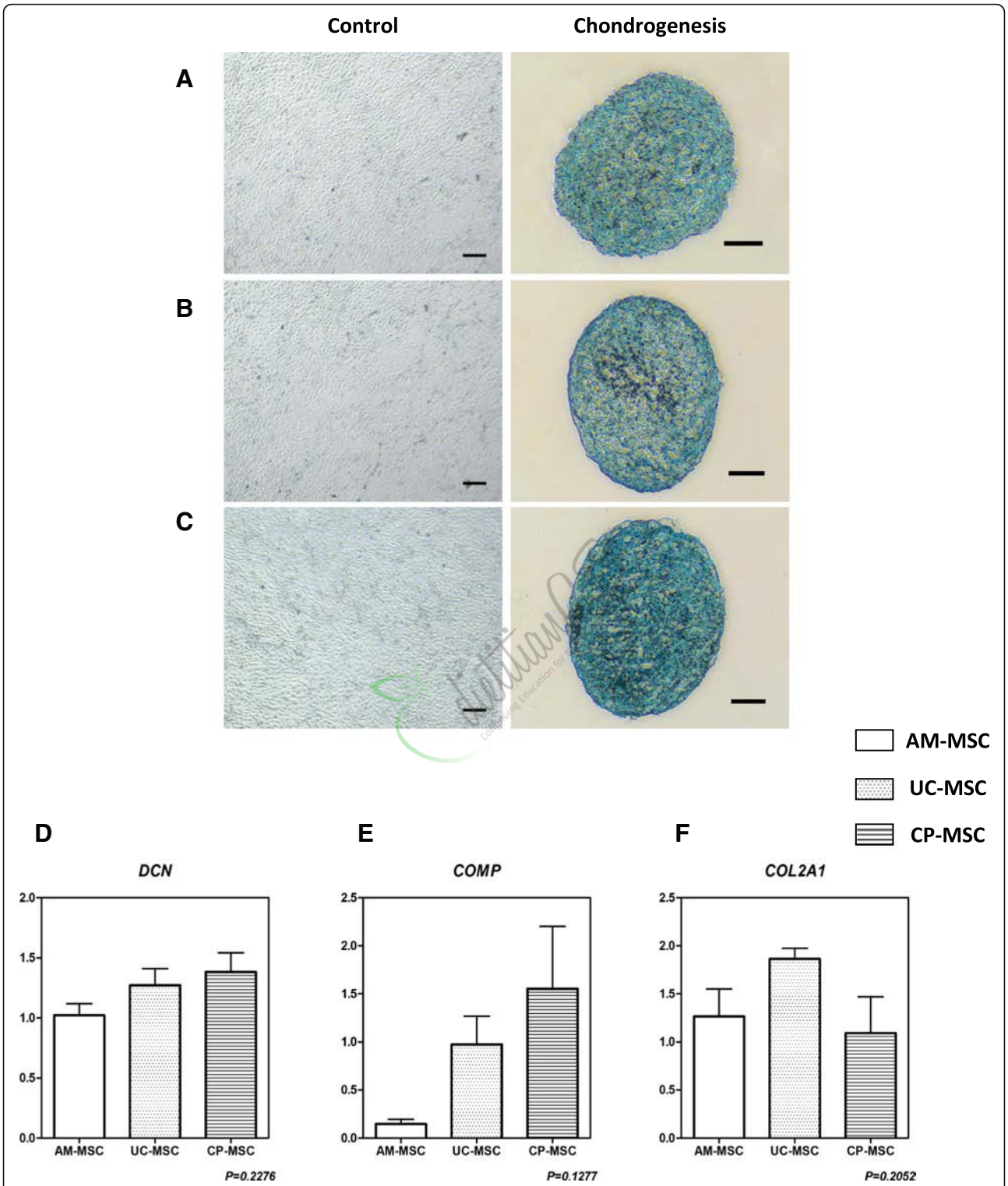

Fig. 4 Chondrogenesis of AM-MSCs, UC-MSCs, and CP-MSCs. **a**–**c** Representative pictures of three MSCs before and after the chondrogenic differentiation were shown. The differentiation results of AM-MSCs (**a**), UC-MSCs (**b**), and CP-MSCs (**c**) were confirmed by Alcian Blue staining. *Scale bar* = 200 μm. **d**–**f** Real-time PCR was performed to measure the relative expression levels of chondrogenic differentiation related genes: *DCN* (**d**), *COMP* (**e**), and *COL2A1* (**f**). All data were presented as the mean ± SEM ($n = 3$). Each sample was replicated in triplicates

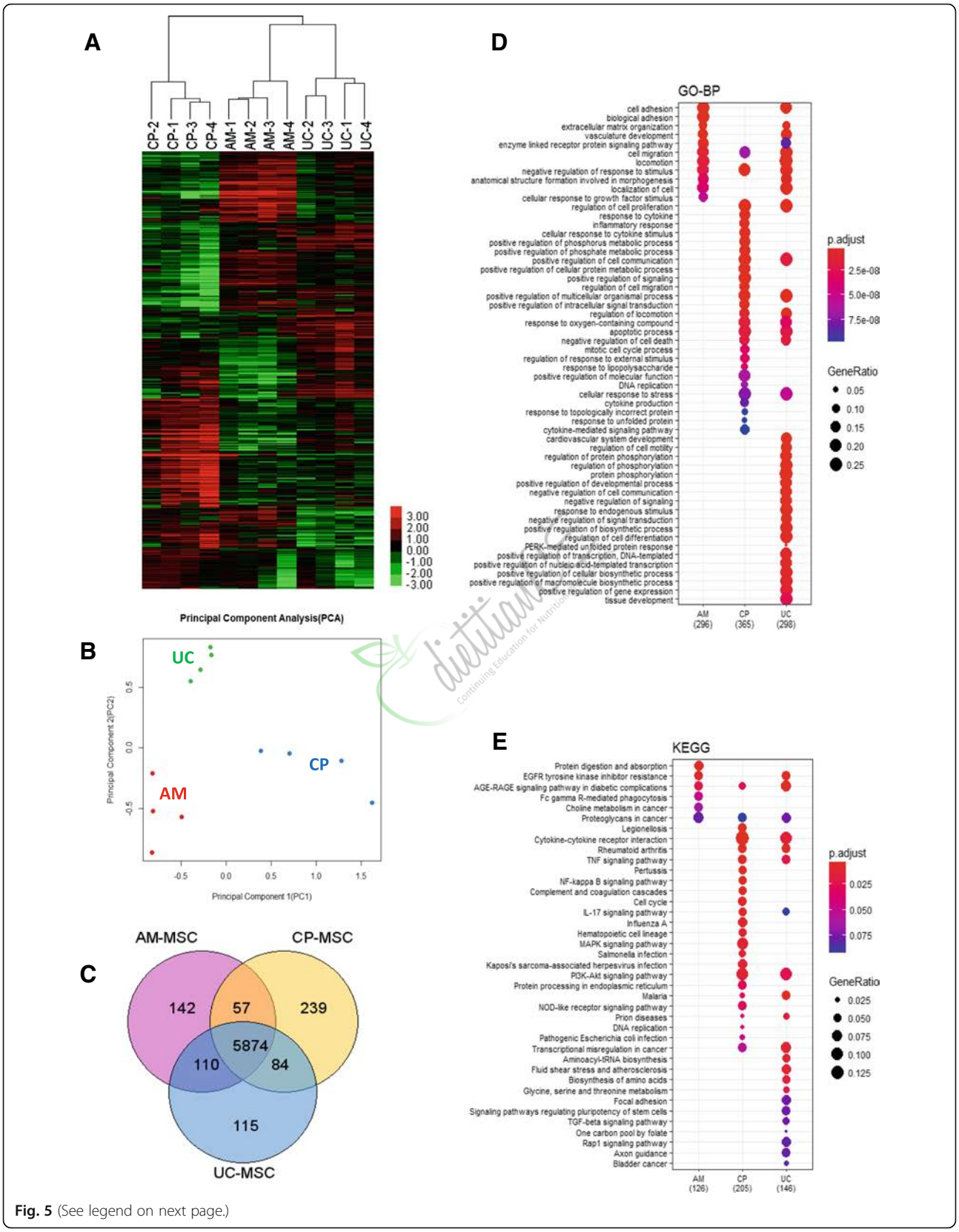

Fig. 5 (See legend on next page.)

(See figure on previous page.)
Fig. 5 Transcriptional analysis of AM-MSCs, UC-MSCs, and CP-MSCs. Hierarchical clustering (**a**) and principal component analysis (**b**) showed a closer relationship between UC-MSCs and AM-MSCs, while CP-MSCs displayed a farther distance from UC-MSCs and AM-MSCs. **c** The number of differentially expressed genes between these three types of MSCs was shown on the Venn diagram. GO-BP (**d**) and KEGG analyses (**e**) were utilized to evaluate the functions of these three types of MSCs based on their differentially expressed genes

Thus, real-time PCR was performed to further evaluate the chondrogenic efficiency. It was found that all these three neonatal MSCs showed a similar chondrogenic potential according to their expression of *DCN*, *COMP*, and *COL2A1* (Fig. 4d–f).

Collectively, the results indicated that MSCs derived from different neonatal tissues exhibited their own superiority to differentiate into different mesodermal lineages when cultured in SFM, suggesting a preferable option of AM-MSCs for osteogenesis and CP-MSCs for adipogenesis.

Transcriptional differences among the three types of MSCs

To investigate the transcriptional differences among these three MSCs expanded in SFM, four individual sample sets of AM-MSCs, UC-MSCs, and CP-MSCs at passage 5 were analyzed using RNA-Seq. The differentially expressed gene information and the relationship among these three MSCs were presented in the heat map (Fig. 5a) and the PCA image (Fig. 5b). It was found that each type of MSCs from four different donors could be clustered into the same group. UC-MSCs together with AM-MSCs could be clustered into a larger group, while CP-MSCs showed a little distant relationship from the former two.

To further understand the functional differences among the three types of MSCs, 142, 115, and 239 specifically expressed genes in AM-MSCs, UC-MSCs, and CP-MSCs were identified respectively (Fig. 5c and Additional file 3: Table S2). The expression patterns of these specifically expressed genes were illustrated and their functions were annotated based on the biological process (Fig. 5d) and signaling pathway (Fig. 5e) involved. Through the GO-BP analysis, it was suggested that AM-MSCs specifically expressed genes involved in biological adhesion. With respect to UC-MSCs, they specifically expressed genes related mainly to cardiovascular system development, cell motility, protein phosphorylation, cell communication, and biosynthetic process. CP-MSCs differentially upregulated genes involved mainly in response to cytokine, cytokine production, and inflammatory response (Fig. 5d), suggesting that CP-MSCs might display specific biological features such as immunological characteristics and cytokine secretion capability. It was also noticed that UC-MSCs specifically expressed genes involved in response to endogenous stimuli, while CP-MSCs highly expressed genes related to regulation of response to exogenous stimuli, in accordance with the biological functions of human placenta during the fetal development. Moreover, it took note that CP-MSCs specifically upregulated genes related to mitotic cell cycle process and DNA replication, consistent with the KEGG pathway analysis results (Fig. 5e), which together suggested that CP-MSCs possessed higher proliferation ability.

CP-MSCs showed higher proliferation ability

To confirm the hypothesis that CP-MSCs might possess the higher proliferation ability, CFU test was performed to compare the proliferation capacity of these three neonatal MSCs. After the toluidine blue staining of cells, stained colonies were counted and then analyzed. The staining results clearly revealed that AM-MSCs exhibited the lowest proliferation ability among these three types of MSCs (see Additional file 4: Figure S2). Through the statistical analysis, it was indicated that CP-MSCs displayed significantly higher proliferation ability than AM-MSCs, while the proliferation ability differences between AM-MSCs and UC-MSCs were of no significance (Fig. 6a). In order to further confirm the higher proliferation ability of CP-MSCs, the three MSCs were then seeded at the same quantity for the CCK8 assay. The results revealed that the viable cell quantity among these three neonatal MSCs was almost the same at the first 3 days, but started to be significantly different from day 4 (Fig. 6b). The tendency of the growth curve once again verified our hypothesis that CP-MSCs possessed higher proliferation ability. Through the analysis of terms of CP-MSCs enriched in GO, we found that many of them were related to the positive regulation of cell proliferation or the negative regulation of cell death (see Additional file 5: Table S3). We then tried to dig further by analyzing CP-MSC specifically high-expressing genes involved in cell cycle pathway (Fig. 6c). We found that 12 genes in the cell cycle pathway were significantly higher expressed in CP-MSCs than in the other two neonatal MSCs. The higher expression of cyclin-dependent kinase gene (*CDK1*, as shown in Fig. 6c) could partly explain why CP-MSCs proliferated faster than the other two neonatal MSCs in SFM, considering its key role in the cell cycle [28]. Moreover, we found that many genes in Mini-Chromosome Maintenance (MCM) complex

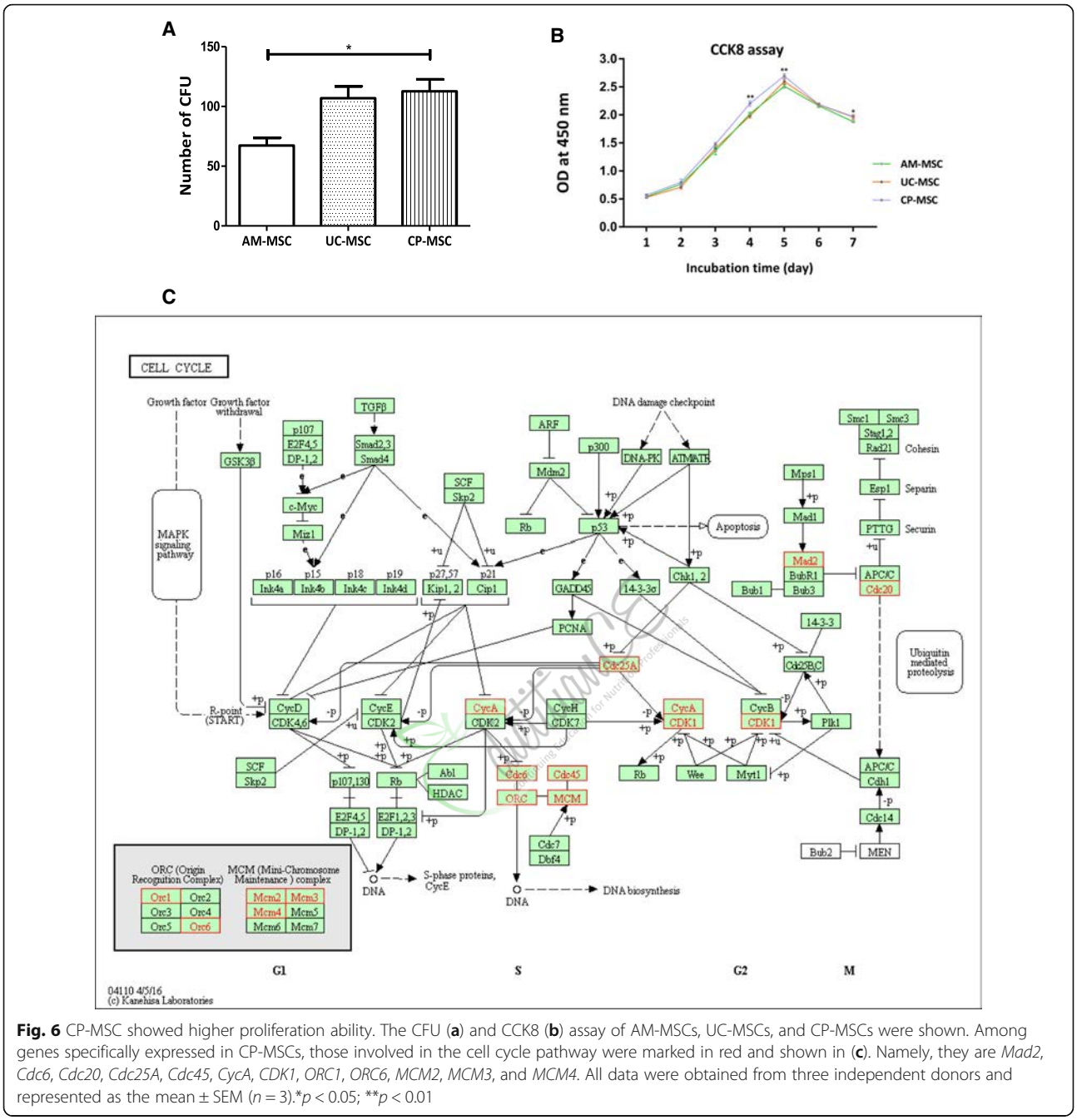

Fig. 6 CP-MSC showed higher proliferation ability. The CFU (**a**) and CCK8 (**b**) assay of AM-MSCs, UC-MSCs, and CP-MSCs were shown. Among genes specifically expressed in CP-MSCs, those involved in the cell cycle pathway were marked in red and shown in (**c**). Namely, they are *Mad2*, *Cdc6*, *Cdc20*, *Cdc25A*, *Cdc45*, *CycA*, *CDK1*, *ORC1*, *ORC6*, *MCM2*, *MCM3*, and *MCM4*. All data were obtained from three independent donors and represented as the mean ± SEM ($n = 3$).*$p < 0.05$; **$p < 0.01$

were also highly expressed in CP-MSCs. As an essential component of the pre-replication complex, MCM is of great importance for the initiation and elongation of DNA replication [29]. The higher expression of MCM might also promote the synthesis of DNA and then accelerate the proliferation of CP-MSCs in the SFM.

Discussion

Human neonatal tissue-derived MSCs have been considered as promising candidates for cell therapy; however, comparative studies have indicated that MSCs of different neonatal origins or cultured under different conditions can exhibit different characteristics. In this study, AM-MSCs, UC-MSCs, and CP-MSCs were isolated and expanded in the chemical-defined commercial SFM, and their morphology immunophenotypes, trilineage differentiation potentials, and global gene expression patterns were systematically compared. The results showed that all these three MSCs exhibited typical MSC morphologies and immunophenotypic profiles, consistent with previous reported results in SCM [18].

As for the detailed trilineage differentiation efficiency, the results turned to be a little confusing. It was reported that the adipogenesis efficiency was higher in CP-MSCs than in UC-MSCs, whereas UC-MSCs exhibited more mineralized matrix accumulation than CP-MSCs in SCM [18], consistent with our results observed in SFM. It was also reported that MSCs of neonatal sources presented lower adipogenic ability but superior efficiency in osteogenesis in SCM [17]; however, when cultured in SFM, it was found that MSCs of different neonatal origins exhibited differently: the adipogenic ability of AM-MSCs was indeed very limited, while the ability of CP-MSCs and UC-MSCs was inspiring; AM-MSCs did show superior efficiency in osteogenic differentiation, whereas CP-MSCs could be hardly induced for osteogenesis. Taken together, our results indicated that MSC trilineage differentiation efficiency could be very different when cultured in SFM. As for the underlying molecular mechanisms, there are barely related researches reported yet. How can MSCs of different neonatal origins possess different trilineage differentiation potentials? To figure out this question, the transcriptome analysis of the three MSCs at serial differentiation points might be one direction remained for further work.

The global gene expression pattern analysis among MSCs derived from different neonatal tissues has been reported previously [15, 30]; however, as far as we know, there has been no comparative analysis of gene expression patterns among AM-MSCs, UC-MSCs, and CP-MSCs cultured in SFM reported yet. Considering that UC-MSCs displayed different gene expression patterns when cultured in SFM [21], our data first provided the differentially expressed gene information among these three neonatal MSCs cultured under the serum-free GMP condition. We were very interested that CP-MSCs specifically expressed genes involved in the mitotic cell cycle process and DNA replication, suggesting a stronger proliferation ability of CP-MSCs. Thus, CFU and CCK8 assay were performed and this speculation was finally validated. GO-BP results showed that CP-MSCs also specifically expressed genes related to the response to cytokine, cellular response to cytokine stimuli, cytokine production, and cytokine-mediated signal pathway, suggesting that placental CP-MSCs could potently secret cytokines and thus might exhibit some specific features, and we would like to take this as one of our future directions. Besides, some comparative studies reported before have discussed the heterogeneity of in vitro cultured MSCs. However, as for the deeper mechanisms whereby MSCs of different tissue origins or culture conditions could exhibit diverse biological features, they are left for more future work to unveil.

Conclusions

In conclusion, our results presented the different trilineage differentiation potentials, gene expression patterns, and proliferation abilities among AM-MSCs, UC-MSCs, and CP-MSCs in SFM. To the best of our knowledge, this is the first systematic comparative work of MSCs from all these three neonatal tissues in the chemical-defined SFM. Our findings provide information and thus will contribute to the development of MSC-based cell therapy when identifying the optimal source of MSCs for a specific clinical application.

Additional files

Additional file 1: Table S1. Primers used for real-time PCR. (PDF 466 kb)

Additional file 2: Figure S1. Immunophenotyping analysis of AM-MSCs, UC-MSCs, and CP-MSCs. (PDF 489 kb)

Additional file 3: Table S2. Differentially expressed gene. (TXT 109 kb)

Additional file 4: Figure S2. Toluidine blue staining results of the CFU test. (PDF 410 kb)

Additional file 5: Table S3. GO term enriched by genes specifically expressed in CP-MSCs (partly). (PDF 439 kb)

Abbreviations

ADIPSIN: Complement factor D; AM: Amniotic membrane; AM-MSC: Amniotic membrane-derived MSC; ANOVA: Analysis of variance; CFU: Colony-forming unit; COL2A1: Collagen type II alpha 1 chain; COMP: Cartilage oligomeric matrix protein; CP: Chorionic plate; CP-MSC: Chorionic plate-derived MSC; CV: Chorionic villi; DCN: Decorin; DPBS: Dulbecco's phosphate-buffered saline; FITC: Fluorescein isothiocyanate; FPKM: Fragments per kilobase million; GMP: Good Manufacturing Practice; GO-BP: Gene ontology–biological process; HLA: Human leukocyte antigen; ISCT: International Society for Cellular Therapies; KEGG: Kyoto Encyclopedia of Genes and Genomes; LEP: Leptin; MHC: Major histocompatibility complex; MSC: Mesenchymal stem cell; OCN: Bone gamma-carboxyglutamate protein; ON: Secreted protein acidic and cysteine rich; PCA: Principal component analysis; PE: Phycoerythrin; PFA: Paraformaldehyde; PPARG: Peroxisome proliferator activated reporter gamma; RUNX2: Runt-related transcription factor 2; SCM: Serum-containing medium; SEM: Standard error of mean; SFM: Serum-free medium; UC: Umbilical cord; UC-MSC: Umbilical cord-derived MSC

Competing interests
The authors declare that they have no competing interests.

References

1. Dominici M, Le Blanc K, Mueller I, Slaper-Cortenbach I, Marini F, Krause D, Deans R, Keating A, Prockop D, Horwitz E. Minimal criteria for defining multipotent mesenchymal stromal cells. The International Society for Cellular Therapy position statement. Cytotherapy. 2006;8(4):315–7.
2. Phinney DG, Prockop DJ. Concise review: mesenchymal stem/multipotent stromal cells: the state of transdifferentiation and modes of tissue repair--current views. Stem Cells. 2007;25(11):2896–902.
3. Schwartz RE, Reyes M, Koodie L, Jiang Y, Blackstad M, Lund T, Lenvik T, Johnson S, Hu WS, Verfaillie CM. Multipotent adult progenitor cells from bone marrow differentiate into functional hepatocyte-like cells. J Clin Invest. 2002;109(10):1291–302.
4. Li Y, Qu YH, Wu YF, Liu L, Lin XH, Huang K, Wei J. Bone marrow mesenchymal stem cells suppressing activation of allogeneic cytokine-induced killer/natural killer cells either by direct or indirect interaction. Cell Biol Int. 2015;39(4):435–45.
5. Friedenstein AJ, Gorskaja JF, Kulagina NN. Fibroblast precursors in normal and irradiated mouse hematopoietic organs. Exp Hematol. 1976;4(5):267–74.
6. Wagner W, Wein F, Seckinger A, Frankhauser M, Wirkner U, Krause U, Blake J, Schwager C, Eckstein V, Ansorge W, et al. Comparative characteristics of mesenchymal stem cells from human bone marrow, adipose tissue, and umbilical cord blood. Exp Hematol. 2005;33(11):1402–16.
7. In 't Anker PS, Scherjon SA, Kleijburg-van der Keur C, de Groot-Swings GM, Claas FH, Fibbe WE, Kanhai HH. Isolation of mesenchymal stem cells of fetal or maternal origin from human placenta. Stem Cells. 2004;22(7):1338–45.
8. Toma JG, Akhavan M, Fernandes KJ, Barnabe-Heider F, Sadikot A, Kaplan DR, Miller FD. Isolation of multipotent adult stem cells from the dermis of mammalian skin. Nat Cell Biol. 2001;3(9):778–84.
9. Bajpai VK, Mistriotis P, Andreadis ST. Clonal multipotency and effect of long-term in vitro expansion on differentiation potential of human hair follicle derived mesenchymal stem cells. Stem Cell Res. 2012;8(1):74–84.
10. Parolini O, Alviano F, Bergwerf I, Boraschi D, De Bari C, De Waele P, Dominici M, Evangelista M, Falk W, Hennerbichler S, et al. Toward cell therapy using placenta-derived cells: disease mechanisms, cell biology, preclinical studies, and regulatory aspects at the round table. Stem Cells Dev. 2010;19(2):143–54.
11. Hass R, Kasper C, Bohm S, Jacobs R. Different populations and sources of human mesenchymal stem cells (MSC): a comparison of adult and neonatal tissue-derived MSC. Cell Commun Signal. 2011;9:12.
12. Blokzijl F, de Ligt J, Jager M, Sasselli V, Roerink S, Sasaki N, Huch M, Boymans S, Kuijk E, Prins P, et al. Tissue-specific mutation accumulation in human adult stem cells during life. Nature. 2016;538(7624):260–4.
13. Martinelli D, Pereira RC, Mogni M, Benelli R, Mastrogiacomo M, Coviello D, Cancedda R, Gentili C. A humanized system to expand in vitro amniotic fluid-derived stem cells intended for clinical application. Cytotherapy. 2016; 18(3):438–51.
14. Bieback K, Brinkmann I. Mesenchymal stromal cells from human perinatal tissues: from biology to cell therapy. World J Stem Cells. 2010;2(4):81–92.
15. Wegmeyer H, Broske AM, Leddin M, Kuentzer K, Nisslbeck AK, Hupfeld J, Wiechmann K, Kuhlen J, von Schwerin C, Stein C, et al. Mesenchymal stromal cell characteristics vary depending on their origin. Stem Cells Dev. 2013;22(19):2606–18.
16. Han ZC, Du WJ, Han ZB, Liang L. New insights into the heterogeneity and functional diversity of human mesenchymal stem cells. Biomed Mater Eng. 2017;28(s1):S29–45.
17. Araujo AB, Salton GD, Furlan JM, Schneider N, Angeli MH, Laureano AM, Silla L, Passos EP, Paz AH. Comparison of human mesenchymal stromal cells from four neonatal tissues: amniotic membrane, chorionic membrane, placental decidua and umbilical cord. Cytotherapy. 2017;19(5):577–85.
18. Kim MJ, Shin KS, Jeon JH, Lee DR, Shim SH, Kim JK, Cha DH, Yoon TK, Kim GJ. Human chorionic-plate-derived mesenchymal stem cells and Wharton's jelly-derived mesenchymal stem cells: a comparative analysis of their potential as placenta-derived stem cells. Cell Tissue Res. 2011;346(1):53–64.
19. Mathews S, Lakshmi Rao K, Suma Prasad K, Kanakavalli MK, Govardhana Reddy A, Avinash Raj T, Thangaraj K, Pande G. Propagation of pure fetal and maternal mesenchymal stromal cells from terminal chorionic villi of human term placenta. Sci Rep. 2015;5:10054.
20. Peltzer J, Montespan F, Thepenier C, Boutin L, Uzan G, Rouas-Freiss N, Lataillade JJ. Heterogeneous functions of perinatal mesenchymal stromal cells require a preselection before their banking for clinical use. Stem Cells Dev. 2015;24(3):329–44.
21. Wang Y, Wu H, Yang Z, Chi Y, Meng L, Mao A, Yan S, Hu S, Zhang J, Zhang Y, et al. Human mesenchymal stem cells possess different biological characteristics but do not change their therapeutic potential when cultured in serum free medium. Stem Cell Res Ther. 2014;5(6):132.
22. Jiang X, Du MR, Li M, Wang H: Three macrophage subsets are identified in the uterus during early human pregnancy. Cellular & molecular immunology. 2018;15(12):1027–37.
23. Hung JH, Weng Z. Analyzing microarray data. Cold Spring Harb Protoc. 2017;2017(3):pdb.prot093112.
24. Law CW, Alhamdoosh M, Su S, Smyth GK, Ritchie ME. RNA-seq analysis is easy as 1-2-3 with limma, Glimma and edgeR. F1000Research. 2016;5:1408.
25. Kanehisa M, Sato Y, Kawashima M, Furumichi M, Tanabe M. KEGG as a reference resource for gene and protein annotation. Nucleic Acids Res. 2016;44(D1):D457–62.
26. Rhee SY, Wood V, Dolinski K, Draghici S. Use and misuse of the gene ontology annotations. Nat Rev Genet. 2008;9(7):509–15.
27. Yu G, Wang LG, Han Y, He QY. clusterProfiler: an R package for comparing biological themes among gene clusters. Omics. 2012;16(5):284–7.
28. Nigg EA. Cyclin-dependent protein kinases: key regulators of the eukaryotic cell cycle. Bioessays. 1995;17(6):471–80.
29. Nakatsuru S, Sudo K, Nakamura Y. Isolation and mapping of a human gene (MCM2) encoding a product homologous to yeast proteins involved in DNA replication. Cytogenet Cell Genet. 1995;68(3–4):226–30.
30. Teng SW, Lo YS, Liu WT, Hsuan Y, Lin W. A genome-wide comparison of mesenchymal stem cells derived from human placenta and umbilical cord. Taiwan J Obstet Gynecol. 2017;56(5):664–71.

Urothelium with barrier function differentiated from human urine-derived stem cells for potential use in urinary tract reconstruction

Abstract

Background: Autologous urothelial cells are often obtained via bladder biopsy to generate the bio-engineered urethra or bladder, while urine-derived stem cells (USC) can be obtained by a non-invasive approach. The objective of this study is to develop an optimal strategy for urothelium with permeability barrier properties using human USC which could be used for tissue repair in the urinary tract system.

Methods: USC were harvested from six healthy adult individuals. To optimize urothelial differentiation, five different differentiation methods were studied. The induced cells were assessed for gene and protein expression markers of urothelial cells via RT-PCR, Western blotting, and immunofluorescent staining. Barrier function and ultrastructure of the tight junction were assessed with permeability assays and transmission electron microscopy (TEM). Induced cells were both cultured on trans-well membranes and small intestinal submucosa, then investigated under histology analysis.

Results: Differentiated USC expressed significantly higher levels of urothelial-specific transcripts and proteins (Uroplakin III and Ia), epithelial cell markers (CK20 and AE1/AE3), and tight junction markers (ZO-1, ZO-2, E-cadherin, and Cingulin) in a time-dependent manner, compared to non-induced USC. In vitro assays using fluorescent dye demonstrated a significant reduction in permeability of differentiated USC. In addition, transmission electron microscopy confirmed appropriate ultrastructure of urothelium differentiated from USC, including tight junction formation between neighboring cells, which was similar to positive controls. Furthermore, multilayered urothelial tissues formed 2 weeks after USC were differentiated on intestine submucosal matrix.

Conclusion: The present study illustrates an optimal strategy for the generation of differentiated urothelium from stem cells isolated from the urine. The induced urothelium is phenotypically and functionally like native urothelium and has proposed uses in in vivo urological tissue repair or in vitro urethra or bladder modeling.

Keywords: Urothelium, Urine-derived stem cells, Barrier function, Tight junctions, Bladder diseases, Tissue engineering

Background

Urothelial cells (UC) are classified as transitional epithelium, and they cover almost the entire luminal surface of the urinary tract. This includes the renal pelvis, ureters, bladder, and the proximal segment of the urethra. Urothelium provides a robust permeability barrier across the urinary tract. This barrier function is dependent on tight-junction complexes that limit the transfer of ions and solutes across the urothelium. In addition, surface glycans, specialized lipid molecules, and uroplakins at the apical surface further reduce the permeability of the urothelium [1]. The barrier function of the urothelium protects underlying tissue from toxic components of urine. Formation and degeneration of the urothelium are critical to inhibit urethral stricture development. In addition, an intact urothelium prevents bladder detrusor muscle over-activity [2], inflammation, and fibrosis. Compromised urothelium leads to several common urologic diseases such as recurrent urinary tract infection, urethral injuries or stricture, interstitial cystitis, overactive bladder, and bladder cancer.

Bioengineered urothelium would provide a valuable tool for both the development of engineered urothelium for urological reconstruction and the study of urothelial dysfunction. Currently, few in vitro urothelial models exist for the development of drugs intended to treat various urologic disorders in the low urinary tract. Thus, there is an urgent need for the generation of engineered urothelium for urinary tract tissue repair. Our group has developed technologies for the generation of engineered multilayer urothelial sheets with barrier function [3–8]. These constructs are currently generated using differentiated cells from healthy urothelial tissue obtained from different species, including rat, pig, and human [3–8]. However, when healthy urothelial tissue is not available, stem cells may be used as an alternative cell source. Mesenchymal stem cells (MSC) derived from bone marrow [9, 10] or adipose tissue [11] maintain some capacity for urothelial cell differentiation. In addition, embryonic stem cells (ESC) [12] and induced pluripotent stem cells (iPSC) [13] have successfully been differentiated into urothelial cells. Despite advances in the controlled differentiation of these progenitor cells, each type has drawbacks and limitations. MSC have limited urothelial differentiation potential, harvesting cells results in donor site morbidity, and there remain concerns regarding the oncogenic potential of iPSC-derived cells as well as persistent ethical issues regarding the use of ESC. An alternative, autologous stem cell source for the generation of UC would benefit the fields of drug development, personalized medicine, and regenerative medicine.

Our previous studies have demonstrated that human urine-derived stem cells (USC) shed from the urinary tract possess beneficial regenerative properties, including robust proliferative potential and multi-potent differentiation potential [14–16]. There are several advantages of human USC over other stem cells. USC can be easily obtained from healthy individuals or patients by non-invasive and low-cost procedures that generate high-quality cells that can be expanded extensively [14, 17–19]. Up to 140 USC clones per 24-h urine collection were consistently obtained from a single healthy individual [20]. Thus, a 24-h urine sample can provide $> 1 \times 10^8$ cells over three passages, a number sufficient for a majority of the intended applications. In addition, cell viability is preserved during isolation [20, 21] as the method used does not require enzymes (such as collagenase) for tissue dissociation. Furthermore, no evidence for oncogenic potential in human USC has been identified over several in vivo studies [14, 17, 22].

Our previous studies have revealed that USC can efficiently give rise to cells expressing urothelial cell markers; however, the barrier function and cellular structure of urothelial cells cultures generated from USC have not yet been investigated [13–16]. The purpose of this study was to optimize a strategy to induce human USC differentiation into functional urothelial cells with barrier function and appropriate cellular 3D architecture. These cells would represent a powerful tool for urological tissue research and urological regenerative medicine.

Methods

Cell isolation, culture and differentiation

Collection of human urine and bladder tissues in this study was approved by the Wake Forest University Health Sciences Institutional Review Board. In total, 28 urine samples were freshly collected from 6 healthy male individuals (28–55 years old). USC were isolated and cultured as previously described [19]. Briefly, urine was centrifuged at 500 g for 5 min and cell pellets were suspended in a mixed medium composed of embryo fibroblast medium (EFM) and keratinocyte serum-free medium (KSFM) (EFM-KSFM, 1:1 ratio) with 10% fetal bovine serum (FBS). The cells were cultured in 24-well plates for 3–5 days, at which point USC clones appeared. When reaching 70–80% confluence (*p0*), USC were passaged to six-well plates (*p1*). USC at *p2–5* were used for all experiments as described below. Human smooth muscle cells (SMC) and human UC were used to provide conditioned medium, and normal UC were used as a positive control. Both cell types were isolated from human bladder biopsies or ureteral tissue from donated kidneys [7]. SMC were cultured in Dulbecco's modified Eagle's medium (DMEM) with 10% FBS and UC were cultured in KSFM with supplements. For all experiments, UC and SMC were used before *p3*.

Flow cytometry

To evaluate stem cell surface markers, cultured USC at *p2* were stained with specific anti-human antibodies:

CD45-FITC, CD31-FITC, CD73-PE, CD90-FITC, CD105-PerCP-Cy™5.5, CD34-FITC, CD44- FITC and CD146-PE. Briefly, following trypsinization, cells (5×10^5) were re-suspended in ice-cold phosphate buffered saline (PBS) containing 1% bovine serum albumin (BSA). Fluorochrome-conjugated antibodies were added to cells in 50 ml PBS containing 3% BSA and incubated on ice for 30 min in the dark. IgG1-PE, IgG1-FITC, IgG2b-FITC, and IgG1-PerCP-Cy™5.5 conjugated isotype control antibodies (BD Pharmingen™, Sparks, MD) were used to determine background fluorescence. Cells were then washed twice in wash buffer, passed through a 70-μm filter, and analyzed by flow cytometry (FACSCalibur BD Biosciences, Franklin Lakes, NJ).

Optimization of urothelial differentiation methods

To efficiently induce USC differentiation into urothelial cells, differentiation methods were optimized under several induction conditions (Table 1), in both dynamic and static cultures for different culture periods (1, 2, or 3 weeks). Assessment of barrier function was accomplished by evaluation of tight junction formation (Western blotting, real-time PCR, immunofluorescence), transmission electron microscopy, and fluorescent dye exclusion.

Conditioned medium was collected 8–12 h after cultured UC or SMC (at p3), respectively. Centrifuged at 1500 RPM for 5 min, the supernatant was filtered with a microfilter (pore size of 0.22 μm, Corning, Tewksbury, MA) to void cell contamination. For urothelial induction, USC were firstly seeded in six-well plates at 5×10^4 cells /cm^2 under ordinary stem cell media [14]. To evaluate urothelial induction conditions, USC were treated with three different types of differentiation media, compared to positive (UC) and negative (non-induced USC) controls, see Table 1. To determine the effect of secretomes of urothelial cell culture on differentiation of USC, conditioned medium from UC culture mixed with EFM-KSFM (1:1), compared to a standard induction method [14, 21], i.e., KSFM containing epidermal growth factor (EGF) at 30 ng/ml. In addition, to evaluate the effect of epithelial-stromal interaction, conditioned medium from SMC culture on urothelial induction of USC will be tested when mixed with KSFM (1:1).

To evaluate the impact of 3D dynamic culture on cellular growth and differentiation, cells of each group were seeded on the culture plates for 6 h and then loaded onto an orbital shaker (Belly Dancer, Stovall, Greensboro, NC) at 40 revolutions per minute (rpm), compared to static culture at different time points (1, 2, or 3 weeks, see below), as described previously [22]. The medium was replaced every 3 days. USC, UC, and SMC controls were cultured under the same conditions described above.

To determine the temporal kinetics of urothelial differentiation, USC and the cells at control groups were cultured in each condition for 1, 2, and 3 weeks.

Permeability determinations

Induced USC were cultured on Falcon® 23.1 mm Permeable Support with 0.4 μm Translucent High-Density PET Membrane (Corning, New York, USA), as previously reported with minor modifications [23]. Briefly, the upper inserts were coated with collagen-IV (3 μg/cm^2), air dried in a laminar hood, and sterilized by a 70% ethanol rinse. The ethanol was allowed to evaporate completely before the inserts were used. To assess the barrier function of UC-induced USC, cells (1×10^5/cm^2) were plated in 1.5 ml of 1 mg/ml tracer-containing medium (FITC-dextran, 4 kDa, Sigma, FD4) in the insert (top chamber) and 3 ml tracer-free medium in the bottom well. Phenol-free medium was used to avoid interference of the indicator in the assay. The media were supplemented with 2 mM $CaCl_2$ solution 24 h before the tracer was added. Three hours after the tracer was added, 100 μl media aliquots from the bottom wells were collected for fluorescence measurements (excitation at 490 nm and emission at 520 nm). Tracer diffusion across the cell layers was calculated by measuring the fluorescent intensity of FITC-dextran in the lower chamber.

Real-time PCR

Total mRNA was extracted from cell pellets based on culturing and grouping above using the RNA isolation

Table 1 Research design for optimization of urothelially differentiated human USC

Group (G)	Dynamic culture		Static culture	
	Single seeding	Triple seeding	Single seeding	Triple seeding
G1 USC	USC (5×10^5 cells/well) as negative control			
G2 UC	UC (5×10^5 cells/well) cultured in KSFM as positive control			
G3 USC + UC/CM	USC (5×10^5 cells/well) cultured with conditioned Media from UC culture			
G4 USC + EGF	USC (5×10^5 cells/well) cultured in induce Media with EGF (30 ng/ml)			
G5 USC + SMC/CM	USC (5×10^5 cells/well) cultured with EGF (30 ng/ml) and conditioned medium from SMC culture (1:1)			

Abbreviations: *USC* urine-derived stem cells, *UC* urothelial cells, *SMC* smooth muscle cells, *CM* conditioned medium, *UC/CM* urothelium-conditioned medium, *SMC/CM* Smooth muscle cell-conditioned medium, *EGF* epidermal growth factor

kit (5Prime, Gaithersburg, MD). According to the manufacturer's instructions, 5 μg of RNA was converted to cDNA in a reaction containing primers, nucleotides, and reverse transcriptase enzyme using a high-capacity cDNA reverse transcription kit (Applied Biosystems, Foster City, CA, USA). The cDNA was used for real-time analysis along with Taqman Universal PCR master mix and gene expression probes. The assay was performed using a 7300 Real-time PCR system (Applied Biosystems, Foster City, CA, USA). The primer sequences used in this study are listed in Additional file 1: Table S1.

Western blotting

Cells were harvested from six-well plates and lysed for Western blotting analysis as previously described [14]. Proteins were separated by 6–10% sodium dodecyl sulfate-polyacrylamide gel (10–50 μg/lane) and then transferred to nitrocellulose membrane. The membrane was probed with primary antibodies at 4 °C overnight and then incubated with secondary antibodies at room temperature for 1 h. Protein hybridization was detected by using the enhanced chemiluminescent assay. Images were captured by a Fujifilm imaging system (LAS 3000). For quantification of signal, the Multi Gauge V3.0 software from Fujifilm was used and the value was presented as relative density to β-actin. The primary antibodies used in this study are listed in Additional file 2: Table S2.

Immunofluorescence

USC were induced following 14 days in dynamic culture conditions, sub-cultured, and then seeded onto chamber slides (Thermo Fisher Scientific Inc., Waltham, MA) and incubated overnight. Cells were fixed with 4% paraformaldehyde, permeabilized with 0.2% Triton for 3 min, and blocked with the blocking buffer (1× PBS/5% normal goat serum/0.3% Triton™ X-100, Cell Signaling Technology, Boston, MA). Urothelial-specific markers (i.e., Uroplakin Ia, Uroplakin III, and CK20, AE1/AE3) and intercellular junction markers (i.e., ZO1, ZO2, E-cadherin, and Cingulin) were used to characterize differentiated USC. An appropriate secondary antibody conjugated to fluorescein isothiocyanate was used. The cells were mounted in a diamidino-2-phenylindole (DAPI, Sigma-Aldrich, St Louis, MO, USA)-containing mount (Vector, Burlingame, CA) for staining nuclei.

All stained sections were evaluated by a single, experienced individual in a double blind manner. All antibodies used for immunofluorescence are listed in Additional file 2: Table S2. To determine the portion of cells expressing positive markers, the number of positive cells were counted and related to the total number of cell nuclei per image. Images were captured from five fields per well at 40× and 200× magnifications with a Zeiss inverted fluorescent microscope (model Axiovert 200 M), filters suitable for DAPI (blue) or fluorescein (green), and a CCD camera from QImaging (model Retiga 2000RV).

Transmission electron microscopy

The ultrastructure of tight junctions between UC-differentiated USC was examined by transmission electron microscopy (TEM) 14 days after induction. The induced USC seeded onto transwell membranes were fixed and sectioned according to standard procedures. Briefly, the cells were fixed in 2.5% glutaraldehyde, then post-fixed with 1% osmium tetroxide, dehydrated in graded alcohols, embedded in Spurr's resin (Polysciences, Warrington, PA), and cut into 80-nm sections using a Reichert-jung Ultracut E ultramicrotome. The sections were viewed and captured using a Tecnai Spirit BioTwin transmission electron microscope (FEI, Hillsboro, OR).

Generation of small intestinal submucosa matrix

A segment of fresh porcine small intestine was obtained from a local slaughter house. Small intestinal submucosa (SIS), a natural collagen-based matrix, was acquired after the mucosa and serosa of intestinal tissue were removed manually and washed in distilled water. For decellularization [3], SIS specimens were immersed in 5% peracetic acid (PAA) for 30 min and then washed in distilled water on a rotary shaker at 200 rpm. SIS material was soaked in 1% Triton X-100 at 4 °C for 2 days and washed in distilled water for 1 day. For disinfection, SIS samples were oxidized in 5% PAA and 20% ethanol for 2 h. Finally, samples were rinsed three times in distilled water and stored in distilled water at 4 °C until needed. SIS scaffolds were firmly secured over a sterile silicone insert for ease of cell seeding.

Multilayer urothelium formation in vitro

To optimize the structures of multilayer urothelium, three different seeding methods were used for USC to seed onto trans-well membranes: (i) 1×10^5 /cm^2 plated at one time (single seeding), (ii) a total of 3×10^5 cells/cm^2 plated in 1×10^5 cells/cm^2 density over 3 days (triple seeding), (iii) 3×10^5 cells/cm^2 plated at one time (single seeding). Certain amounts of cells were detached during culture with the last seeding method (i.e., 3×10^5 cells/cm^2 on single seeding); therefore, the first two seeding methods were used in the rest of study. These cells were induced in urothelial-conditioned medium under dynamic culture conditions for 14 days. Culture plates were placed on a rotator in an incubator at 40 rpm, 24 h after seeding. Cell proliferation of UC-induced USC was measured at 490 nm on days 0, 2,

4, 6, 8, 10, 12, and 14 using an MTT assay (Promega, Madison, WI, USA).

To determine the impact of natural collagen matrix on multilayer urothelium formation by induced USC, cells at were cultured on SIS scaffolds compared to cells on polyester membrane in transwell. Induced USC at $1 \times 10^5/cm^2$ were seeded onto the matrix each day over the first 3 days under static culture and then cultured in dynamic culture for extra 11 days. The cell-seeded SIS and cell transwell membrane constructions were cut into 1-cm^2 pieces for histological analysis.

Histology and immunohistochemistry

Cell-seeded matrix samples were analyzed using immunohistochemistry. The samples were fixed in 10% buffered formalin and embedded in paraffin. After deparaffinization and high temperature citrate-based antigen retrieval, the slides were blocked with BLOXALL solution (Vector Laboratory Inc., Burlingame, CA, USA) and 5% goat serum. The slides were then washed in PBS and incubated in anti-cytokeratin antibodies (AE1/AE3, GA053, Dako, CA, USA) and incubated with the secondary antibody, i.e., Biotinylated Goat Anti-Mouse IgG Antibody (Vector Laboratory Inc., Burlingame, CA, USA) diluted at 1:400 for 30 min at room temperature. Finally, after incubation with the ABC reagent, i.e., Vectastain ABC Kit (Vector Laboratory Inc., Burlingame, CA, USA), slides were treated with DAB substrate, i.e., ImmPACT DAB Substrate Kit (Vector Laboratory Inc. Burlingame, CA, USA) and counterstained with hematoxylin.

Statistical analysis

The values are expressed as means and standard errors of the mean (SEM), with $n = 3$ or 6. All results were reproduced in experiments at least three times. Statistical analyses were performed by using one-way ANOVA. Student-Newman-Keuls post hoc test was used for multiple comparisons. SPSS16.0 software was used for analyses. Differences were considered statistically significant at $p < 0.05$.

Results

USC adopted a "rice-grain" like appearance 2–3 days after initial seeding. These cells subsequently formed clones over 4–6 days. Fluorescence activated cells sorting (FACS) analysis showed that USC consistently expressed stem cell surface markers (CD73, CD90, CD105) (Fig. 1), but did not express hematopoietic stem cell markers (CD31, CD34, CD45) or endothelial cell markers (CD31) as described previously [13–16]. The induced USC converted to cobblestone morphology, which appeared similar to normal UC. When cultured under conditioned medium, the cells became smaller and more densely packed, as compare to non-induced USC.

In the present study, we compared the addition of urothelial-conditioned medium with or without dynamic flow culture (Fig. 2a), in combination with convention methods (i.e., EGF and static culture) for directing the differentiation of USC to urothelial cells. Barrier function testing is one of most important and effective parameters for the evaluation of urothelial cell differentiation. As such, in vitro assays using a fluorescent tracer on USC cultured on transwell membranes demonstrated a 60% reduction in passage of the tracer across the urothelium over 3 h, as compared to undifferentiated USC. Urothelial cells differentiated in this conditioned medium form continuous cell layers that possess barrier function similar to that of normal urothelium (Fig. 2b). Importantly, the combination of urothelial-conditioned medium and dynamic culture significantly increased urothelial differentiation and barrier function, similar to that of normal urothelium, as compared to other methods, including EGF only or bladder SMC-conditioned medium (Fig. 2b–d, Additional file 3: Table S3, Additional file 4: Table S4) at 2 weeks post-induction ($p < 0.01$).

Temporal analysis of the data indicated that urothelial cell differentiation progresses in a time-dependent manner. Over a 2-week induction period using a combination of conditioned medium and dynamic culture, progressively greater levels of functional proteins and tight junctions formed (Fig. 2c). By comparison, a 1-week induction using EGF produced only modest expression of urothelial cell-specific markers ($p < 0.01$). In addition, dynamic culture alone was sufficient to enhance urothelial transcript and protein marker expression and promoted formation of multilayered urothelial structures (Fig. 2d).

Our current data demonstrate that the optimal material for inducing urothelial cell differentiation from USC is a urothelial-conditioned medium. Immunostaining and Western blotting showed that uroepithelial transcript and protein marker expression by USC for all urothelial cell subtypes (i.e., Uroplakin Ia, Uroplakin III, CK20 for superficial or umbrella cells; AE1/AE3 for all urothelial cells) are significantly increased following combined use of urothelial-conditioned medium and dynamic culture, as compared to other induction conditions ($p < 0.01$, Fig. 3a–c). Cytometer analysis showed that 72.6% of induced USC and 94.5% of UC expressed AE1/AE3, as compared to 15.1% of EGF-induced USC, 19.4% SMC/CM-induced USC, and 18.2% of USC (Additional file 3: Table S3). Dynamic culture conditions significantly improved the barrier function of USC-derived urothelial cells, as evidenced by increased uroplakin expression (Fig. 3a–c). This effect was observed for both

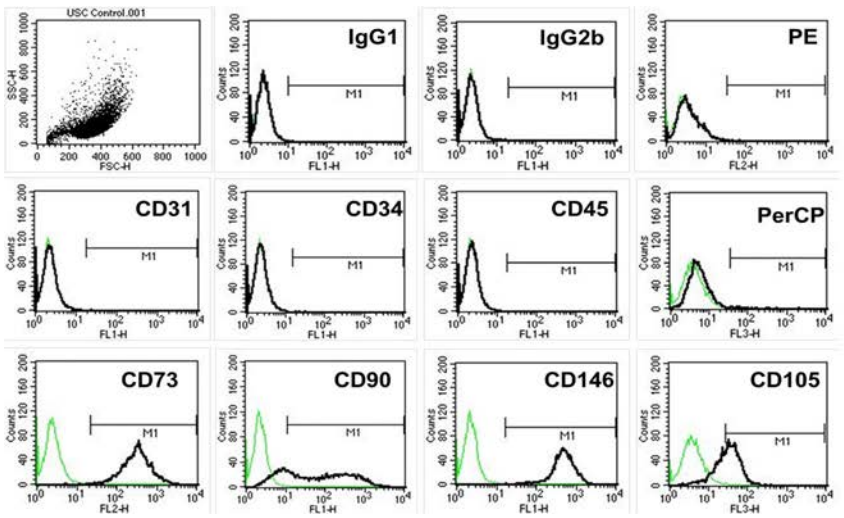

CD markers	Percentage (%) of USC expressing positive antibodies
CD44	100.0±0.0
CD146	98.3±1.0
CD31	≤1
CD34	≤1
CD45	≤1
CD90	69.2 ± 24.8
CD73	99.7 ± 0.3
CD105	70.2 ± 28.5

Fig. 1 Cell surface markers and morphology of USC and UC-induced USC. Human USC expressed MSC surface marker profiles (CD73, CD90, CD 105, and CD146), but not hemoprotein stem cell markers (CD 31, CD34, and CD45) assessed by flow cytometry

native urothelial cells and urothelium differentiated from USC.

Similarly, several tight junction gene and protein markers (ZO-1, ZO-2, Cingulin, and E-cadherin) are significantly higher with both of UC and USC induced by UC-conditioned medium treatment, as compared to other treatments. This is illustrated by immune-fluorescence staining and Western blotting analysis. Interestingly, high concentrations of EGF (30 ng/ml) in the culture medium also promoted formation of tight junctions, whereas culturing with SMC-CM had little effect (Fig. 4 a–c, Additional file 4: Table S4). Tight junction formation by urothelial cells in vitro requires a confluent cell layer. The structural integrity of tight junctions is one of the most critical components of normal urothelial barrier function. As a barrier, tight junctions functionally block the passing of molecules and ions through the channel between plasma membranes of neighboring cells. By using TEM, the ultrastructure of tight junctions and desmosomes between neighboring cells were identified clearly on both low- and high-definition views of UC and induced USC, including UC-conditioned medium, EGF, and SMC medium treatment; however, they were not found on non-induced USC (Fig. 4d).

Triple-seeded USC presented significantly more cells on days 2, 4, 6, and 8 compared to single-seeded USC, but not on days 10, 12, and 14. Numbers of single-seeded USC grew up and caught up the number of triple-seeded USC on the last three time points in Fig. 5. Based on permeability analysis, it appears that single-seeding can form the similar barrier function as triple-seeding during 2-week induction culture, indicating that it requires time to fully develop tight junctions regardless of the number of cells present. However, urothelium tended to detach from transwell after 2-week induction.

In addition, triple-seeded USC formed a cell sheet on SIS that was five to six cells deep over 14 days under dynamic culture conditions (Fig. 6). No evidence of generation of internal necrotic regions was identified. This indicates that dynamic culture promotes USC proliferation and generates a healthy multilayer urothelium with a cellular microarchitecture. Immunochemical staining of USC-derived urothelium generated on decellularized SIS showed normal multilayered urothelial structures with well-organized luminal surface expression of AE1/AE3. These cells penetrated into the SIS with porous structure, providing good anchorage that limited the occurrence of detachment from the substrate (Fig. 6). Despite cells growing well on polyester membrane, the portions of the multilayer urothelium often separated from the rigid synthetic material were also washed away during immunocytochemical staining (not shown in figures). Remarkably, soft SIS matrix provides favorite subtract for multilayer urothelium formation in vitro. In order to obtain optimal histological slides with entire cell structures, the mechanical properties (such as hardness) of biomaterial should match to the soft cellular sheet for the histology processes to evaluate the microarchitecture of multiple layers of UC.

Discussion

The overarching goal of this study is to develop an optimized method for increasing uroplakin expression and barrier function of human urothelium differentiated from USC by urothelial conditional media and dynamic culture system for potential use in urethra or bladder

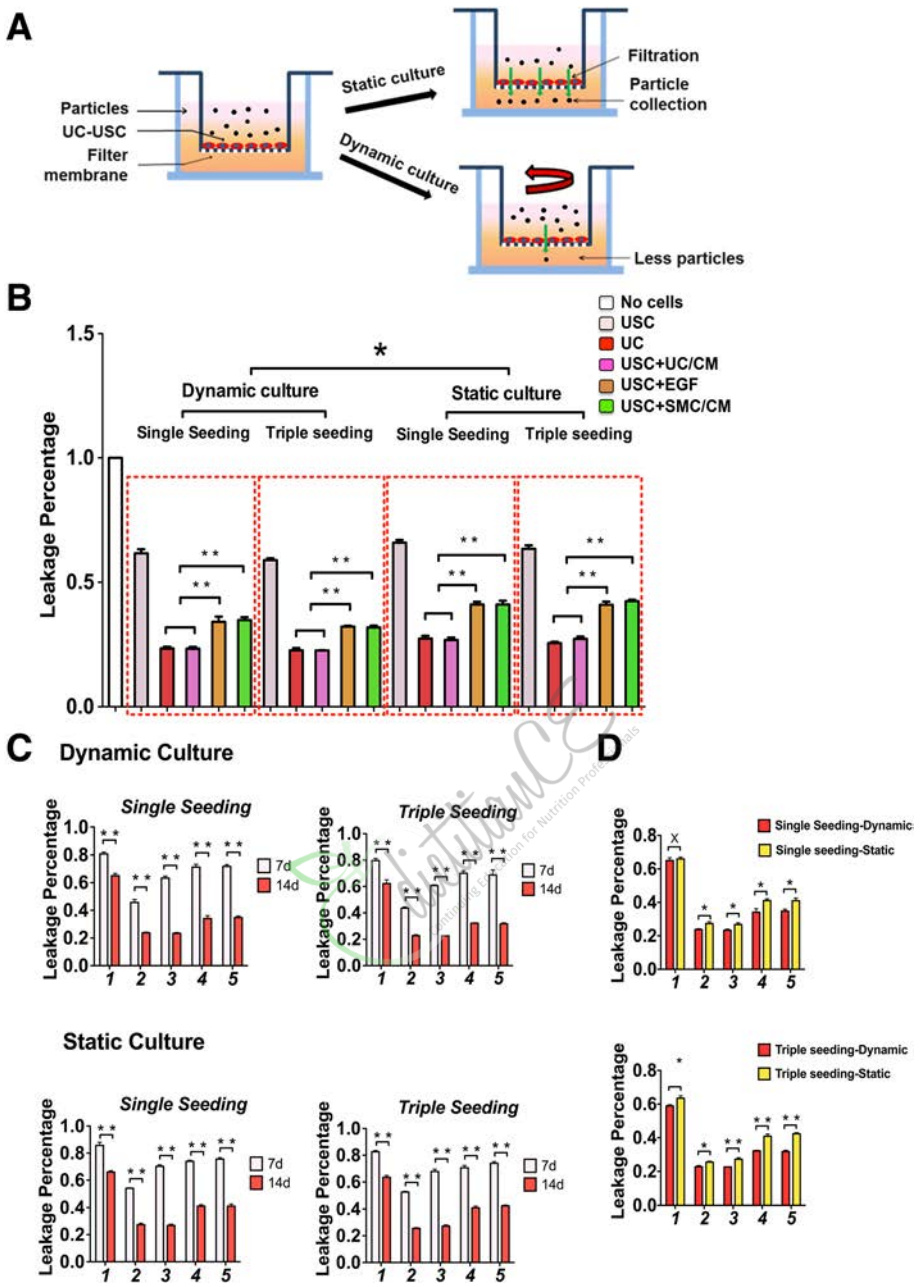

Fig. 2 Permeability barrier function test of urothelial differentiation of USC. **a** In vitro permeability test model of UC-induced USC in dynamic culture condition vs. static culture condition. **b** Urothelial induction of USC in different conditions of differentiation culture for 2 weeks. **c** Effect of time-dependent induction on urothelial differentiation of USC on weeks 1 and 2, respectively. **d** Impact of dynamic culture on permeability barrier function of USC 2 weeks after urothelial induction. Notes: Foot numbers in graphs **c** and **d** represent: (1) USC, (2) UC, (3) USC + UC/CM, (4) USC + EGF, (5) USC + SMC/CM. Abbreviations: USC = urine-derived stem cells, UC = urothelial cells, SMC = smooth muscle cells, CM = conditioned medium, UC/CM = urothelium-conditioned medium SMC/CM = smooth muscle cell-conditioned medium EGF = epidermal growth factor. Single seeding = seeding cells only once, Triple Seeding = seeding cells each at first 3 days

reconstruction. The underlying thought was that urothelium condition medium provides differentiation cues that guide USC to differentiate into urothelial cells in a more efficient manner than EGF alone. In addition, dynamic culture generated mechanical signals that promoted the formation of tight junctions. The present study demonstrated that the combination of urothelial conditional media and dynamic culture system provides preferred induction method for multiyear urothelium formation from stem cells in the urine.

Terminally differentiated urothelial cells are the most commonly used cells for the generation of multilayer

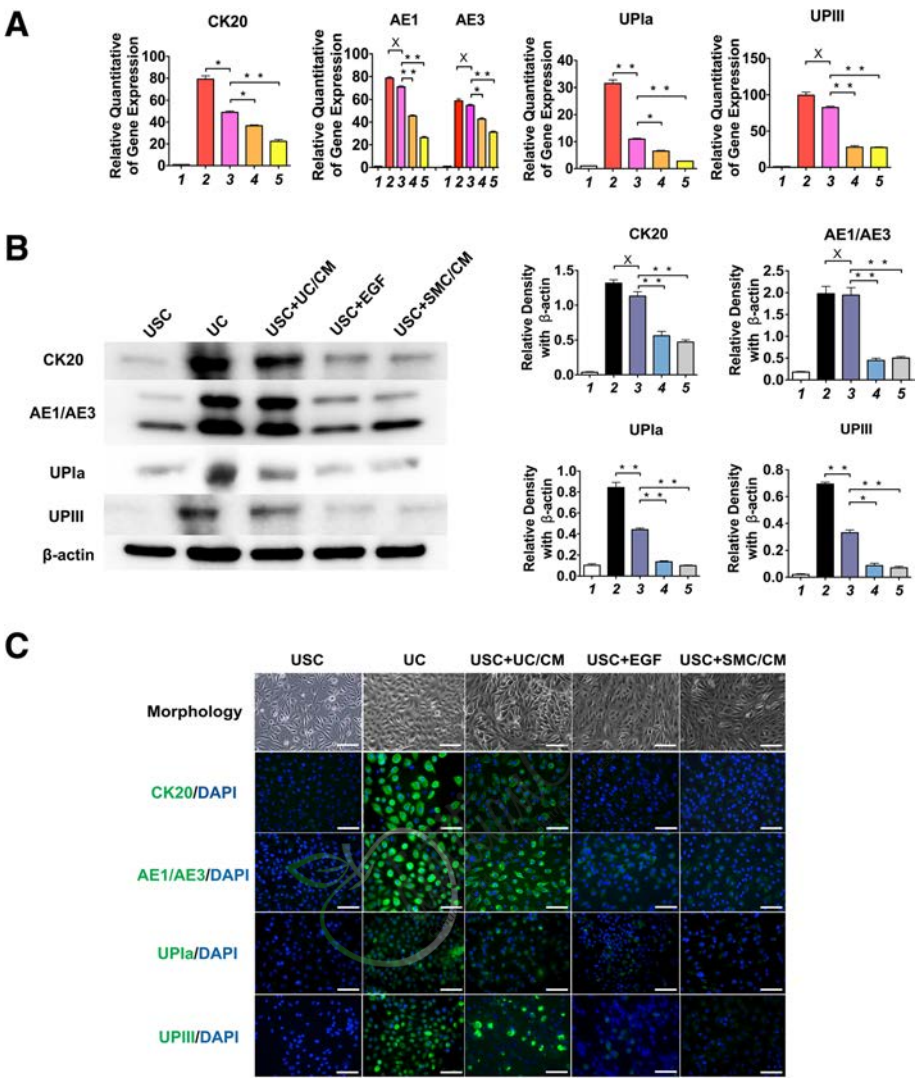

Fig. 3 UC-induced USC expressing urothelial cell gene and protein markers. Expression level of urothelial cell transcripts and protein markers (Uroplakin Ia/III, AE1/AE3, and CK20) under different induction culture conditions assessed by: **a** real-time PCR, **b** Western blotting, and **c** immunofluorescence staining 14 days after urothelial differentiation. Cell morphology of USC, UC, and induced USC are also illustrated. Notes: Foot numbers in graphs (**a**) and (**b**) represent: (1) USC, (2) UC, (3) USC + UC/CM, (4) USC + EGF, (5) USC + SMC/CM. Abbreviations: UPIa = Uroplakin Ia, UPIII = Uroplakin III. USC = urine-derived stem cells, UC = urothelial cells, SMC = smooth muscle cells, CM = conditioned medium, UC/CM = urothelium-conditioned medium SMC/CM = Smooth muscle cells conditioned medium EGF = epidermal growth factor. Scale bar = 50 μm

urothelium intended for drug testing and use in urological tissue repair. However, patient-derived urothelial cells often cannot be obtained due to urethral stricture or bladder infection diseases or trauma. In addition, urothelial cells in certain patients may be affected by conditions such as bladder stones or other foreign bodies, presenting challenges in isolation and expansion of a sufficient cell population. Urothelial differentiation of USC offers a virtually limitless source of cells for model fabrication or tissue engineering. Several different types of stem cells, including MSC [10, 11], ESC [12], and iPSC [13], have been studied for urothelial cell differentiation. iPSC or ESC can give rise to functional urothelial cells, but the differentiation process is long and expensive. In addition, the differentiated cells carry the risk that rare, undifferentiated cells may retain the potential for teratoma formation. Although many reports describe urothelial cell differentiation from adult stem cells, most of these cells only display urothelial cell marker expression and do not measure barrier functionality. MSC give rise to very few urothelial cells with barrier function and the ability to form a multilayer structure. These cells have more limited differentiation potential than ESC, and typically only give rise to cell types within the same germ layer lineage. This produces enormous challenges when

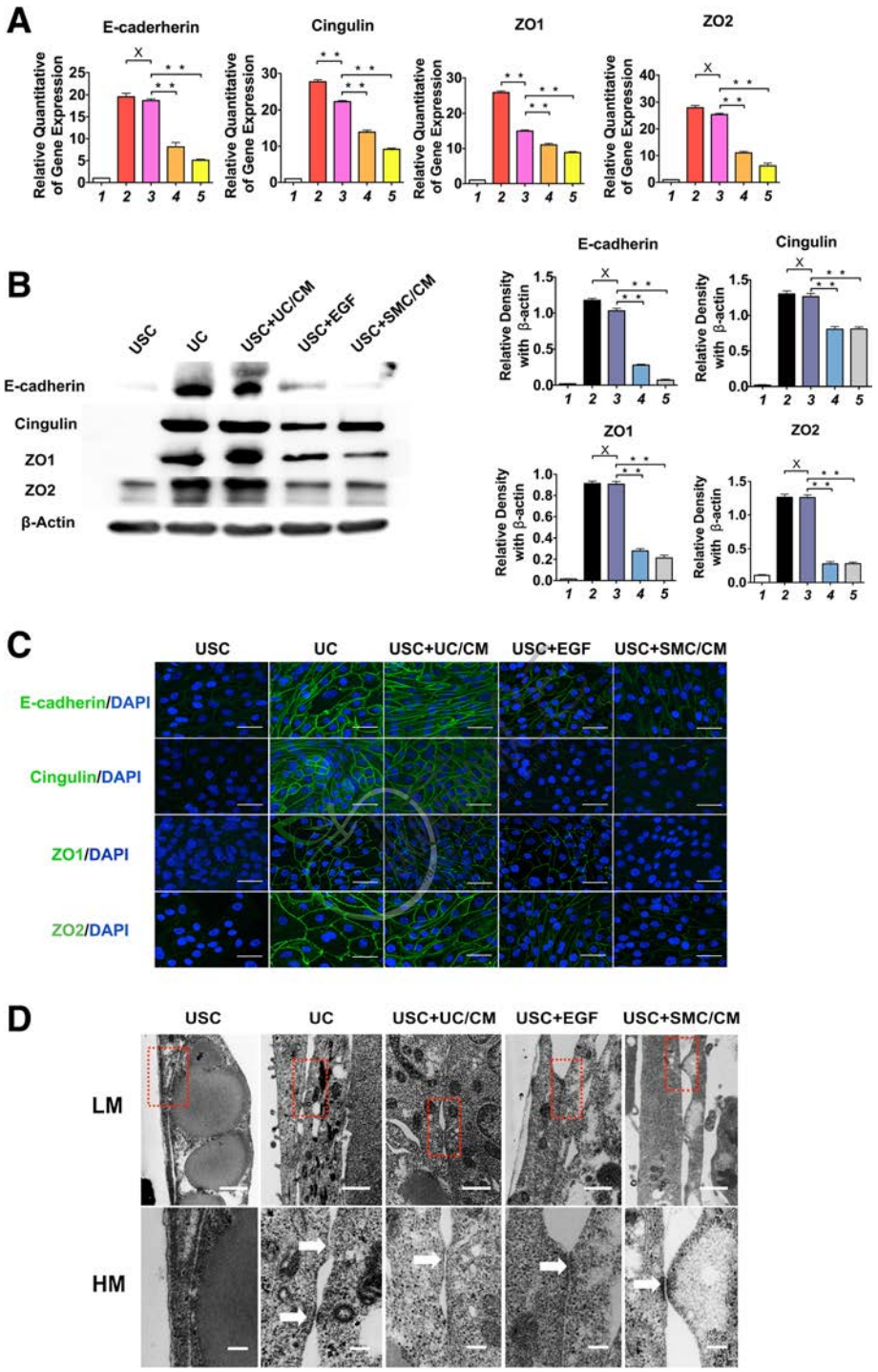

Fig. 4 UC-induced USC expressed gene and protein markers of tight junction markers 14 days after differentiation. Tight junction markers (E-cadherin and Cingulin, ZO1, ZO2) displayed on cell membrane boundaries between cells in the urothelially induced USC and UC, but not in USC, assessed by **a** real-time PCR, **b** Western blotting, and **c** immunofluorescent staining assessed under confocal microscope. Scale bar = 40 μM. **d** Tight junctions or desmosomes between neighboring cells in the induced USC and UC groups, but not in non-induced USC, examined by transmission electron microscopy. LM scale bar = 500 nm, HM scale bar = 100 nm. Notes: Foot numbers in graphs **a** and **b** represent (1) USC, (2) UC, (3) USC + UC/CM, (4) USC + EGF, (5) USC + SMC/CM. Abbreviations: USC = urine-derived stem cells, UC = urothelial cells, SMC = smooth muscle cells, CM = conditioned medium, UC/CM = urothelium conditioned medium SMC/CM = Smooth muscle cells conditioned medium EGF = epidermal growth factor. LM = low magnitude, HM = high magnitude

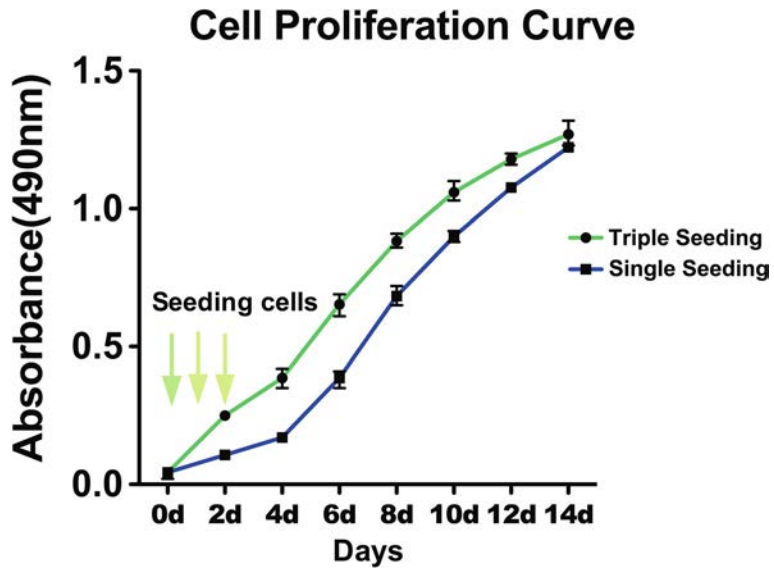

Fig. 5 Cell proliferation curves of urothelially induced USC at different seeding cell concentrations. Cell growth pattern of single seeding was similar with that of triple seeding pattern. Dotted square showed at the 14th day the cell proliferation curve goes to almost same metric. Both groups were urine-derived stem cells cultured in urothelial-conditioned medium under dynamic culture environment. Notes: Single seeding = seeding cells only once, Triple seeding = seeding cells each at first 3 days

attempting to differentiate mesodermal MSC into endodermal urothelial cells.

USC are native to the urinary tract and can survive contact with urine, in the same manner as normal urothelial cells. USC are neither urothelial cells nor MSC, but they offer advantages over other multipotent cell types [24]. USC possess robust proliferation and multipotent differentiation potential [14, 19, 21]. Our previous studies have demonstrated that USC can be efficiently differentiated into urothelial cells in vitro and in vivo. Furthermore, USC isolation is trivial via a non-invasive method, and the cells expand extensively, in vitro [14, 20, 21]. Age and gender do not appear to impact the ability to harvest USC from urine.

Although urothelium possess multiple functions including sensory mechanisms (i.e., thermal, mechanical, and chemical sensors) and release chemical mediators, it serves mainly as a passive barrier to ions and solutes in urine. As a key protective attribute, urothelium barrier function is maintained by three structures: (1) uroplakin proteins in the apical cell membrane, (2) tight junctions localized between the superficial umbrella cells, (3) urothelial glycosaminoglycan (GAG) and proteoglycans, covering the umbrella cells [26]. Thus, uroplakin proteins, tight junction proteins, and histological or ultra-structure of cell/cell attachments are often assessed for evaluation of urothelial barrier function. Thus, urothelial barrier function is crucial in studies intended

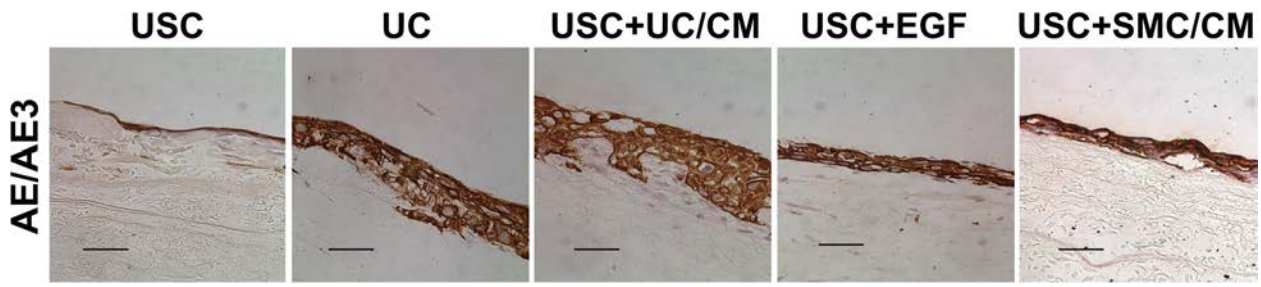

Fig. 6 Effect of nature collagen matrix on multilayer formation of urothelium of UC-induced USC. Urothelially induced USC developed urothelium with five to seven cell layers stained positive for AE1/AE3 onto a SIS matrix under dynamic culture, which is similar to urothelial cells. In contrast, USC treated with EGF or SMC/CM grew thinner layer and USC alone formed a single layer. In addition, the induced USC penetrated into the porous SIS matrix to a great depth to form well adhesion structure of cell-matrix. Scale bar = 50 μm. Abbreviations: USC = urine-derived stem cells, UC = urothelial cells, SMC = smooth muscle cells, CM = conditioned medium, UC/CM = urothelium conditioned medium SMC/CM = smooth muscle cell-conditioned medium EGF = epidermal growth factor

to identify treatments for a host of urinary tract diseases such as infection, interstitial cystitis, radiation cystitis, calculus formation, and cancer. Therefore, barrier function and histology are critical elements in the characterization of bioengineered urothelium. To date, most studies have shown that urothelial cells derived from adult stem cells displayed a certain amount of urothelial markers, but generally lack appropriate barrier function and histological structure [10, 11]. In this study, we demonstrate that urothelial cells differentiated from USC not only express urothelial specific markers, but also form tight junctions, arrange into an appropriate cellular architecture and maintain robust barrier function. Glycosaminoglycan layer is an important defense mechanism for the transitional epithelium mucosal surface of urinary tract. It allows adaptation to the constant exposure to urine and controls the permeability of urinary substances to the transitional cell. Urine appears necessary for induced stem cell to form elaboration of a GAG layer on the surface of multilayer urothelium [27]. As human urine was not used to induce GAG layer formation in this study, it is worthwhile to determine the GAG layer formation when differentiated USC are exposed to urine in a future study.

It is challenging to induce stem cell differentiation into functional cells because the molecular and mechanical factors that govern the differentiation program are not fully understood. Conditioned medium from cultured target cells is commonly used for induction of stem cells to differentiate renal tubule epithelial cells [27], germ cells [28], skeletal muscle cells, osteocytes [29], and chondrocytes [30]. Paracrine factors (i.e., growth factors, cytokines, tissue-specific genes, and microRNAs) that are released into the medium can regulate cell phenotype and are likely responsible for directing the differentiation of multipotent cells towards the intended cell type. Our previous studies have demonstrated that EGF alone may be used to promote differentiation of USC to cells that express urothelial cell markers [14, 19, 25]. The current study suggests that urothelial cell-conditioned medium provides a favorable source of inductive signals that initiate differentiation of USC towards the urothelial cell lineage. These urothelial-inductive factors remain incompletely characterized, although EGF is likely one of the major mediators of urothelial differentiation [14, 19, 25]. To understand the mechanism driving urothelial differentiation of USC, factors secreted by cultured urothelial cells would need to be separated by chromatography and characterized. The elucidation of these factors will need to be accomplished in future studies. This would provide a better understanding of the mechanisms driving urothelial cell differentiation and allow for the formation of even more physiologically normal USC-derived urothelium that could be used for generating in vitro models and for urological regenerative medicine therapies.

The urothelium is constantly exposed to fluctuating osmotic conditions, hydrostatic pressure, and mechanical strain, due to the dynamic environment produced by cyclic retention and voiding of urine. Our previous studies demonstrated that dynamic culture significantly enhanced cell growth and myogenic differentiation of bone marrow stromal cells (BMSC) by SMC-conditioned medium, as compare to static culture. By testing a series of dynamic conditions, it was determined that the optimal rotational rate for producing was 40 rpm [31]. However, dynamic culture in the absence of molecular differentiation cues promoted only cell proliferation but did not induce SMC differentiation from BMSC [22]. In this study, dynamic culture conditions significantly promoted barrier function in USC-derived urothelium, regardless of the differentiation protocol employed. The dynamic culture conditions most likely promoted cell/cell communications and promoted tight junction formation through increase mechanical stress. It appears that induced USC formed multipliers of urothelium so that number of cells did not continue increasing at the end of 14 days' culture. These data suggest that dynamic culture conditions, mimicking the flow of urine, prompted the USC-derived UC to adopt a more normal phenotype and arrange into a normal urothelial cellular architecture.

The induction time frame is important for urothelial differentiation of stem cells. The state-of-the-art method for urothelial cell differentiation from USC uses EGF in static culture for 1 or 2 weeks. Our previous studies have shown that conditioned medium enhance urothelial cell differentiation and proliferation of rat urothelial progenitors [8], and dynamic culture promotes bladder SMC differentiation from USC [22] at different time periods. It is apparent that different time frames are required to induce stem cells to give rise to different cell types. Based on our previous studies, it takes approximately 4 weeks to induce human USC into skeletal muscle cells [14, 17, 20], 2 weeks for differentiation of SMC with contractile function [14, 20], and 1 to 2 weeks for endodermal differentiation with barrier function [14, 20]. However, many groups induce USC differentiation to UC that express urothelial markers over a single week. Our study indicates that the standard 1-week induction is not sufficient to give rise to a urothelial cell population with normal tight junctions (Fig. 2c). Of note, urothelium has tendency to detach from the substrate after 3 weeks of induction and tight junction is not fully developed at 1-week induction, indicating that 2 weeks is the optimal time frame for urothelial differentiation from USC.

One highly important characteristic of urothelium is its multilayer structure. Multilayer urothelium provides the bladder with the physical attributes required for

urine storage (stretching) and voiding (contracting). Urothelial cells usually require a serum-free and calcium/magnesium-free culture condition [31]. Our previous studies and other laboratories have demonstrated that after urothelial cells reach confluence in serum-free keratinocyte medium, increasing extracellular calcium from 0.09 to 0.9 mM [32], or the addition of serum, promoted urothelial cell stratification and formation of tight junctions [14, 20, 21, 33]. Though not evaluated in the current study, calcium and serum might provide additional differentiation cues that could further enhance the functionality of the induced USC. In addition, natural collagen-based biomaterials possess beneficial properties, which promote urothelial cell growth, formation of a multilayer structure, and expression of urothelial cell functional markers. This multilayer urothelium derived from USC may provide an excellent model for research on human urothelial tissue and serve as a potential material for urological regenerative medicine therapies. It would be interesting to examine whether normal urothelium structures including three layers: basal, intermediate, and apical, form in the tissue engineered multilayer urothelium in a future study. Additionally, characterization of organelle structure, urothelial mechanical properties, and additional functional biomarkers needs to be conducted to confirm the functional potential of USC derived urothelium.

In addition, it is critical to consider interactions of the drug with both normal and diseased urothelium to improve the safety and efficiency of drugs delivered locally to the bladder. Thus, tissue-engineered urothelium also provides a convenient tool for studying these interactions, beside urological tissue repair. The development of disease-specific urothelium models based on the technologies described herein would increase our understanding of locally delivered bladder drug kinetics in both normal and diseased tissue.

Conclusions

Tissue engineered urethra or bladder and in vitro bladder mucosa models for anti-cancer or interstitial cystitis drug development require urothelial cells for production. However, urothelial cells are often obtained by invasive bladder tissue biopsy. Although adult stem cells maintain urothelial differentiation potential, affecting this differentiation remains challenging. In this study, we have demonstrated that stem cells present in urine can efficiently differentiate into urothelial cells with robust barrier function that form multilayered structures similar to normal urothelium. USC-derived urothelium induced by urothelial cell-conditioned medium showed multiple functional improvements over previous differentiation methods. Urothelium generated from patient-derived USC would provide an excellent platform for the study of mechanisms underlying urological diseases including interstitial cystitis, overactive, neurogenic, or obstructive bladder and provide a testbed for the development of therapies to treat these diseases. In addition, induced urothelium can be used in evaluating the impact of pharmacological treatment on urothelial barrier function in both normal bladder and in bladder that has been compromised by diseases. Furthermore, multiple layer urothelium formed on a natural collagen-based matrix may be used for the reconstruction of urological tissues that have been damaged by trauma or disease.

Additional files

Additional file 1: Table S1. Primers for real-time PCR used in this study. (DOCX 13 kb)

Additional file 2: Table S2. Antibodies used in this study. (DOCX 14 kb)

Additional file 3: Table S3. Percentage of USC expressing urothelial cell markers 2 weeks after urothelial induction assessed by immunofluorescence. (DOCX 14 kb)

Additional file 4: Table S4. Percentage of USC expressing tight junction markers 2 weeks after urothelial induction assessed by immunofluorescence. (DOCX 16 kb)

Abbreviations

BMSC: Bone marrow stromal cells; BSA: Bovine serum albumin; CM: Conditioned medium; DAPI: Diamidino-2-phenylindole; DMEM: Dulbecco's modified Eagle's medium; EFM: Embryo fibroblast medium; EGF: Epidermal growth factor; ESC: Embryonic stem cells; FBS: Fetal bovine serum; GAG: Glycosaminoglycan; iPSC: Induced pluripotent stem cells; KSFM: Keratinocyte serum-free medium; MSC: Mesenchymal stem cells; PAA: Peracetic acid; PBS: Phosphate buffered saline; SIS: Small intestinal submucosa; SMC: Smooth muscle cells; TEM: Transmission electron microscopy; UC: Urothelial cells; USC: Urine-derived stem cells

Competing interests
The authors declare that they have no competing interests.

References

1. Floyd RV, Winstanley C, Bakran A, Wray S, Burdyga TV. Modulation of ureteric ca signaling and contractility in humans and rats by uropathogenic E. coli. Am J Physiol Renal physiol. 2010;298(4):F900–8.
2. Akkad T, Pelzer AE, Mitterberger M, et al. Influence of intravesical potassium on pelvic floor activity in women with recurrent urinary tract infections: comparative urodynamics might lead to enhanced detection of dysfunctional voiding. BJU Int. 2007;100(5):1071–4.
3. Zhang Y, Atala A. Bladder regeneration. In: Ma PX, editor. biomaterials and regenerative medicine. Cambridge: Cambridge University Press; 2015. p. 669-79.
4. Zhang Y, Kropp BP, Lin HK, Cowan R, Cheng EY. Bladder regeneration with cell-seeded small intestinal submucosa. Tissue Eng. 2004;10(1–2):181–7.
5. Zhang Y, Kropp BP, Moore P, et al. Coculture of bladder urothelial and smooth muscle cells on small intestinal submucosa: potential applications for tissue engineering technology. J Urol. 2000;164(3 Pt 2):928–34 discussion 34–5.
6. Zhang Y, Liu G, Kropp BP. Re-epithelialization of demucosalized stomach patch with tissue-engineered urothelial mucosa combined with Botox a in bladder augmentation. BJU Int. 2012;110(2 Pt 2):E106–12.
7. Zhang YY, Frey P. Growth of cultured human urothelial cells into stratified urothelial sheet suitable for autografts. Adv Exp Med Biol. 2003;539(Pt B):907–20.
8. Zhang YY, Ludwikowski B, Hurst R, Frey P. Expansion and long-term culture of differentiated normal rat urothelial cells in vitro. In Vitro Cell Dev Biol Anim. 2001;37(7):419–29.
9. Tian H, Bharadwaj S, Liu Y, Ma PX, Atala A, Zhang Y. Differentiation of human bone marrow mesenchymal stem cells into bladder cells: potential for urological tissue engineering. Tissue Eng A. 2010;16(5):1769–79.
10. Ning J, Li C, Li H, Chang J. Bone marrow mesenchymal stem cells differentiate into urothelial cells and the implications for reconstructing urinary bladder mucosa. Cytotechnology. 2011;63(5):531–9.
11. Zhao Z, Yu H, Fan C, Kong Q, Liu D, Meng L. Differentiate into urothelium and smooth muscle cells from adipose tissue-derived stem cells for ureter reconstruction in a rabbit model. Am J Transl Res. 2016;8(9):3757–68.
12. Oottamasathien S, Wang Y, Williams K, et al. Directed differentiation of embryonic stem cells into bladder tissue. Dev Biol. 2007;304(2):556–66.
13. Kang M, Kim HH, Han YM. Generation of bladder urothelium from human pluripotent stem cells under chemically defined serum- and feeder-free system. Int J Mol Sci. 2014;15(5):7139–57.
14. Bharadwaj S, Liu G, Shi Y, et al. Multipotential differentiation of human urine-derived stem cells: potential for therapeutic applications in urology. Stem Cells. 2013;31(9):1840–56.
15. Zhang D, Wei G, Li P, Zhou X, Zhang Y. Urine-derived stem cells: a novel and versatile progenitor source for cell-based therapy and regenerative medicine. Genes Dis. 2014;1(1):8–17.
16. Qin D, Long T, Deng J, Zhang Y. Urine-derived stem cells for potential use in bladder repair. Stem Cell Res Ther. 2014;5(3):69.
17. Liu G, Pareta RA, Wu R, et al. Skeletal myogenic differentiation of urine-derived stem cells and angiogenesis using microbeads loaded with growth factors. Biomaterials. 2013;34(4):1311–26.
18. Wu R, Soland M, Liu G, et al. Immunomodulatory properties of urine-derived stem cells.[abstract]. In: Atala A, editor. Wake Forest Institute for Regenerative Medicine Retreat Meeting. Winston Slem: Wake Forest Institute for Regenerative Medicine; 2013. p. 3.
19. Zhang Y, McNeill E, Tian H, et al. Urine derived cells are a potential source for urological tissue reconstruction. J Urol. 2008;180(5):2226–33.
20. Lang R, Liu G, Shi Y, et al. Self-renewal and differentiation capacity of urine-derived stem cells after urine preservation for 24 hours. PLoS One. 2013;8(1):e53980.
21. Bharadwaj S, Liu G, Shi Y, et al. Characterization of urine-derived stem cells obtained from upper urinary tract for use in cell-based urological tissue engineering. Tissue Eng A. 2011;17(15–16):2123–32.
22. Tian H, Bharadwaj S, Liu Y, et al. Myogenic differentiation of human bone marrow mesenchymal stem cells on a 3D nano fibrous scaffold for bladder tissue engineering. Biomaterials. 2010;31(5):870–7.
23. Higashida T, Kreipke CW, Rafols JA, et al. The role of hypoxia-inducible factor-1alpha, aquaporin-4, and matrix metalloproteinase-9 in blood-brain barrier disruption and brain edema after traumatic brain injury. J Neurosurg. 2011;114(1):92–101.
24. Kang HS, Choi SH, Kim BS, et al. Advanced properties of urine derived stem cells compared to adipose tissue derived stem cells in terms of cell proliferation, immune modulation and multi differentiation. J Korean Med Sci. 2015;30(12):1764–76.
25. Liu G, Wang X, Sun X, Deng C, Atala A, Zhang Y. The effect of urine-derived stem cells expressing VEGF loaded in collagen hydrogels on myogenesis and innervation following after subcutaneous implantation in nude mice. Biomaterials. 2013;34(34):8617–29.
26. Birder L, Andersson KE. Urothelial signaling. Physiol Rev. 2013;93(2):653–80.
27. Baer PC, Bereiter-Hahn J, Missler C, et al. Conditioned medium from renal tubular epithelial cells initiates differentiation of human mesenchymal stem cells. Cell Prolif. 2009;42(1):29–37.
28. Lacham-Kaplan O, Chy H, Trounson A. Testicular cell conditioned medium supports differentiation of embryonic stem cells into ovarian structures containing oocytes. Stem Cells. 2006;24(2):266–73.
29. Caballe-Serrano J, Schuldt Filho G, Bosshardt DD, Gargallo-Albiol J, Buser D, Gruber R. Conditioned medium from fresh and demineralized bone enhances osteoclastogenesis in murine bone marrow cultures. Clin Oral Implants Res. 2016;27(2):226–32.
30. Alves da Silva ML, Costa-Pinto AR, Martins A, et al. Conditioned medium as a strategy for human stem cells chondrogenic differentiation. J Tissue Eng Regen Med. 2015;9(6):714–23.
31. Wu S, Liu Y, Bharadwaj S, Atala A, Zhang Y. Human urine-derived stem cells seeded in a modified 3D porous small intestinal submucosa scaffold for urethral tissue engineering. Biomaterials. 2011;32(5):1317–26.
32. Southgate J, Hutton KA, Thomas DF, Trejdosiewicz LK. Normal human urothelial cells in vitro: proliferation and induction of stratification. Lab Investig. 1994;71(4):583–94.
33. Bodin A, Bharadwaj S, Wu S, Gatenholm P, Atala A, Zhang Y. Tissue-engineered conduit using urine-derived stem cells seeded bacterial cellulose polymer in urinary reconstruction and diversion. Biomaterials. 2010; 31(34):8889–901.

"This course was developed and edited from the open access article: Comprehensive characterization of chorionic villi-derived mesenchymal stromal cells from human placenta - Ventura Ferreira et al. Stem Cell Research & Therapy (2018) 9:28 (DOI 10.1186/s13287-017-0757-1), used under the Creative Commons Attribution License."

"This course was developed and edited from the open access article: The multi-functional roles of menstrual blood-derived stem cells in regenerative medicine -Chen et al. Stem Cell Research & Therapy, (2019) 10:1, (https://doi.org/10.1186/s13287-018-1105-9), used under the Creative Commons Attribution License."

"This course was developed and edited from the open access article: Comparative analysis of mesenchymal stem cells derived from amniotic membrane, umbilical cord, and chorionic plate under serum-free condition - Ma et al. Stem Cell Research & Therapy (2019) 10:19, (https://doi.org/10.1186/s13287-018-1104-x), used under the Creative Commons Attribution License."

"This course was developed and edited from the open access article: Urothelium with barrier function differentiated from human urine-derived stem cells for potential use in urinary tract reconstruction - Wan et al. Stem Cell Research & Therapy, (2018) 9:304 (https://doi.org/10.1186/s13287-018-1035-6), used under the Creative Commons Attribution License."